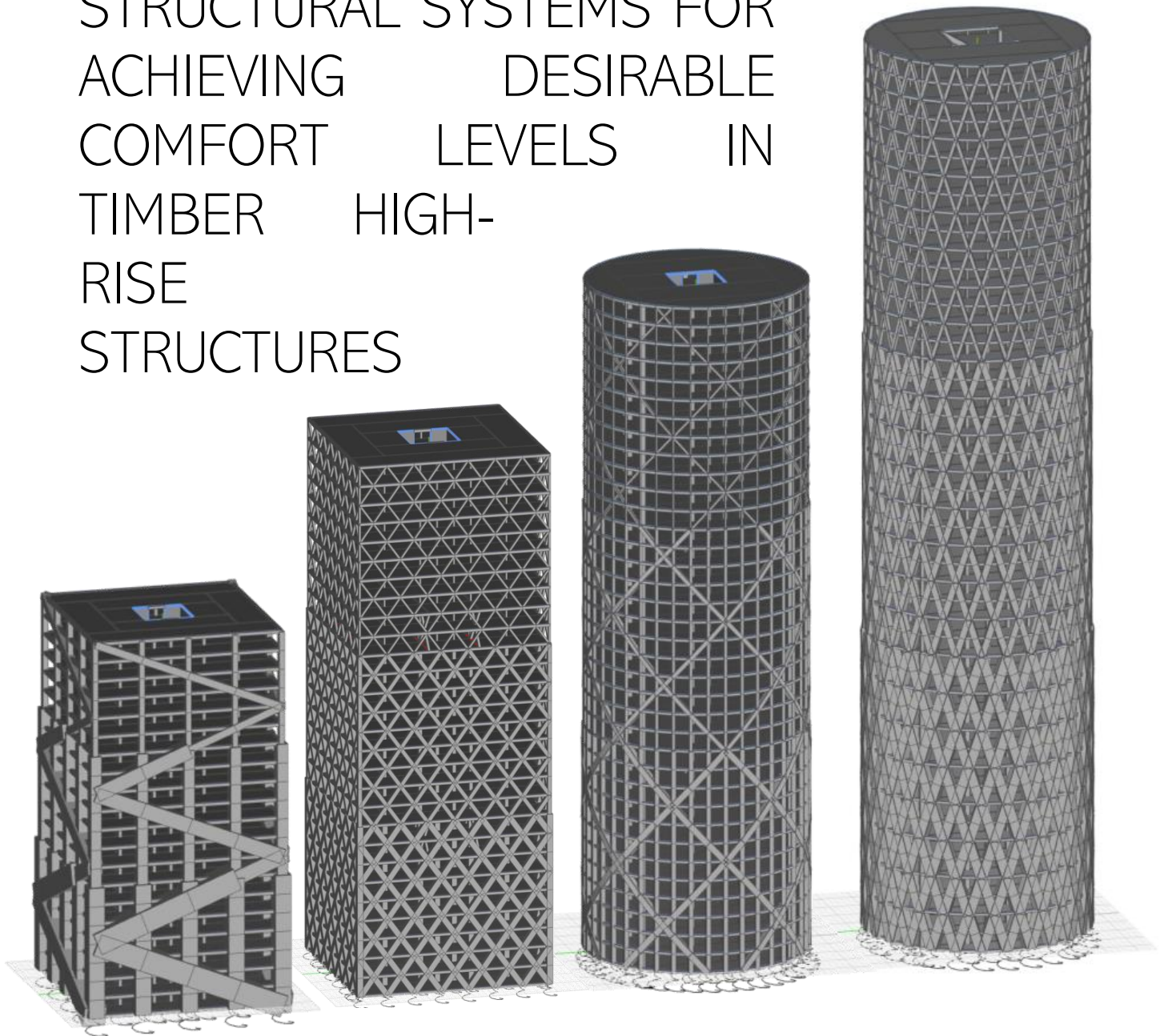


A COMPUTATIONAL STUDY ON THE APPLICATION OF EFFICIENT DUAL STRUCTURAL SYSTEMS FOR ACHIEVING DESIRABLE COMFORT LEVELS IN TIMBER HIGH-RISE STRUCTURES



Jacob Versteeg Conlledo

29-09-2022



A COMPUTATIONAL STUDY ON THE APPLICATION OF EFFICIENT DUAL STRUCTURAL SYSTEMS FOR ACHIEVING DESIRABLE COMFORT LEVELS IN TIMBER HIGH-RISE STRUCTURES

By

Jacob Versteeg Conlledo

A Master's thesis submitted for partial fulfilment of the requirements for the degree of

Master of Science

In Building Engineering – Structural Design

at Delft University of Technology

September 2022



Author

Jacob Luis Fernando Versteeg Conlledo

4351576

+31 (06) 15 68 67 90

jversteegconlledo@gmail.com

University

Delft University of Technology

Faculty of Civil Engineering and Geosciences

Master Building Engineering

Specialisation in Structural Design

Graduation committee

Ass. Prof. Dr. M.A. (Mariana) Popescu Chair	<i>Delft University of Technology Applied mechanics</i>
Ir. M.P. (Maria) Felicita	<i>Delft University of Technology Bio-based Structures & Materials</i>
Ir. R. (Roy) Crielaard	<i>Delft University of Technology Applied mechanics</i>
Ir. R.H.A. (Rick) Titulaer	<i>Arup Senior Structural Engineer</i>
Dr. ir. G.j.P. Ravenshorst	<i>Delft University of Technology Bio-based Structures & Materials</i>
Dr. ir. H.R. Schipper	<i>Delft University of Technology Applied Mechanics</i>

PREFACE

The Master's thesis is the final step in obtaining a Master of Science in Civil Engineering, with a Master degree in Building Engineering at Delft University of Technology. During the Master Building Engineering I have specialized in Structural Design, due to my interest in Architecture and Structural Engineering.

With this research, my goal was to push the limits for timber construction by performing a mass variant study using my favourite tool, Parametric Design. Through parametric engineering, numerous studies have been performed, exploring what is, would be or should be possible for timber high-rise structures. By studying the possibilities for previously unexamined timber structural system configurations, I hope to open doors for further applications of structural timber in high-rise structures. In my personal opinion, I strongly believe that materials should be used where they are most fit for, if a sustainable and holistic design is considered.

I would like to thank my committee members, Mariana Popescu, Maria Felicita, Roy Crielaard and Rick Titulaer for all the help and feedback throughout this thesis. They have helped me understand how to acquire results that are comparable and based on what criteria the variants should be evaluated. Also, I would like to thank everyone at Arup that took the time to help me with my thesis. Many colleagues at Arup took the time to help me with questions about timber, wind dynamics, circularity or one of my three, non-stop running, remote desktops.

Lastly, I would like to thank my fellow students during my Master's for thinking along with this thesis, my friends for being patient with me when I'd be too busy to meet and most importantly my parents, sister and girlfriend for being so considerate and attending me throughout the process.

Amsterdam, September 2022

Jacob Versteeg Conlledo

ABSTRACT

The Paris Agreement formulates the ambition that global warming should be limited to 1.5 degrees Celsius above pre-industrial temperatures. This may have tremendous impact, in particular for the construction sector. While the built environment is already accountable for 39% of human-caused CO₂ emissions, the expected population growth, growing from 7.7 billion in 2019 to 9.7 billion in 2050 and up to 11 billion in 2100 will demand large urbanization development. More specifically, as the Netherlands aim to construct over 650.000 houses before 2030, a fast, sustainable and area-efficient solution is needed. A solution may be the development of residential timber high-rise structures as a timber structure has a low environmental impact due to its capability to store CO₂. Timber structures are also quicker to erect due to its potential for prefabrication. By constructing high-rise buildings with timber structures, more sustainable homes can be constructed in dense areas.

When looking at the challenges for high-rise structures, it has been found that these structures are of increasing complexity when built from timber-only elements. One of the main design criteria for high-rise structures is the assessment of the vibration levels based on comfort levels. Due to lateral wind loads, slender structures tend to oscillate at a frequency and an acceleration. High frequencies and accelerations can become noticeable to the building's users and can, in some cases, cause motion sickness. Reducing accelerations is key when designing high-rise structures, measures taken may include increasing either the global stiffness or the building's mass. Complications arise for realizing comfortable high-rise with structural timber, as it is generally complex to increase the global stiffness with timber elements. In addition, the relative density of wood is considerably lower than concrete or steel, causing complications when a heavier structure is desired.

Since increasing global stiffnesses of high-rise buildings is more complex when structural timber is used, unexamined structural methods for timber construction should be considered. Tube-in-tube systems for example rely on the collaboration of the stiffnesses of the inner- and the outer tube. For timber high-rise, combining structural systems may offer a solution to overcome challenges regarding required stiffnesses. Therefore, the main research question of this thesis is:

“How can dual structural systems be applied for achieving desirable comfort levels in efficient timber high-rise”

Hence, the goal of this thesis is to acquire knowledge on the dynamic behaviour of timber high-rise, explore the possibilities of configurations with combined structural systems and to be able to make recommendations on how dual structural systems should be applied in order to realise an efficient design while complying to the required comfort levels.

In this thesis, two exterior systems have been studied in combination with four interior systems, based on 2 different floorplan shapes over varying heights. Whereas the façade systems are the diagrid and megaframe, interior systems are a cross laminated timber (CLT) core, a braced frame core and the combination of each with an outrigger system. Combinations of interior and exterior systems have been applied on circular and rectangular floorplans, which have been analysed on heights varying from 60 m to 144 m.

Due to the complexities to obtain joint rigidity in structural timber, all assessed structural systems are chosen to be form stable structures, except for the CLT core. Therefore, all connections in the structural models are modelled as perfect hinges. The connections between perpendicular panels in the CLT core have been modelled as rigid joints. In order to resemble the CLT core's structural capacity, which is governed by the core's connections, the bending stiffnesses of CLT elements have reduced by 70%.

In order to perform such an extensive variant study, with numerous variables per system configuration, a parametric structural model has been set up. Utilizing this model each of the 3072 alternatives have been checked on acceptance levels based on strength, stability and accelerations, according to EN 1995-1-1: Eurocode 5: Design of timber structures, EN 1995-1-1: Eurocode 1: Actions on structures, NEN 6702, Nationaal Convenant Hoogbouw and their corresponding Dutch National Annexes.

In this thesis, in order to size structural elements accordingly for the fulfilment of abovementioned acceptance levels, an estimator function has been developed. The estimator function is a multiplication factor based on the structure's height. Moreover, the function is an approach to gather adequate element dimensions with a method that is faster than the brute force method, with more accurate estimates. By incorporating this method, element sizes correspond to the acceptance levels, making all configurations comparable based on their material use.

Results from this thesis are measured in the structure's efficiency, indicated by the efficient use of timber [kg/m²]. Main conclusions drawn from this thesis are:

1. Dual structural systems can achieve up to 50% material reduction if systems are connected with an outrigger, increasing the participation of the exterior system by 10%.
2. The effect of dual structural systems without an outrigger is negligible, as the stiffness of a timber core system is below 3% of the global stiffness.
3. The effectiveness of a configuration depends on the bending stiffness – shear stiffness ratio. A higher ratio results in lower natural frequencies, decreasing the required material.
4. Most efficient configurations are shown in Figure 1, with continuous lines showing feasible results, as discussed in sections 5.3.1 and 5.3.2. Dotted lines resemble results that are beyond the, to this point, viable realm for timber high-rise structures :
 - a. 20 – 33 floors, a circular 56.9° diagrid with a braced core and an outrigger system shows to be the most efficient alternative
 - b. 33 – 37 floors, a circular 47.5° megaframe with a braced core and an outrigger system shows to be the most efficient alternative

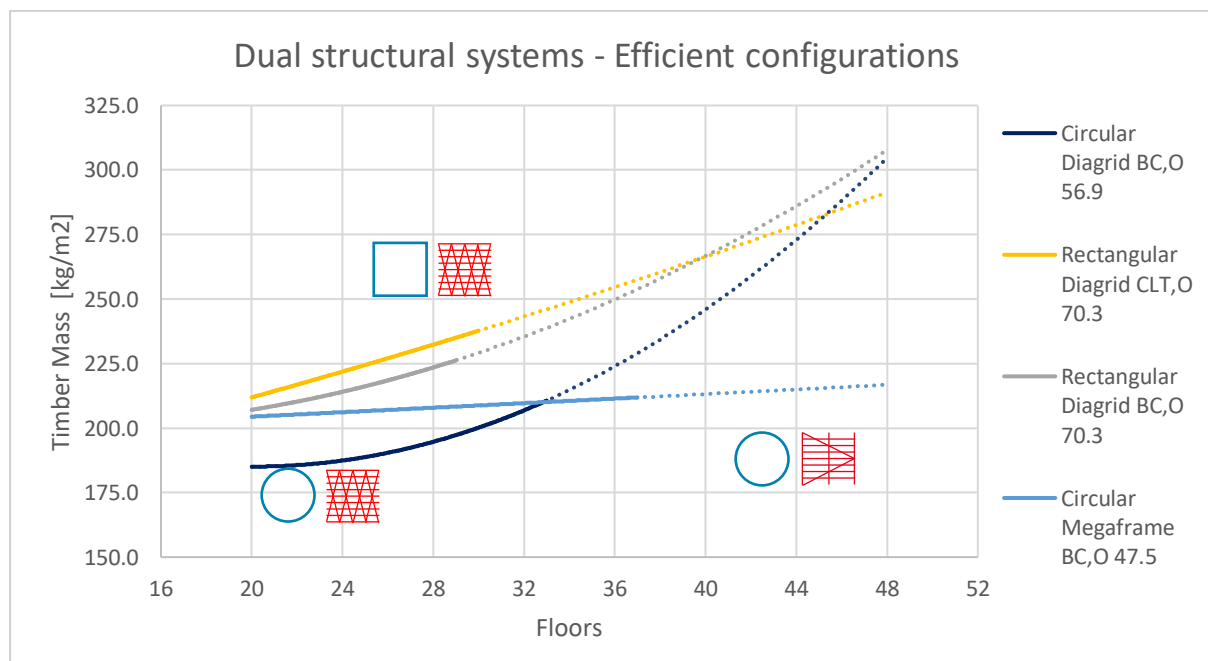


Figure 1: Dual structural systems - configuration effectiveness

When designing efficient and comfortable timber-only high-rise structures a few design considerations need to be taken into account. First it has been found that the floorplan shape is of major influence on the accelerations. The force coefficient (c_f) of a circular shaped building is 0.84, whereas the force coefficient of a square shaped building is 1.47, as much as 75% higher than the circular force coefficient.

The efficiency of the exterior system can be improved by considering a higher bay density, increasing the number of load paths in the façade decreases the gap between the required sizing of critical and non-critical elements.

For taller structures, bending resistances become more influential over shear resistances, altering the optimal bay angle from 30° (shear) to 90° (bending moments), making the megaframe structure most efficient for taller structures due to the presence of columns. The megaframe is not impacted by the brace angle, as braces and columns collaborate in resisting shear and bending in the structure and helps reducing the shear lag effect.

Results from this thesis show that the interior plain core contribution to the moment resistance is below 2%, caused by its negligible stiffness compared to the exterior system. The outrigger system shows to be highly beneficial for improving the efficiency of the structure, connecting core system to either interior columns or the structure's perimeter. The outrigger can achieve up to 50% material reduction if the outrigger's stiff arms extend to both exterior systems of the structure, having the largest lever arm and connecting opposite facades. By connecting opposite facades, additional webs are created that improve and activate the collaboration between opposite flanges, increasing bending stiffness – shear stiffness ratio.

TABLE OF CONTENTS

PREFACE	4
ABSTRACT	5
TABLE OF CONTENTS	9
1 INTRODUCTION	12
1.1 MOTIVATION	12
1.2 GOALS AND OBJECTIVES	14
1.3 RESEARCH QUESTIONS	15
1.4 METHODOLOGY	15
1.5 SCOPE.....	16
2 THEORY	18
2.1 TIMBER.....	18
2.1.1 MATERIAL PROPERTIES.....	20
2.1.2 GLUED LAMINATED TIMBER.....	21
2.1.3 CROSS LAMINATED TIMBER	22
2.1.4 CONNECTIONS	23
2.1.5 TIMBER CALCULATIONS.....	24
2.1.6 HIGH-RISE	24
2.2 INFLUENCE PARAMETERS.....	28
2.2.1 EIGENFREQUENCY	29
2.2.2 ACCELERATIONS.....	31
2.2.3 DAMPING	35
2.2.4 FORCE COEFFICIENT	36
2.2.5 SHEAR LAG.....	36
2.3 STRUCTURAL SYSTEMS.....	37
2.3.1 CASE STUDIES.....	37
2.3.2 DIAGRID	40
2.3.3 MEGAFRAME.....	42
2.3.4 CORE SYSTEMS.....	43
2.3.5 OUTRIGGER	45
2.4 SOFTWARE.....	46
2.5 DIMENSIONING METHODS	47

3	STRUCTURAL MODEL	49
3.1	GEOMETRY GENERATION	51
3.1.1	FLOORPLAN SHAPE	51
3.1.2	EXTERIOR SYSTEMS.....	54
3.1.3	INTERIOR SYSTEMS	59
3.1.4	OUTRIGGER	64
3.2	ANALYSIS.....	66
3.2.1	GSA INPUTS	66
3.2.2	GSA OUTPUTS	71
3.3	ACCEPTANCE CHECK	74
3.3.2	ELEMENT DIMENSIONS	77
4	RESULTS	78
4.1	GEOMETRY GENERATION	78
4.1.1	FLOORPLAN SHAPE	78
4.1.2	EXTERIOR SYSTEM.....	79
4.1.3	INTERIOR SYSTEM	83
4.1.4	OUTRIGGER	85
4.2	ANALYSIS.....	87
4.2.1	COMPARISON OF SYSTEMS	87
4.2.2	MASS INFLUENCE.....	88
4.3	ACCEPTANCE CHECK	89
5	DISCUSSION	91
5.1	GEOMETRY GENERATION	91
5.1.1	FLOORPLAN SHAPE	92
5.1.2	EXTERIOR SYSTEM.....	93
5.1.3	INTERIOR SYSTEM	97
5.1.4	OUTRIGGER	101
5.2	ANALYSIS.....	107
5.2.1	COMPARISON OF SYSTEMS	107
5.2.2	ESTIMATOR FUNCTION.....	108
5.2.3	DAMPING	109
5.3	ACCEPTANCE CHECK	110
5.3.1	ELEMENT DIMENSIONS	110
5.3.2	ELEMENT LOADS	111

5.3.3	DESIGN CODES	112
6	CONCLUSION	113
7	RECOMMENDATIONS FOR FURTHER RESEARCH	116
8	BIBLIOGRAPHY	118
APPENDICES		1
A	TIMBER CALCULATIONS	1
B	ALONG-WIND ACCELERATIONS	6
C	ACROSS WIND ACCELERATIONS	9
D	ELEMENT DIMENSIONS.....	10
E	ESTIMATOR FUNCTION	15
E.1	CALIBRATION MODEL & FIRST ANALYSIS.....	16
E.2	DETERMINATION OF BANDWIDTH.....	18
E.3	DIMENSIONING FACTOR.....	19
E.4	VERIFICATION BANDWIDTH	21
E.5	ADJUSTING ESTIMATOR FUNCTION	22
E.6	VERIFICATION ESTIMATOR FUNCTION	24
F	STIFFNESS CALCULATION CORE VS FAÇADE	25

1 INTRODUCTION

A global challenge that cannot be ignored anymore is the fact that, on a world scale, carbon emissions should be reduced in order to limit global warming to 1.5 degrees Celsius above pre-industrial temperatures (Paris Agreement, 2015). While the built environment is already accountable for 39% of human-caused CO₂ emissions, there is an increasing demand for new buildings in urban areas (IEA, 2018). The world's population is expected to grow from 7.7 billion in 2019, to 9.7 billion in 2050 and even up to 11 billion in 2100 (UN, 2021). In addition, due to an increase in urbanization, most of the population growth will be in densely urbanized areas (The World Bank, 2022). The single most widely used construction material, in the Netherlands as well as worldwide, is concrete which is one of the large producers of carbon dioxide (Metabolic, 2020). The combination of the growing urbanization and the increasing emissions of the building industry are alarming.

A possible solution to these two growing issues is timber construction. Timber constructions have several large advantages, such as low environmental impact, capability to store CO₂ and large-scale industrial production (TNO, 2021). Moreover, looking at the current housing shortage in the Netherlands, using timber as a construction material could accelerate the construction of domestic buildings. Which is very interesting, as the Dutch market aims to construct +650/700k houses before 2030. For this, timber offers a lower construction time compared to steel or concrete structures due to the prefabrication of structural elements. In other words, timber construction could be a real game-changer.

1.1 MOTIVATION

To approach abovementioned problems, developments are needed in the building industry. It has become clear that there is a demand for tall and sustainable buildings as ground will become scarce in urban areas and buildings need to be built with a lower carbon footprint. High-rise buildings could offer an area efficient solution to the housing problem that will arise. By constructing high-rise buildings, more sustainable homes can be constructed in dense areas (Urban Taskforce, 2022).

For the environmental issues the world is facing today, timber as a building material offers a reduction in the carbon footprint of future buildings. It is known that, in contrast to steel and concrete, timber absorbs CO₂ during growth and stores it until it is decomposed. Other benefits of timber are a higher strength to volume ratio, quicker construction time and the potential for disassembly. However, like every material, timber does have a number of disadvantages compared to other materials.

Timber has considerably lower relative density, strength and stiffness and timber is a hygroscopic material, making it vulnerable to moisture. Lastly, timber is vulnerable for deterioration, both biotic as abiotic deterioration could be problematic for timber elements.

If timber could be used for high-rise structures, it could be a suitable and more sustainable alternative for current construction methods. If used properly, high-rise timber constructions offers an integral solution for space-efficient and environmental friendly buildings.

To research possibilities for timber as a sustainable construction material is in line with the Dutch ambitions to become completely circular in 2050 (Rijksoverheid, 2016). A circular economy decouples economic activity from the consumption of finite resources. In design this means eliminating waste and pollution, circulating products and materials at their highest value and regenerating nature (Ellen MacArthur Foundation, 2016). Circularity is not limited to choosing building materials with a low carbon footprint, as many may think. In a circular economy, it's essential to achieve an elongated lifespan for material use. According to the Ellen MacArthur Foundation, to extend the lifespan of materials and components, there are three circular design principles that should be taken into account: design for disassembly (DfD), design for material efficiency (DfME) and design for adaptability (DfA). To ensure alignment with the Dutch government's circular ambitions, these three design strategies will be used to create focus within the scope of the research. In other words, the three DfX strategies are considered when assessing structural systems, to be able to narrow down the scope in this thesis. The three strategies are briefly introduced below, but will not be researched as part of the Master's thesis.

Design for disassembly (DfD) – the strategy aims at enabling the potential for disassembly at the end of the service life. It is possible that the useful life of some building components outlast their service life as part of the full system. It is important to design this strategy upfront, to make sure the components can be disassembled in order to recover residual value of the components at the end of their service life (Arup, 2022).

Design for material efficiency (DfME) – this strategy aims at minimizing the material consumption, while meeting the project requirements. The purpose and objective is to ensure efficient use of materials at a maximum performance level (Arup, 2022).

Design for adaptability (DfA) – the final strategy aims at ensuring the adaptability potential during the use stage of the building. Often, the functional life spans of the building are short. It is important that building have the ability to accommodate to new functions to retain the value at the highest level (Arup, 2022).

This current thesis investigation proposes to further research possibilities for a variation of structural systems for timber high-rise structures, while accommodating circular design principles.

1.2 GOALS AND OBJECTIVES

The goal of this Master's thesis is to explore the possibilities for dual structural systems in order to realise efficient and comfortable high-rise structures. The research aim is to achieve structurally efficient timber high-rise structures by combining interior and exterior structural systems for the purpose of increasing global stiffnesses in order to reduce high-rise accelerations and comply to serviceability limits.

To determine this goal a few objectives have been defined:

1. Determine influence of parameters on accelerations regarding wind induced building dynamics
2. Evaluate efficient and accurate approaches for eigenfrequencies
3. Assess feasibility of structural systems
4. Determine method for quantification of collaboration and stiffness of dual structural systems
5. Implement quantification method for stiffness into parametric structural model
6. Verify parameter influence on structural accelerations
7. Configurate structural systems for comfort levels
8. Compare configurations for material efficiency and draw conclusions

1.3 RESEARCH QUESTIONS

The research questions have derived from the problem definition. This Master's thesis will give answer to a main research question. To be able to answer the main research question seven sub questions are formulated.

The main research question of this Master's thesis is:

“How can dual structural systems be applied for achieving desirable comfort levels in efficient timber high-rise”

The sub-questions have been listed below:

1. *“What parameters influence high-rise serviceability levels?”*
2. *“How can the collaboration of dual structural systems be quantified?”*
3. *“How does the collaboration of dual structural systems influence high-rise accelerations”*
4. *“How can a 3D structural parametric model be used to determine high-rise accelerations for combined structural systems?”*
5. *“What configuration of parameters achieves desirable comfort levels for timber high-rise?”*
6. *“What strategy can be used to improve the collaboration of dual structural systems?”*
7. *“What recommendation can be made on how dual structural systems can achieve comfortable timber high-rise”*

1.4 METHODOLOGY

For this Master's thesis a parametric structural model has been created which can give insights in the parameters of structural accelerations for required comfort levels in timber high-rise. This will be done while conforming the three circular design principles (DfD, DfME and DfA). Several structural systems will be assessed both individually and collectively to determine their influence on reducing accelerations.

By doing a literature study, answers will be found for the following sub-questions:

1. *“What influence do parameters have on high-rise serviceability levels?”*
2. *“How can circular design strategies be quantified for timber high-rise buildings?”*
3. *“How can the collaboration of dual structural systems be quantified?”*
4. *“How does the collaboration of dual structural systems influence high-rise accelerations”*

To be able to evaluate the different alternatives, a number of building requirements need to be aligned on which the different systems will be compared. Based on the findings from the first three sub-questions, the boundary conditions, design parameters and key performance indicators (KPI's) can be determined. Once this information is derived, the parametric model can be constructed, answering sub-question 5:

5. *“How can a 3D structural parametric model be used to determine high-rise accelerations for combined structural systems?”*

Lastly, by doing a parametric study and analysing the KPI's, conclusions can be drawn over the final sub-questions:

6. *“What configuration of parameters achieves desirable comfort levels for timber high-rise?”*
7. *“What strategy can be used to improve the collaboration of dual structural systems?”*
8. *“What recommendation can be made on how structural systems comply to circular principles?”*

1.5 SCOPE

The following chapter will delineate the scope boundaries of the research. First, serviceability of timber high-rise needs to be assessed. In-depth knowledge on wind induced dynamics is needed and influence parameters need to be established. Also, it is necessary to gain insights on what influence which parameter has, and which designs would give more satisfying results. By analysing the wind dynamics first, a preliminary set of parameters is determined which influence the serviceable accelerations of the building. Once the dynamics of wind induced accelerations are clear, several circular design strategies are to be looked into.

Three circular design strategies are assessed to select applicable structural systems for timber-only high-rise: Design for Adaptability (DfA), Design for Material Efficiency (DfME) and Design for Disassembly (DfD).

The selected structural systems should be in line with the three DfX strategies. To ensure this, an initial selection took place. In this preliminary stage of the research, some of the systems can be disregarded and are therefore neglected. For example, when structural systems are selected that fulfil DfA requirements; floorplans need to be able to be rearranged without structural renovations. These structural systems should then include perimeter- or core active systems such as diagrid system, tube system, tube-in-tube system, braced frames, CLT cores and outrigger systems.

Due to complications with timber connections, which will be elaborated further on, only structural systems will be assessed where connections can be modelled as hinges. However, CLT-cores are to be assessed in this thesis because of its benefits in terms of accessibility of the core. According to Polastri et al., 2018, the structural performance of CLT-cores mostly depend on the strength of their connections, which is why assumptions need to be made in order to model CLT cores properly.

However, since increasing global stiffness for timber high-rise is less feasible, unconventional structural methods for timber construction should be considered. Tube-in-tube systems for example rely on the collaboration of the stiffnesses of the inner- and the outer tube. For timber high-rise, combining structural systems might offer a solution to overcome challenges regarding comfort levels. For example by combining an outrigger system with an external diagrid system the global stiffness, and thus the comfort levels can be increased. These will be further investigated in the report.

Lastly, when wind dynamics, circular design principles and structural systems are assessed a parametric structural model is made to determine the consequences of different design parameters. By using the model the influence of combined stiffnesses on serviceability levels are assessed while calculating each design alternative on circularity principles.

Much effort is being done in realising comfortable timber high-rise but unfortunately, these designs include non-circular aspects. This thesis aims to make substantiated design recommendations on how to realise timber high-rise while complying to DfX strategies. Also insights need to be given into the effects of design parameters on certain design strategies.

2 THEORY

In this chapter the theory is presented which has been gathered from a literature study. The literature study is performed on timber, high-rise dynamics, structural systems, applicable software and dimensioning methods. With the knowledge gathered from this theory, the structural model can be created in order to do the research in this thesis

2.1 TIMBER

In the general campaign to battle climate change, traditional materials are reconsidered on their carbon footprint and impact on global warming. It has become clear that concrete and steel are highly polluting materials, making it necessary to investigate structural possibilities using other materials. By doing this, better decisions can be made on when to apply which material, considering material properties and embodied carbon. Therefore, it has become needed to investigate biobased materials with a lower carbon footprint on their material properties. Although timber is a weaker material which makes it is less suitable for structural purposes, it is a material that is considered to have a low carbon footprint, as it allows carbon storage (WPMA, 2020).

Carbon sequestration, the process of capturing and storing atmospheric carbon dioxide, happens on a global level. Carbon dioxide (CO₂) is stored in forests and vegetation, in the ocean and in products (such as building materials). Amongst others, the global carbon cycle can be improved by stopping deforestation, planting trees and increasing the application of wood in (durable) construction products. Trees absorb sunlight and carbon dioxide to create wood (Climate Change Committee, 2019). Sustainable use of wood in products reduces the rise in CO₂ levels and therefore also acting as a restraint on the greenhouse effect. Although its depended on the type of wood and the way of sourcing (Van der Lugt, 2012). Each cubic metre of wood holds about a tonne of CO₂ - sequestered from the atmosphere.

An adequate way to compare different materials is to perform a Life Cycle Assessment (LCA). It's a technique to evaluate the lifetime environmental impact of products and materials in a quantitatively. An Life Cycle Assessment takes into consideration all the steps of a material, that lead from raw material, to processing and manufacturing, to the use phase and finally disposal. An LCA does not only calculate the carbon footprint, but many other dimensions, such as eutrophication, human health impact, ozone depletion and more (Ghattas et al., 2016). By doing an LCA, designers can reduce environmental impact by comparing design alternatives to choose the lowest impact ones. This information shall be used in the further analysis of this thesis.

Wood is an organic material, which grows over time with the help of photosynthesis. In this process CO₂ is extracted from the air and the carbon is incorporated into the wooden biomass. If wood does not break down, for example by burning or rotting, the obtained carbon is stored into the wood.

Once wood is prepared to be used for carpentry or as structural elements, wood is considered to be called timber. Timber construction is an effective way of carbon storage since the elements are withhold from burning or rotting (Hafner, A. & Schäfer, S., 2017). As described by Hafner, S. & Schäfer, S. (2017), it is evident that timber construction is a more sustainable alternative. However, from a structural point of view it is also clear that “raw” sawn timber does not nearly compete with steel and, depending on strength classes, narrowly competes with concrete, since its mechanical properties are broadly speaking inferior. Furthermore, because sawn timber can hardly compete with conventional building materials (e.g. steel and concrete), new techniques are being developed to improve the material properties. By studying the strengths and weaknesses of the material, improvements can be made to enhance its performance. For example, in the timber industry the development of cross laminated timber (CLT) and glue laminated (glulam) elements combine properties to battle some of the flaws of “normal” sawn timber.

2.1.1 MATERIAL PROPERTIES

The composition of timber is related due to its organic nature, being built up from cells giving it its hygroscopic and anisotropic properties. Because it is an anisotropic material, timber has different physical properties in different directions. For timber the physical properties depend on the orientation of the cut with respect to the grain, the longitudinal composition of fibres (Blass, H.J., & Sandhaas, C. (2017)). This behaviour of timber is important to consider when designing structures, as it might affect many aspects of the design. Directions employed in timber depend on the orientation of the grain, whereas the longitudinal direction is along the grain axis, other directions include the radial and tangential direction, as can be seen in Figure 2.

In addition, timber is a hygroscopic material, meaning that it is capable of absorbing and exuding water vapor. In practice, moisture contents are continuously adjusted to the surrounding air humidity. Because timber absorbs and exudes moisture, the material will shrink and swell correspondingly.

To illustrate on timber's anisotropic behaviour, the shrinking and swelling in the grain direction is roughly 10 to 20 times smaller than the shrinking and swelling perpendicular to the grain (Eckelman, C.A., 1998). In order to apprehend this phenomenon, Figure 2 should be looked at. The figure shows that at fibre level the grains could be compared to a bundle of straws, making them very susceptible to deformations in tangential and radial directions. Due to the anisotropy of timber, wooden elements might have a high strength in the longitudinal direction while the direction orthogonal to it might be particularly weak. Due to these properties sawn timber has been used for elements loaded in one direction only, for example for beam elements.

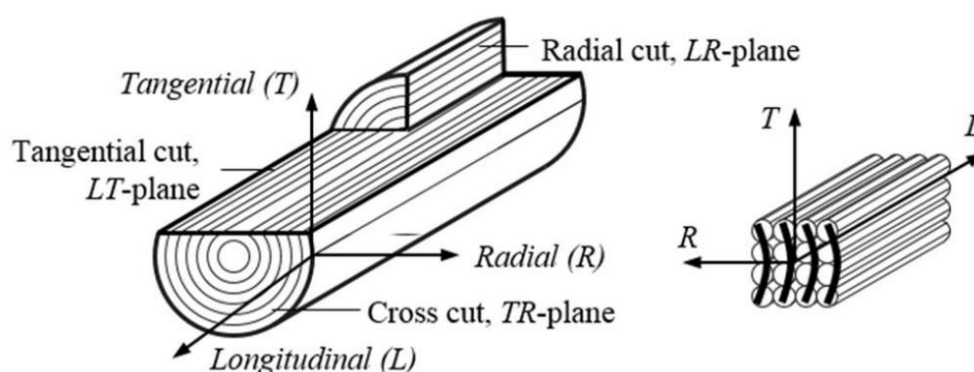


Figure 2: Anisotropy of wood showing the longitudinal, radial and tangential directions on trunk level (left) and fibre level (right) (Ehrhart, T., Steiger, R., & Frangi, A., 2017)

2.1.2 GLUED LAMINATED TIMBER

Glued laminated timber, also known as glulam, is a technique for the homogenisation of wood for its application as a construction material. In glulam, various lamellas are glued together in the same direction, parallel to the grain. By gluing timber elements together, less quality segments of sawn timber can be removed and more homogenic elements can be created. For example, segments like knots or bark ingrowths are removed because of their lower strength. Not only are impurities removed, but also can the assembly be modified. For example, by placing higher grade timber on the outside of the glulam element, and lower grade timber in between. Evidently, by gluing timber lamellae together, element dimensions are not restricted by sawn timber sizes and higher element dimensions can be achieved (Issa, C.A., & Kmeid, Z., 2005).

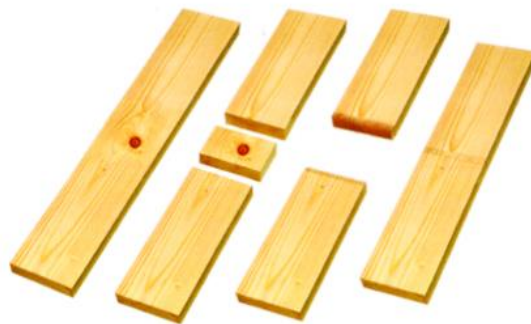


Figure 3: Glued laminated timber

2.1.3 CROSS LAMINATED TIMBER

To understand the benefit of cross laminating timber lamellas (as done in CLT) it is essential to understand consider timber's varying mechanical properties in various directions.

Cross laminating timber layers averages timber properties in cross spanning directions, making timber elements suitable for 2D elements such as walls and floors. Mechanical properties in cross-directions show less variation. In addition, when looking at hygroscopic properties, shrinking and swelling ranges are also flattened out, making them differ less than the case of sawn timber. Also, since CLT elements are load bearing in two directions, it can be said that CLT elements behave like diaphragms.

Due to the fact that for CLT different types of lamellas are cross-laminated, an added value is that less quality wood can be used and combined to obtain superior mechanical performance (Znabei, T., 2020). Although often 3, 5 or 7 layers are cross-laminated, the possibilities are limitless and larger dimensions are possible when cross laminating lamellas. Limitations in dimensions are often set by producers.

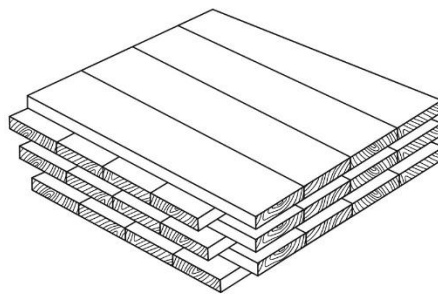


Figure 4: Cross laminating timber layers (side/top view)



Figure 5: Cross laminating timber layers (cross sectional view) (Znabei, T., 2020)

2.1.4 CONNECTIONS

In order to connect all elements it is also essential to investigate timber connections. Connections in timber structures are mostly assumed to perform as hinges or semi-rigid connections because creating a rigid or semi-rigid connection is very complex and expensive. Leichti (1999) states that obtaining true rigidity in a timber connection is unlikely and unwanted. The joint stiffness is a function of both the beam flexural stiffness and the rotational stiffness of the connection and full rigid joints cannot be realised due to stiffness orthotropy. However, it is possible to make moment-resisting joints with 50% rigidity. Lesko (2016) has also studied the behaviour of moment resisting timber connections by using finite element methods to model a joint with both an isotropic and an orthotropic material. Findings from this study are that the orthotropic material had a larger deformation and gave much larger stresses on the steel anchor connection, resulting in the fact that the connection can be seen as moment-resistant but not as rigid. Therefore the connection should be modelled as semi-rigid for orthotropic materials such as timber. Sanner (2017) also mentions that rigid connections in timber should be avoided because of their limited performance and considering that nearly rigid timber connections is also incredibly expensive. In addition to limitations due to rigidity in timber connections, it should also be considered how timber elements are converged in a joint. Creating a joint where many structural elements meet is quite a challenge in timber, this challenge is mostly solved by applying a large steel node to connect all elements. The more elements converge, the higher the complexity and costs of construction, which is why it should, if possible, be avoided to converge too many elements.

2.1.5 TIMBER CALCULATIONS

For timber elements certain calculations should be performed, in order to determine whether chosen element dimensions would suffice strength unity check criteria. This is performed based on the following checks obtained from EN 1995-1-1: Eurocode 5: Design of timber structures and the Dutch National Annex:

Strength checks

1. Tensile utilisation check
2. Compressive utilisation check
3. Bending utilisation check
4. Combined bending and axial tension check
5. Combined bending and axial compression check

And stability checks

6. Flexural buckling checks
7. Shear check

2.1.6 HIGH-RISE

As is described in the research motivation, timber high-rise structures would be highly fit to respond to the demand for an increasing built environment with a responsible and space-efficient strategy. Also, with regard to the housing shortage, timber would be an appropriate building material for its lower construction time due to its degree of prefabrication. Lastly, it is emphasized that circular design principles are extremely relevant and need to be considered during this research.

According to Smith and Coull (1991), high-rise structures are structures where wind or seismic forces are governing for the structural design. This would mean that when serviceability state is applied as the criterium, the building could be considered as high-rise. Furthermore, at this moment there is no leading definition for a certain height to be considered as high-rise. However, the Council of Tall Buildings and Urban Habitat (CTBUH, 2011) stated that the limit for high-rise was at 20 floors, due to the necessity for more advanced vertical means of transport. Although currently the CTBUH does not maintain this definition, since it proposes that buildings can be categorized as high-rise whenever several attributes and requirements are met, in this thesis high-rise structures are defined by buildings with 20 or more floors (Gregoletto, D., & Da Luz Reis, A. T., 2019).

When designing high-rise structures, designs cannot be approached only as static structures, as due to their height, slenderness and exposure to high horizontal loads the structures starts behaving in a dynamic way. The structure will start oscillating at a certain frequency, and the acceleration of the oscillation will determine the comfort level of the buildings occupants.

For high-rise structures, achieving certain comfort levels in terms of structural serviceability is the governing threshold. These serviceability levels include maximum deflections and accelerations combined with natural frequencies. When reducing deflections and the combination of accelerations and natural frequencies, desirable comfort levels of high-rise structures can be accomplished. The accelerations of a high-rise structure depend on the structure's self-weight, global stiffness, height, natural frequency and structural damping. Hurdles appear for timber high-rise because of timber's material properties. Due to the lower stiffness and building mass, it is more complicated to reduce accelerations of timber high-rise structures. Therefore it is a challenge to realize levels of comfort in terms of structural serviceability for timber high-rise structures.

First, the state of the art for high-rise structures is reviewed. For high-rise buildings, different principles determine what is critical for element dimensions. To give an idea, for conventional towers strength is the dominating principle for slenderness up to 1:8, whereas deformation might be dominating up to slenderness ratio of 1:20. For slenderness ratio's higher than 1:20 the "feelable" vibrations, so the dynamic behaviour, is dominating for dimensioning elements (Nijssen, R., 2020). These slenderness ratio's and critical principles apply to conventional towers using concrete and steel structural elements. For timber, a material with a considerably lower stiffness, these ratios are assumed to be lower.

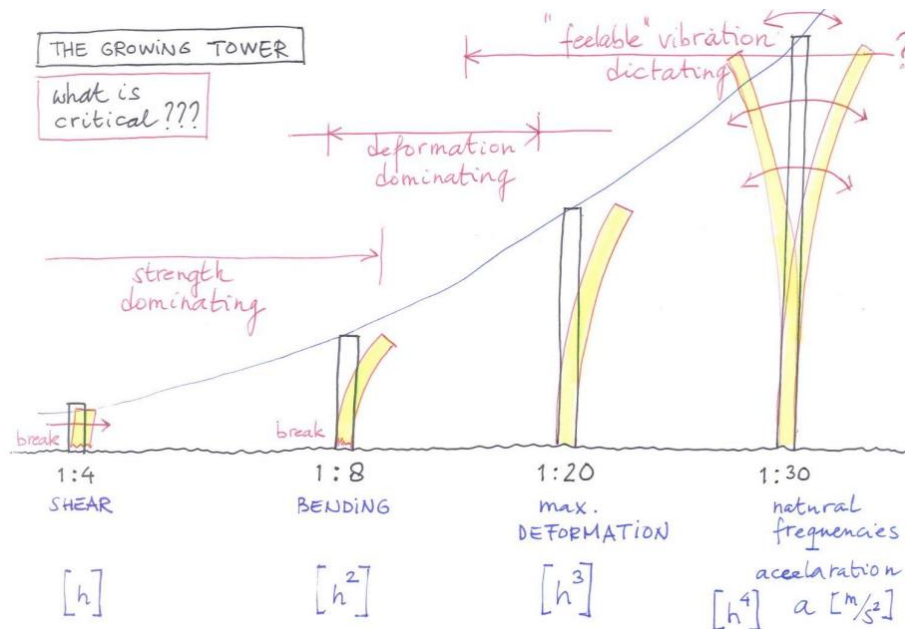


Figure 6: The growing tower (Nijse, R., 2020)

Consequently, the structure's acceleration does not solely depend on the material's stiffness; geometry and structural systems affect a building's global stiffness, which also has an influence. A higher global stiffness could reduce accelerations and therefore improve comfort (Green, 2012). For increasing global stiffness in timber high-rise structures it is recommended to first look at relevant case studies, to analyse which structural systems have been applied and with what effects, taking the scope of this thesis into consideration.

One of the objectives in this Master's thesis is to determine the influence of parameters on accelerations regarding structural dynamics. This will help in answering research question:

"What influence do parameters have on high-rise serviceability levels?"

In order to be able to answer this question, basics of wind dynamics need to be understood. By learning the Eurocode standards with Covenant Hoogbouw as a reading Guide general knowledge is gathered on structural, wind induced dynamics (Eurocode 1, 2010) (Covenant hoogbouw, 2012).

Figure 7 shows evaluation curves for the relation between accelerations and eigenfrequencies. As can be seen in the figure two evaluation curves are shown. The first curve represents serviceability limits for office buildings, the second curve represents residential buildings. For buildings to meet serviceability requirements, the relation of the eigenfrequency to the acceleration should be below the curve.

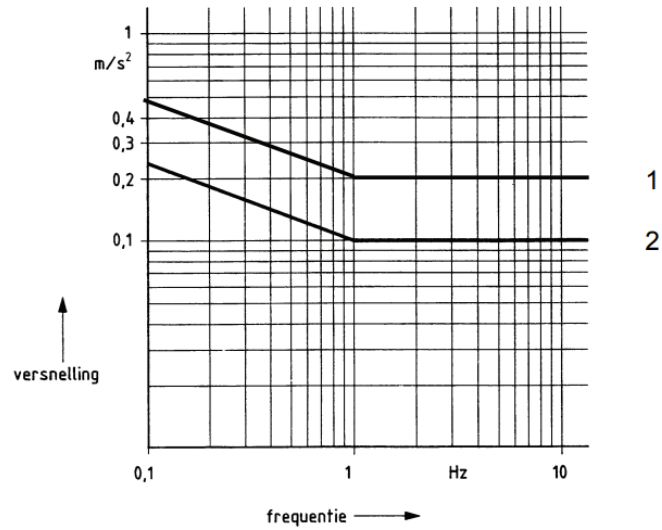


Figure 7: Evaluation curves for horizontal wind induced vibrations in a high-rise building (Convenant hoogbouw, 2012)

According to Figure 7, the combination of eigenfrequency and acceleration determine whether a building complies to serviceable requirements. Therefore, accelerations and eigenfrequency's need to be properly understood and computed. In the following paragraphs more insights are given on accelerations and natural frequency.

2.2 INFLUENCE PARAMETERS

When evaluating parameters for structural dynamics it is clear which parameters adjustable for lowering the building's accelerations. Figure 8 below shows in red which parameters are adaptable and in black what other factors are influenced by it. Building geometry, system configuration and material properties determine how the structure behaves dynamically. Superimposed mass is also shown in a red box since it is highly influential and could, if the accelerations are much higher than allowed, be added later on.

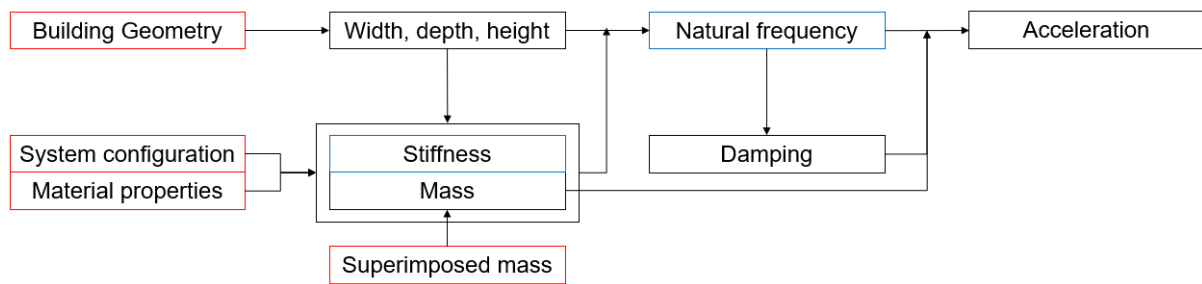


Figure 8: Parameters for structural dynamics (adaptable parameters in red)

2.2.1 EIGENFREQUENCY

Eigenfrequency, also known as natural frequency, is the frequency of oscillations of a system when damping forces are absent (College Physics, 2012). As mentioned in section 2.1.6, the relationship between the acceleration and the natural frequency need to be below certain service lines to guarantee serviceable high-rise buildings. In addition, the acceleration also depends on the structures eigenfrequency. Determining a structure's eigenfrequency can be challenging, there are various ways to estimate the actual frequency.

According to Eurocode 1, the natural frequency can be estimated with:

$$n_{x,1} = \frac{46}{h}$$

Equation 1: Natural frequency (Eurocode 1)

h is the building height [m]

However, this is an estimation for concrete and steel structures meaning that when timber structures are assessed this estimation is much too inaccurate. Smith & Coull, 1991 propose a more accurate estimation:

$$n_0 = \frac{1}{2\pi} \left(\frac{g * \sum F_i u_i}{\sum W_i u_i^2} \right)^{1/2}$$

Equation 2: Natural frequency (Smith & Coull, 1991)

g is the gravitational acceleration

F_i is the equivalent lateral load at the floor levels

u_i is the calculated static horizontal deflection at level i

W_i is the weight of the floor i

Disadvantageous of this approach is that it can only be used when preliminary design is made and the stiffness, and thus the deflections are known. Depending on whether the structure acts in bending or in shear the natural frequency changes. Smith & Coull, 1991 did not consider it in their approximation. However, Van Oosterhout, 1996, did take that into account with a more accurate estimation:

$$n_{1,x} = f(\alpha h) * \sqrt{\frac{q_w * h}{\mu * \delta_{max}}}$$

$$\alpha^2 = \frac{(GA)_{tot}}{(EI)_{tot}}$$

Equation 3: Natural frequency (Van Oosterhout, 1991)

q_w is the uniformly distributed horizontal load due to wind

h is the height of the structure

μ is the mass distribution over height

δ_{max} is the maximum lateral horizontal displacement

$$0 \leq \alpha h \leq 1$$

$$f(\alpha h) = \sqrt{\left[\frac{0.3131}{(\alpha h)^2} + 0.1148 \right] * \left[\frac{-1 - \alpha h * \sinh(\alpha h) + \cosh(\alpha h)}{(\alpha h)^2 * \cosh(\alpha h)} \right]}$$

$$\alpha h \geq 1$$

$$f(\alpha h) = \sqrt{\left[\frac{0.2365}{(\alpha h - 0.3)^{1.22}} + \frac{1}{16} \right] * \left[\frac{-1 - \alpha h * \sinh(\alpha h) + \cosh(\alpha h)}{(\alpha h)^2 * \cosh(\alpha h)} + \frac{1}{2} \right]}$$

Equation 4 Determination of $f(\alpha h)$ (Van Oosterhout, 1991)

Both for Smith & Coull as for van Oosterhout's formulas the deflections and stiffnesses can be found with the following formula:

$$\delta_{bending} = \frac{q_w * H^4}{8 * (EI)_{eff}} \text{ and } \delta_{shear} = \frac{q_w * H^2}{2 * (GA)_{eff}}$$

Equation 5: Deflection and stiffness (Smith & Coull, 1991)

Lastly, natural frequencies can also be found using finite element modelling software, such as Oasys GSA. With this software, modal analysis can be performed, by which natural mode shapes and frequencies are determined. The eigenfrequency calculation using FEM software is considered to be the most accurate compared to abovementioned alternatives. Moreover, if finite element analysis is being done, truthful results can be collected on the structure's stiffness and deformation. Whereas the earlier mentioned alternatives are approximations where stiffnesses and deformations should be known. Since this thesis will focus on dual structural systems, determining stiffnesses and deformations might be too complex. Therefore by doing the entire analysis in FEM software, the most accurate results can be collected. In this thesis FEM software will be applied, both for finding the building's stiffness as for doing the modal analysis to find corresponding natural frequencies.

2.2.2 ACCELERATIONS

This paragraph describes the principles of accelerations in structures. There are three types of building accelerations identified which are governing for certain cases. These accelerations are wind induced and their direction is relative to the wind direction. Hence, the accelerations are:

1. Along-wind, accelerations in the same direction of the wind load
2. Cross-wind, accelerations in the transverse direction of the wind load. Caused by vortex shedding
3. Torsional, accelerations of rotation along an internal axis

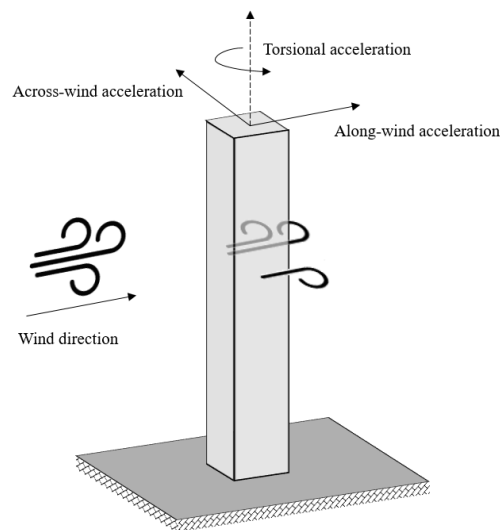


Figure 9: Figure showing wind induced acceleration directions

Important for the acceleration of a building are human perception levels of these accelerations. Smith and Coull (1991) set up Table 1 below. The design of a building based on dynamic behaviour is thus determined by the serviceability of the structure, if large accelerations occur this might influence the building's occupants. To avoid residents becoming seasick on the top floors, evaluation curve 2 (the threshold for residential buildings) is set to the 90% level of perception probability. Exceeding the curve would not be a "make or break" scenario, however it should be pursued to satisfy the threshold.

Range	Acceleration [m/s ²]	Effect
1	<0.05	Humans cannot perceive motion
2	0.05–0.10	Sensitive people can perceive motion; hanging objects may move slightly
3	0.1–0.25	Majority of people will perceive motion level of motion may affect desk work long-term exposure may produce motion sickness
4	0.25–0.4	Desk work becomes difficult or almost impossible ambulation still possible
5	0.4–0.5	People strongly perceive motion difficult to walk naturally standing people may lose balance
6	0.5–0.6	Most people cannot tolerate motion and are unable to walk naturally
7	0.6–0.7	People cannot walk or tolerate motion
8	>0.85	Objects begin to fall and people may be injured

Table 1: Human perception levels and corresponding building accelerations (Smith and Coull, 1991)

2.2.2.1 ALONG-WIND ACCELERATION

Along-wind accelerations are the accelerations of the excitations in the same direction as the wind loads. These excitations result from frontal wind loads on the building's façade.

$$a_{along}(y, z) = \sigma_{a,x}(y, z) * k_p$$

Equation 6: Along-wind accelerations

$\sigma_{a,x}(y, z)$ standard deviation of the characteristic along-wind acceleration

k_p is the peak factor

Complete calculations of the standard deviation and peak factor for Equation 6 can be found in Appendix B. When analysing the parameters used for calculating along-wind accelerations it can be seen that there are environment-dependent parameters such as air density and wind velocities and building-dependent parameters. Building dependent parameters include building measurements, damping coefficients, mass distributions and most importantly natural frequencies.

2.2.2.2 ACROSS-WIND ACCELERATION

Across-wind accelerations are accelerations in the transverse direction of the wind load. Across-wind excitations occur due to vortex shedding. Shed vortices occur because wind streams pass the building which causes the flow to revolve around it. Vortex shedding is a periodic process where the vortices alternate each other from both the building's sides. The vortices create alternating low pressure zones which enable the building to shift, and thus accelerate in the direction of the vortices. Since vortices occur on both sides of the building the building will move in the transverse direction with respect to the wind load. Wind velocities, building shape and size influence vortex shedding and the across-wind accelerations that are caused by it (Kwok et al., 1982).

According to Covenant Hoogbouw, 2012, vibrations in across-wind direction are significantly smaller than along-wind vibrations. And therefore across-wind accelerations don't need to be calculated. Eurocode 1, 2010 mentions that the effect of vortex shedding does not need to be investigated when:

$$v_{crit,i} > 1.25 * v_m$$

Equation 7: Pre-requisite for neglecting across-wind accelerations (Eurocode 1, 2010)

$v_{crit,i}$ is the critical wind velocity for mode i

v_m is the characteristic 10 minutes mean wind velocity

Additional approaches for determining the across-wind accelerations can be found in Appendix C.

2.2.2.3 TORSIONAL ACCELERATIONS

As mentioned above, torsional accelerations are accelerations of the movement of the building along an internal axis. Torsional vibrations are caused by uneven load distribution on the building's façade, affecting parts of the building to displace more relative to other parts, causing rotation. To calculate the torsional accelerations the torsional eigenfrequency $n_{1,t}$ needs to be determined together with the torsional mode shape constants. Unlike along-wind accelerations both mode shape variations along the horizontal and the vertical axes have linear distributions. Resulting in the following mode shape constants:

$$G_y = 3/8, G_z = 3/8, K_y = 3/2, K_z = 3/2$$

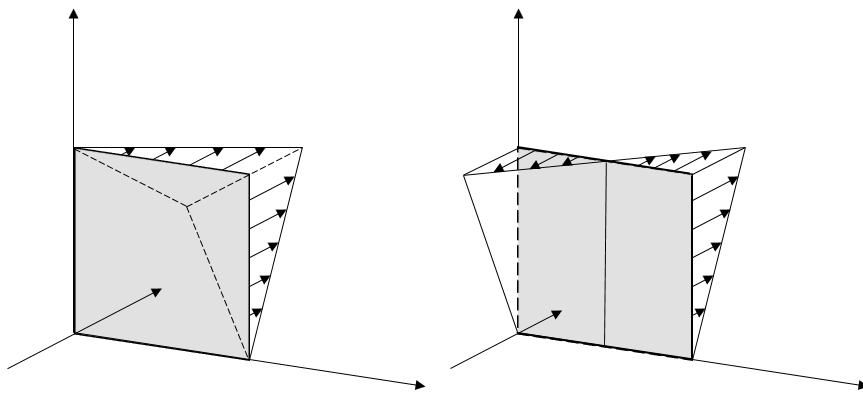


Figure 10: Linear distributions along the horizontal and vertical axes for both mode shape variations

2.2.3 DAMPING

The damping of a structure is the decrease of the amplitude the structure's vibrations. Damping reduces the wind induced or seismic effect by dissipating the energy transferred through the building. Although damping has a complex physical nature, it is known that there are three types of damping: material damping, non-material damping and damping through material devices such as tuned mass dampers. The latter is not applied in this thesis as it is regarded to be out of scope.

Material damping is a type of damping that occurs in each material, and is the result of small deformations due to altering loading. Non-material damping is caused by the interaction between structural elements, this type of damping depends on the amount and type of connections. For example, when slip is allowed in timber connections, dynamic energy is absorbed by the structure, making the slipped connections serve as a form of additional damping. For timber high-rise, structural damping varies from 0.64 to 2.7%, depending on the type of structure, connections and finishing of the building (Feldmann, H., 2006).

2.2.4 FORCE COEFFICIENT

The force coefficient (c_f) is a factor that largely affects the along wind acceleration of a timber structure, as shown in Equation 46, Appendix B. The force coefficient depends on the shape of the structure, determining the engagement of the wind pressure to the structure. As shown in Figure 11, each floorplan shape corresponds to another force coefficient, resulting in a 75% higher coefficient for a rectangular structure compared to a circular structure.

Gebouwworm ^a	c_f^b
Rechthoek, $d/b < 0,2$	1,40
Rechthoek, $d/b = 0,7$	1,68
Rechthoek, $d/b = 1$	1,47
Rechthoek, $d/b = 2$	1,15
Rechthoek, $d/b = 5$	0,70
Rechthoek, $d/b > 10$	0,63
Cirkel	0,84
Hexadeca (16 hoeken)	0,84
Dodeca (12 hoeken)	0,91
Deca (10 hoeken)	0,91
Octa (8 hoeken)	1,02
Hexa (6 hoeken)	1,12
Penta (5 hoeken)	1,26

^a Voor tussenliggende waarden van d/b kan c_f door lineaire interpolatie worden bepaald.
^b Voor verschillende aanstroombindingen kan een andere waarde voor c_f worden gevonden.

Figure 11 Force coefficients (Convenant Hoogbouw, table 2, 2012)

2.2.5 SHEAR LAG

Many tall buildings, mostly framed tube systems, are susceptible to the shear lag effect. The shear lag effect is a nonlinear distribution of axial stresses due to lateral loads occurring over the perimeter of the building at its foundation. The expected stress distribution without shear lag effect could be compared to the stress distribution of a cantilevered beam with a hollow cross-section. In the case of a hollow cantilevered beam the stress distribution would be linear to the beam location, as shown in Figure 12. Lastly, it needs to be taken into consideration when evaluating the shear lag in a diagrid structure, that the diagrid angle should not exceed 70° . Else, shear lag will not be reduced (Kim and Lee, 2010).

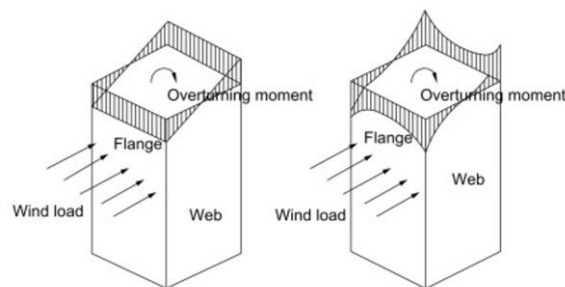


Figure 12: Axial stress distribution in the columns of the building in web as well as in flange panels (Fu, 2018)

2.3 STRUCTURAL SYSTEMS

To realise timber-only high-rise structures it is critical to evaluate alternative structural systems as creating some systems with timber elements will generate many complexities, and therefore be unrealistic alternatives. Structural systems for high-rise buildings can be classified into two categories (Thanh Dat et al., 2017): interior structures and exterior structures. To discover which systems might be suitable for timber only realisation, this chapter starts with covering case studies. From the case studies on, possible systems are elaborated on and discussed.

2.3.1 CASE STUDIES

The first case that is evaluated is the case of Brock Commons Tallwood House in Vancouver, Canada. In this timber high-rise project a hybrid structure has been applied, where a concrete core has been combined with mass timber floors and panels (Staub-French et al., 2020). Although this project realised 18 stories and 53 meter in height, using a concrete core does not conform the design for disassembly principle and therefore case studies with a concrete core will be disregarded in this research.

When discounting cast in situ concrete structural systems, non-hybrid timber high-rise is looked into. For example in Brumunddal, Norway where the Mjøstårnet has been constructed. The structures stiffness has been realized by large scale glulam trusses, transferring horizontal loads to the buildings foundation (Abrahamsen, 2017). Also with 18 stories but 85 meter, Mjøstårnet is the highest timber building in the world. Because the structural system is entirely constructed with timber elements, this results in very large cross-sectional elements with dimensions of the corner elements up to 1485 x 625 mm², resisting axial loads of 11500 kN.

Although the structural system does not contain any concrete, concrete has been applied on the 7 top floors to increase the weight of the structure. By adding concrete to the floors, the building's weight increases which reduces accelerations and conforms buildings comfort levels. However, in the case of Mjostarnet, top floors still do not satisfy the dynamic threshold, but in consultation with the client it was agreed that the perception levels would be acceptable. Pouring concrete on timber floors might be a solution for ensuring comfort, however, it does not conform circular principles such as design for disassembly and design for material efficiency. In terms of disassembly, it is not possible to properly strip the poured concrete from a timber floor, making it unsuitable for disassembly. Also, in terms of material efficiency it does not seem effective material use if concrete is added just for adding mass to the structure's top floors. If these circular principles are to be taken into account in the design, systems should be developed where adding (non-structural) mass to the structure should be avoided.

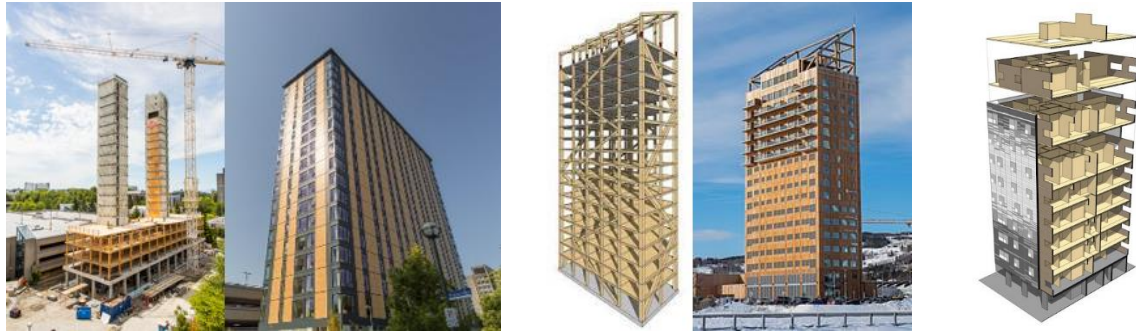


Figure 13: Brock Commons Tallwood House during construction and finished (left), Mjøstårnet during construction and finished (middle) & Stadthaus rendered

Moreover, another case for timber-only high-rise that needs to be assessed is the Stadthaus in London, United Kingdom. The Stadthaus is a 9 stories high tower that makes use of CLT shear walls as its stabilising structural system. For every wall in the floor plan CLT walls have been applied, which act as shear walls in their respective transverse directions. By using many shear walls, a structure with a high global stiffness, and thus acceptable accelerations, is realised. Stadthaus in London complies to serviceability requirements regarding (wind induced) comfort levels. Unfortunately, the design strategy of applying a high amount of shear walls does not conform the last circular principle; design for adaptability. By achieving structural stability with shear walls, the floor plan is locked in the sense of adaptability. With these type of structural systems adapting floor plans is impossible and, if a different layout is desired it is not possible to adjust the floorplan without mayor renovations.

To stay within boundaries of the abovementioned circular principles, comfort levels for structural serviceability of efficient, adaptable, demountable high-rise structures will be researched. By complying to circular principles, challenges for comfort levels emerge with regard to the building's accelerations, more specific concerning mass and global stiffness. These obstacles need to be faced with timber structural solutions.

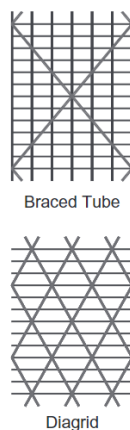


Figure 14: Braced tube and Diagrid

When looking at potential and feasible structural systems that are within the predetermined circularity boundaries and buildable with timber, it is clear that systems where diagonal elements are applied in the façade are most compelling. For timber structures, this theory is consistent with the information found in chapter 2.1.4 on connections. Structural façade active systems that are incorporated in this thesis are the diagrid and the mega frame. Both effective systems, because the majority of the forces are taken by axially loaded façade elements. According to Merza and Zangana (2014) axial loading is the most efficient method of load transfer. Major difference between the mega frame and the diagrid is the presence/absence of columns, influencing element dimensions and grid densities. Both properties are influenced by each other, the horizontal (wind) load and vertical load transfer.

Further systems that are considered in this thesis are core active systems, because a collaboration of structural systems might offer solutions for timber high-rise. In addition, it is most probable that high-rise structures will need a way of vertical transport, suggesting that space for a core active structural system will be present. However, it must be said that timber core systems are far from common practice. In this thesis a CLT core is considered, since it is the most common of timber core techniques and some literature is available. Further timber core systems that are considered are the braced frame and an outrigger structure. Braced frames are hardly used for high-rise, but the efficiency of the system makes it worth investigating. Just like the system would be applied in the façade, a braced frame could be a probable system for the core of the building. Lastly, outrigger are also investigated for it is an efficient structural system which is applied for tall to super tall buildings and it is realisable with timber only elements.

2.3.2 DIAGRID

The diagrid structure is known for its sole use of diagonal elements and beams in the structure's façade. Whereas most high-rise structures would mostly use columns and beams for vertical load transfer and an additional system for horizontal load transfer, the diagrid system discards orthogonal columns for vertical load transfer. Instead, the diagrid elements act like inclined columns and bracings simultaneously. The diagrid system is also an efficient structure, because the elements are predominantly loaded axially, minimizing shear deformation (Moon, 2007). Therefore, deformation behavior of a diagrid is assumed to be similar to that of a cantilevered beam, as also assumed in the studies of Fang, D. & Liu, C. (2021). The elements carrying shear by axial action indicates that minimal moment resistance is required in the connections, making it a useful structure to be realized with timber elements. In addition, studies have shown that diagrid structures have higher material utilization and are applicable for taller structures, which is why the diagrid system is to be assessed in this thesis (Liu, C. et al (2017)).



Figure 15: Example of the diagrid structure (Moon, 2007)

The diagrid can be qualified as a space truss system combined with a tubular system, providing both bending and shear rigidity. However, diagrid structures are less susceptible to shear lag than tubular systems, since the diagonal elements “even out” the load distribution over the perimeter (Kim and Lee 2010). Figure 16 and Figure 17 show the shear lag effect for a tubular and diagrid structure. Notable is that the shear lag effect of diagrid structures is remarkably less along the flange and more fluently distributed over the web side, suggesting higher in-plane shear stiffnesses for diagrid structures compared to tubular structures. This is in agreement with the knowledge that axially deformation generally has a higher stiffness than flexural deformation. The higher the diagrid angle, the more the diagrid elements become vertical oriented and behave like columns. To minimize shear lag effect the diagrid angle should not exceed 70° (Kim and Lee, 2010).

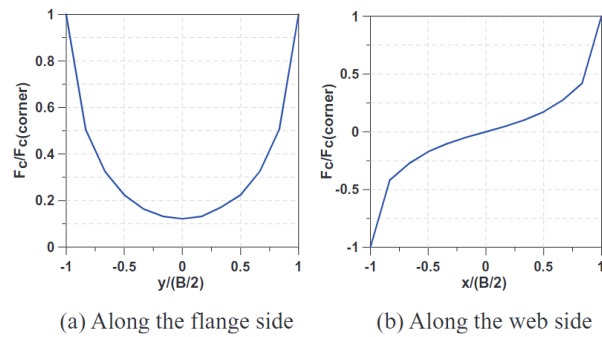


Figure 16: Shear lag effect of the tubular structure (Kim and Lee, 2010)

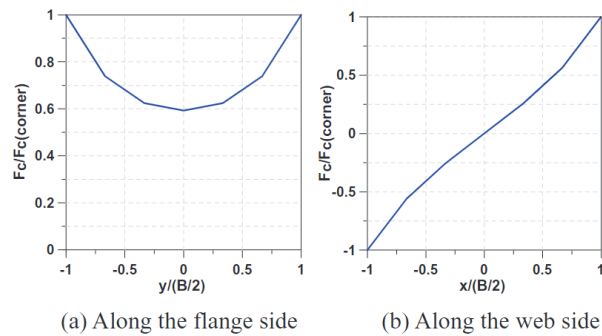


Figure 17: Shear lag effect of diagrid system (67.4 degree) (Kim and Lee, 2010)

2.3.3 MEGAFRAME

A mega frame, also known as a truss-braced structure applied on large scale, is a structural system where beams, columns and diagonal bracings are applied. In this system, the beams and columns are used for gravitational load transfer and the bracings for transfer of lateral loads. Unlike a diagrid structure, the bracings are not involved in gravitational load transfer. Because of this, columns are present in the structure's façade and the density of brace elements can be highly reduced. As an illustration, one bracing can be sufficient for resisting lateral load. This would mean that the element would span over multiple floors and large parts of the façade, as is the case for Mjøstårnet (see Figure 16). In-plane shear stiffness is also realized by axially loaded brace elements, making a mega frame efficient and realizable with timber only elements.

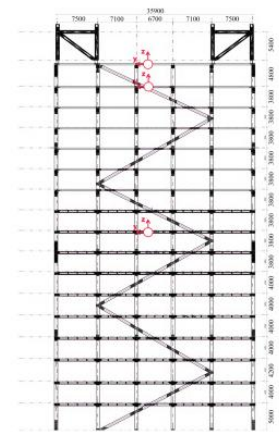


Figure 18: Case for Mjøstårnet - one bracing for resisting lateral load (Abrahamsen, 2017)

Characteristic for a mega frame is the deformation based on the systems compounds. Flexural deformation is caused by axial strain of the columns and shear deformation is generated by axial strain of the braces and beams in the structure. For the mega frame strain could be either lengthening or shortening. Figure 17 displays this principle well, for different deflections correspond to shear and flexural deformation. For mega frames, both deformations need to be considered. A combined deformation can be seen in Figure 17 (Smith and Coull, 1991).

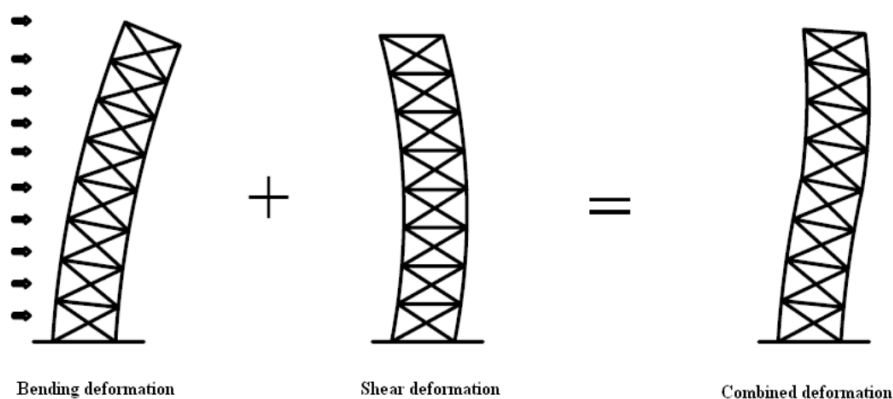


Figure 19: Shear and flexural deformation (Smith and Coull, 1991)

2.3.4 CORE SYSTEMS

A core system is a structure system that, in contrary to a perimeter structure, is located at the core of a building. Core structures are most commonly created in concrete but alternative designs with steel elements are also occurring. For a concrete core, the general idea is that the core would act as a vertical cantilevered beam, withstanding lateral loads through its flexural stiffness and being able to resist large bending moments at its supports. Steel cores act like a truss-braced structure which has been elaborated in section 2.3.3.

For high-rise, a core does not solely have a structural purpose, as it might also offer a vertical passage through every floor. This vertical path is obviously interesting for vertical transport, and it is very often the position where stairs and elevators are located. Not only the vertical passage, but also its centered location makes a core very suitable for stairway and elevator location. In addition, it is also found in Equation 8 that core dimensions are governed by its capacity for vertical transport (Arup, 2022). A general estimator function used at Arup (2022) references that core width and depth are depending on the building height:

$$width = depth = \frac{height}{10}$$

Equation 8: Core dimension estimator function (Arup, 2022)

Lastly, it is also possible to improve the structural core's performance by incorporating an outrigger structure in the design. By applying an outrigger, one or multiple very stiff floors will be computed which activate vertical elements in the perimeter of the building to help resist lateral deflections.

For realizing core systems with timber elements, it is important to consider which system can or cannot be reproduced with timber. As is the case with timber, the majority of complications are in the connections of the elements. In this thesis a timber braced core, a CLT core and the combination with outriggers will be assessed.

2.3.4.1 BRACED CORE

The braced core researched in this thesis is a timber braced frame, located in the center of the structure. Braced frames are built up by a timber frame, connected with a timber diagonal element, which braces the frame structure (Figure 20). This bracing enables the system to have lateral stability, as the frame becomes a shape retaining system. Also, due to the application of the braces, large horizontal loads can be withheld without moment resisting connections. Instead, loads are transferred through axial loading, making it an efficient system that is suitable to be built in timber.

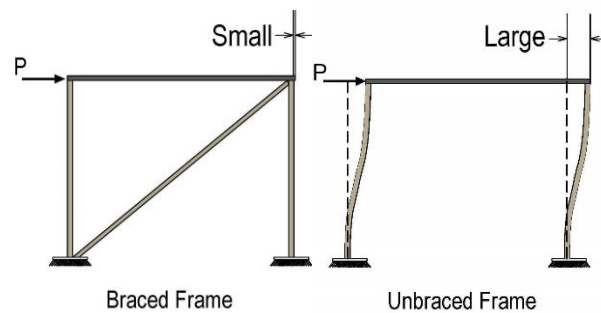


Figure 20: Braced and unbraced frame (Patil, Naringe, & Rama, 2018)

2.3.4.2 CLT CORE

The CLT core is an interior system that acquires stiffness through the shear wall behavior of a CLT panel. Two or more CLT walls are located orthogonally to the loaded direction, carrying bending moments through the façade. Just like conventional, concrete cores, a CLT core is designed as a stiff tube with high bending and shear stiffnesses. However, these properties are limited by CLT core connections, which are governing for the capacity of such a system. Modelling of the CLT core's is explained further on in this thesis, in section 3.1.3.3.

2.3.5 OUTRIGGER

An outrigger system is a truss system that serves as a lever arm, connecting the core of a structure to its perimeter. The ends of the outrigger are supported by columns, through which axial loads are transferred when the outrigger transfers overturning moments. The columns are either loaded in tension or compression, depending on the column's location with respect to the wind direction. Bending moment of the core of the structure is reduced by placing one or more outriggers, as the stiff outrigger transfers overturning moments to the columns in the façade, as can be seen in Figure 21. It is an efficient structural system for high-rise as it increases the moment capacity of the interior system, making it suitable for high-rise structures.

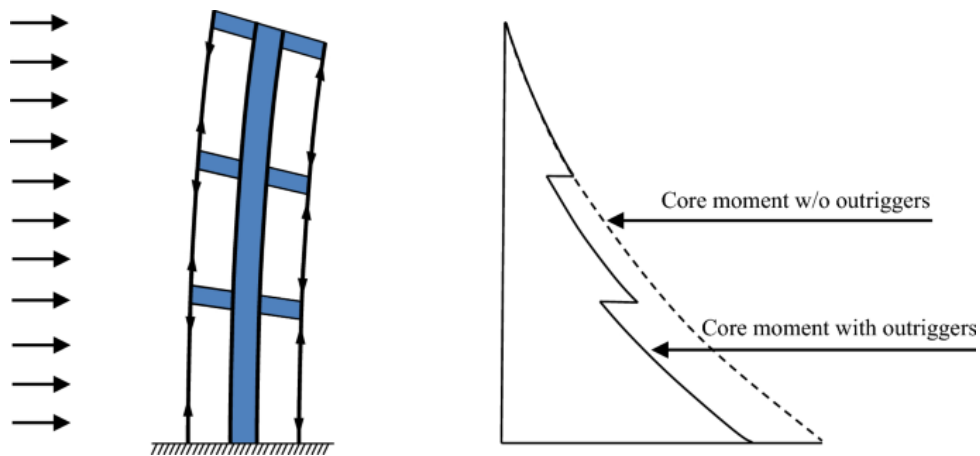


Figure 21: Schematic drawing of an outrigger system (Vasseghi, A. and Khoshkalam, V., 2020)

2.4 SOFTWARE

In this thesis, several software is required in order to generate results necessary to be able to answer the research question. To research the possibilities for dual structural systems in timber high-rise, a variant study is to be performed. Large variant studies can best be modelled with the help of parametric software, such as Grasshopper. Grasshopper is a visual programming software that runs on Rhinoceros 3D. Advantages of Rhino and Grasshopper are the numerous plug-ins that are developed, allowing additional extensions to be made for this software. For example, timber calculations are incorporated into the model using Arup Compute, a plug-in that performs engineering calculations in the cloud.

Another essential plug-in used in this thesis is Geometry Gym, allowing the geometry created in Grasshopper to be transferred to a Finite Element Modelling software, such as Oasys GSA. By analysing the geometries created in Grasshopper with GSA, more complex and comprehensive calculations can be made, including calculating the natural frequency (as explained in section 0).

Results from GSA are retrieved by Geometry Gym and saved by another Grasshopper plug-in called Colibri. Allowing automatic iterations to be made in Grasshopper and saving requested outputs into an Excel file. All software can be managed from Grasshopper, which is the main location where the models are constructed.

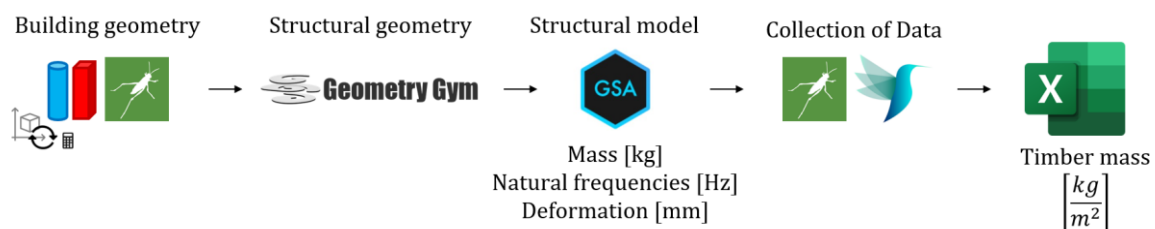


Figure 22: Workflow required software

2.5 DIMENSIONING METHODS

As stated earlier, alternative systems and their configurations can only be compared if ultimate and serviceability states of the building are within acceptable thresholds. The previous chapter described these acceptance levels, whose purpose is to quantify the building's behaviour. In order to have alternative models suffice to the same criteria, sizing of elements should be sized for each specific case. In general, there are two main approaches for finding appropriate dimensions in this parametric model:

1. Element optimisation
2. Brute force method

Element optimisation would consist of a script with an iteration based optimisation focused to reach a pre-set target value. As an illustration, a parametric model with a target value of 0.9 would iterate, evaluate result and re-iterate to be able to reach a value of 0.9. Setting up such a script would require a looped workflow, allowing iterations to be assessed and alternatives to be recalculated, oftentimes with an incorporated maximum of iterations. Although the creation of such a model might be more complicated, general practice shows that it is a quick and "smart" solution for finding optimum values. This type of solver would require less computational power but it is deemed that more knowledge is prerequired, in order to avoid local maxima and minima. Beneficial from this approach is that with less calculation time highly detailed results can be found. This is due to the fact that the solver aims to optimise its result until satisfied, discarding unsuitable alternatives.

Using an optimisation solver is the opposite approach to the brute force method, where the solver would step-by-step calculate each alternative. The brute force method is considered to be a simple solver since there is no processing of calculated values, meaning that also highly unfeasible dimensions are calculated. In addition, brute force calculations are extremely time consuming, whereas the duration has a linear relation to the accuracy of the outcomes. Ten times the accuracy equals ten times the time consumption.

Although it would be ideal to incorporate an optimising solver for finding optimal element dimensions, complications arise when optimisation is done for multiple configurations. Complications arise when Grasshopper and Colibri are used to run optimisations consecutively, i.e. after one configuration is optimised the model records the (optimised) data and starts optimisation for the next design. Due to the linear nature of Grasshopper, there are limitations when building nested loops in the model, especially using the Colibri plug-in. Barriers for creating nested loops for element optimisation makes it necessary to reject this alternative for approaching correct element dimensions.

The brute force method proposes an alternative to the -not achievable- optimisation solver. However, when brute force is considered, it is important to examine the design space first. The design space consists of all possible solutions of the designs, so multiplying each variable range by each other, summing up to a total quantity of results resembling each possible outcome. Variables in the design space are the same variables discussed previously, with an additional variable for element dimensioning. Element dimensioning could, for the tallest structures, be up to 4 times the size of an element sized on strength only. However, having element cross-sections sized as 1 to 4 times the dimension on strength would be a much too rough estimate. Therefore, the accuracy needs to be increased by narrowing down the interval within the dimensioning range. To make an estimation of the accuracy that would be required, the cross-section library of Hasslacher Norica Timber (Hasslacher Group, 2022), an Austrian timber producer, is reviewed. On average, element dimensions increase by 10% per type of profile, making it sensible to set the dimensioning interval to 0.1. The design space for the circular diagrid system is shown below, assuming a dimensioning interval of 0.1.

Circular Diagrid			
Variable	Range	Interval	Total
Horizontal segments	4 – 7	1	4
Vertical storey span	1 – 4	1, 2, 4	3
Height	60 – 148	3	24
Interior systems	CLT – BC – Outrigger	1	3
Dimensioning factor	1 – 4	0.1	40
Total	$4 * 3 * 24 * 3 * 40$		46080

Table 2: Design space circular diagrid.

Now for the circular diagrid only the design space would have 46080 alternatives. Calculated at ± 1 minute per iteration it is estimated that it will take 768 hours or 32 days to calculate. For the complete thesis not only the circular diagrid is assessed, also the circular megaframe and rectangular diagrid and megaframe need to be computed. All together this would sum up the total calculation time to 128 days if all calculations are performed flawlessly. In this thesis, a method has been developed to make the brute force method faster without compromising on result accuracy. The process applied in this thesis is explained in section 3.3.2 and in Appendix E.

3 STRUCTURAL MODEL

In this section the creation of the structural model is further explained. The model is created as such that a large variety of configurations can be generated and eventually compared. Each section in this chapter will focus on a segment of the parametric model, which have the workflow described in section 3.1 in common. Structural models are generated for each structural system and floorplan combination, meaning that 16 different alternatives are created:

Diagrid system

1. Rectangular Diagrid
 - a. Cross Laminated Timber core
 - b. Braced core
2. Rectangular Diagrid outrigger
 - a. Cross Laminated Timber core
 - b. Braced core
3. Circular Diagrid
 - a. Cross Laminated Timber core
 - b. Braced core
4. Circular Diagrid outrigger
 - a. Cross Laminated Timber core
 - b. Braced core

Megaframe system

5. Rectangular Megaframe
 - a. Cross Laminated Timber core
 - b. Braced core
6. Rectangular Megaframe outrigger
 - a. Cross Laminated Timber core
 - b. Braced core
7. Circular Megaframe
 - a. Cross Laminated Timber core
 - b. Braced core
8. Circular Megaframe outrigger
 - a. Cross Laminated Timber core
 - b. Braced core

Besides the variables that are to be discussed in each section, the prime variable for high-rise will be present in each set of configurations: the height of the structure. In this thesis the structure will be analysed over 7 different heights. Starting at 20 floors and ending at 48 floors, with steps of 4 floors at the time. With a fixed floor height of 3 m it results in a height range of 60 m to 144 m, with steps of 12 m. The workflow of the building geometry can be seen in Figure 23. First, the building geometry is defined, describing which shape, exterior and interior systems and whether an outrigger has been applied.

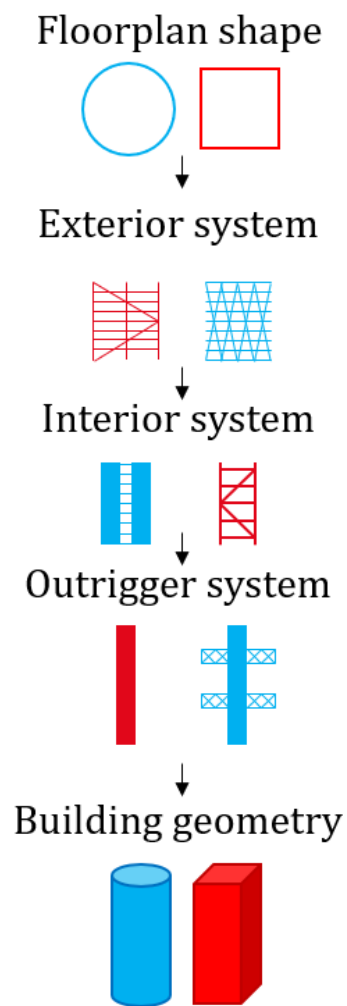


Figure 23: Organisation of the building geometry

3.1 GEOMETRY GENERATION

3.1.1 FLOORPLAN SHAPE

3.1.1.1 CLT FLOORS

When creating the parametric model, it is important to make assumptions for modelling the floor systems. The floors behave like semi-rigid diaphragms, transferring lateral forces from one end of the floor system to the other Ashtari (2012). For example, from the façade, which is susceptible for wind loads, to the structure's core. For doing the study on dual structural systems, it is needed to assess the material properties of the floor system, as it affects the diaphragm action and thus the collaboration between dual structural systems. Unfortunately, since the floors behave like semi-rigid diaphragms, the floors can translate, rotate and also deform, decreasing the diaphragm action and thus the cooperation of dual structural systems. As mentioned earlier, for timber and CLT elements it is important to look at the orientation of these elements, including the floor systems. Figure 24 shows the orientation of the floors, as assumed in the model. However, for the ease of modelling the structure, a few assumptions are made on modelling CLT floors in this study.

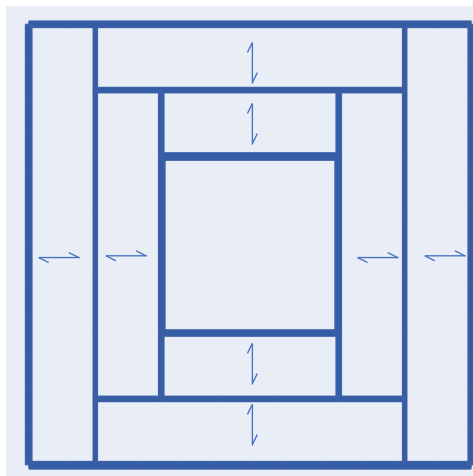


Figure 24: Floor orientation, assumed by model

1. Isotropic CLT properties

Just like the CLT core, the floor systems are modelled as 2D elements without considering element orientation. Floor properties were not critical in this study, which is why the anisotropic characteristic of CLT elements are disregarded. By modelling the floors in that fashion, the diaphragm action will falsely be improved, which is why another assumption needs to be made on its properties to be able to model the system truthfully. Material properties of the CLT floors are shown in Table 3 below.

	$E_{0,mean}$ [N/m ²]	ν	G [N/mm ²]	ρ [kg/m ³]	Thickness [mm]
CLT260	7900	0.3	500	500	260

Table 3: Material properties CLT floors

2. Bending modifier

A bending modifier is applied to the model, to make up for the isotropic CLT properties and to resemble the connections of the CLT floors to be hinged. In GSA there are complications when modelling hinged floors, which is why an alternative is sought for. By adding the bending modifier, the floors are ensured to behave as hinged links, as can be seen in Figure 25 (left). By doing so, it is established that floor elements only transfer axial loading, whereas no torsional bending will be transferred from the floors to their supporting elements. This way it is avoided that the floors make the structure act like a rigid frame (Figure 25 (right)). By adding the bending modifier, floors can be modelled with the assumptions mentioned above without affecting the behaviour of the rest of the structure.

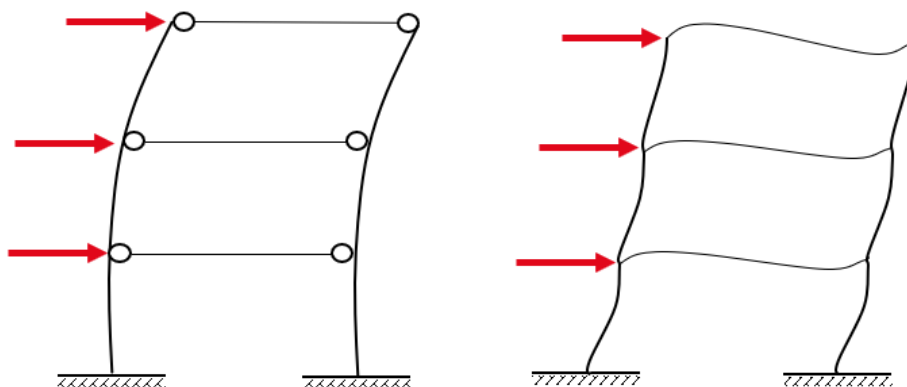


Figure 25: Effect of the bending modifier (left) to avoid rigid frame behaviour (right)

Sensitivity study

The graphs in Figure 26(a) and Figure 26 (b) below show a study done on the influence of the bending modifier. In this study the bending modifier is the variable for an 84 m circular diagrid with a braced core. The graph on the left (Figure 26(a)) shows the influence of varying the modifier from 0.001 to 1.0, making it seem that the bending modifier has an enormous influence on the dynamic behaviour of the building. However, as can be seen in Figure 26 on the left, the influence is not that powerful. In the model used for further studies the bending modifier is set to 20% (0.2).

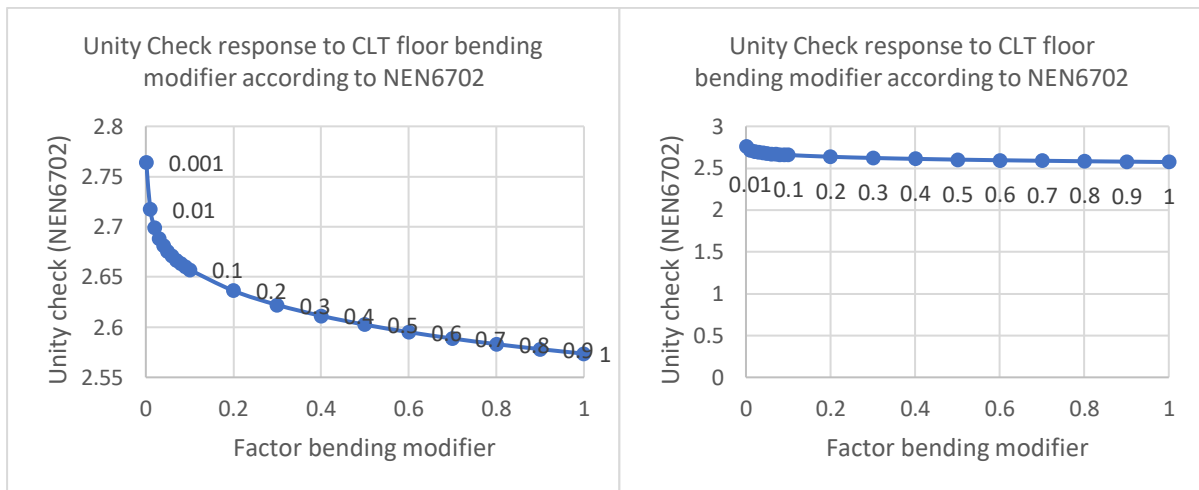


Figure 26: Unity check response to CLT floor bending with varying modifier from 0.001-1.0 (a) and unity check response to CLT floor bending with varying modifier from (b) according to NEN 6702.

3.1.2 EXTERIOR SYSTEMS

In the following sections the parameters determining the exterior systems are discussed. First variable that accounts for both systems is the floorplan shape. For this thesis two different floorplan shapes are considered: the square and the circle. As discussed previously floorplan shape largely affects the susceptibility of the building to lateral wind loads, measured with the force coefficient. To be able to compare two types of buildings with varying shapes, it is ensured that the floorplan area is nearly equal. Table 4 below shows dimensions for each shape.

	Width/radius [m]	Area [m ²]
Square	30	900
Circle	35	962

Table 4: Floorplan shape dimensions

In the following sections the parameters for the configurations of each exterior system are elaborated. Element dimensions are discussed in section 3.3.2. However, over the height of the building it is assumed that the dimensions of exterior systems will lessen in size, as more material is required in structural elements on the bottom floors in relation to the top floors. In each model the sizing of elements will vary over every third of the building, as shown by the example of a 20-floor building in Table 5 below.

Floors	Element dimensions
0 – 7	Original element dimensions – $(b_0 \times h_0)$
8 – 14	Middle element dimensions – $\frac{2}{3} * (b_0 \times h_0)$
15 – 20	Top element dimensions – $\frac{1}{3} * (b_0 \times h_0)$

Table 5: Example 20 floor (60 m) building, sizing variation over height

3.1.2.1 DIAGRID

3.1.2.1.1 RECTANGULAR

The rectangular diagrid is built up from diagonal elements combined with larger edge columns. Two variables for the diagrid structure are the number of horizontal segments and the storey span of the diagrid. The horizontal segments being the amount of support point at the foundation of the diagrid façade, also referred to as the diagrid bay density. The storey span of the diagrid determines over how many floors the diagrid bay passes before intersecting with its neighbouring bay element. The figure below (a) shows the case for a 4 segmented, 1 storey span diagrid whereas Figure 27 shows a diagrid configuration with 7 horizontal segments spanning 4 floors.

Horizontal segments

Range: 4, 5, 6, 7

Storey span diagrid

Range: 1 storey, 2 storeys, 4 storeys

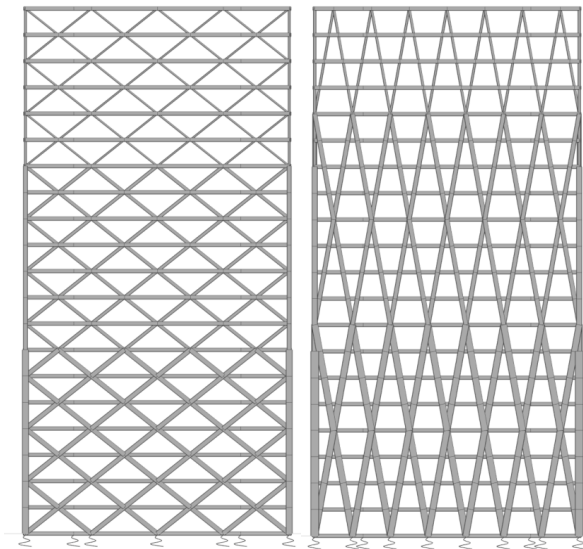


Figure 27: Configuration set-up for a rectangular diagrid

3.1.2.1.2 CIRCULAR

The circular diagrid is built up in the same manner as the rectangular diagrid. Whereas for the rectangular diagrid each façade is divided into horizontal segments for the diagrid, for the circular pattern the same thing has been done. However, the total perimeter has been split up into 4 sides, each being one fourth of the circumference. Each fourth of the periphery is treated as if it were a façade of the rectangular system, resulting in an equal number of horizontal segments over the outline of the façade. Once again, Figure 28 (a) and (b) show the configurations of the circular diagrid with 4 and 7 horizontal segments and 1 and 4 storey spans, respectively.

Horizontal segments

Range: 4, 5, 6, 7

Storey span diagrid

Range: 1 storey, 2 storeys, 4 storeys

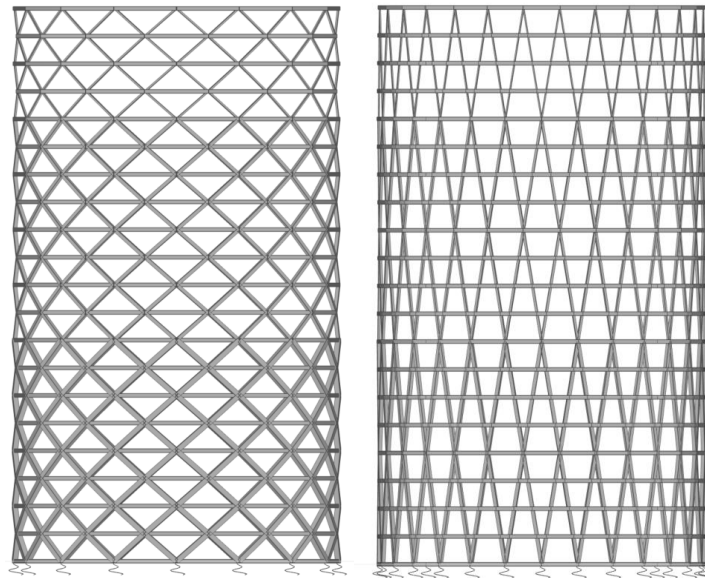


Figure 28: Configuration set-up for a circular diagrid

3.1.2.2 MEGAFRAME

3.1.2.2.1 RECTANGULAR

The rectangular megaframe is constructed based on two variables which apply to each façade, parameters for this system are the width and the storey span of the megaframe. Whereas the width determines the distance of the frame from the centre towards the edge of the façade the storey span defines the vertical configuration, similar to the diagrid system. It is noteworthy that the side columns at which the megaframe elements have much higher dimensions compared to the other columns, as the vast majority of vertical loading will pass through these columns. Figure 29(a) shows a rectangular megaframe with a width of 8 m and 4 storeys span, Figure 29(b) shows the configuration of the 30m width and a 1 storey span.

Megaframe width

Range: 8, 12.4, 16.8, 21.2, 25.6, 30

Storey span megaframe

Range: 1 storey, 2 storeys, 4 storeys

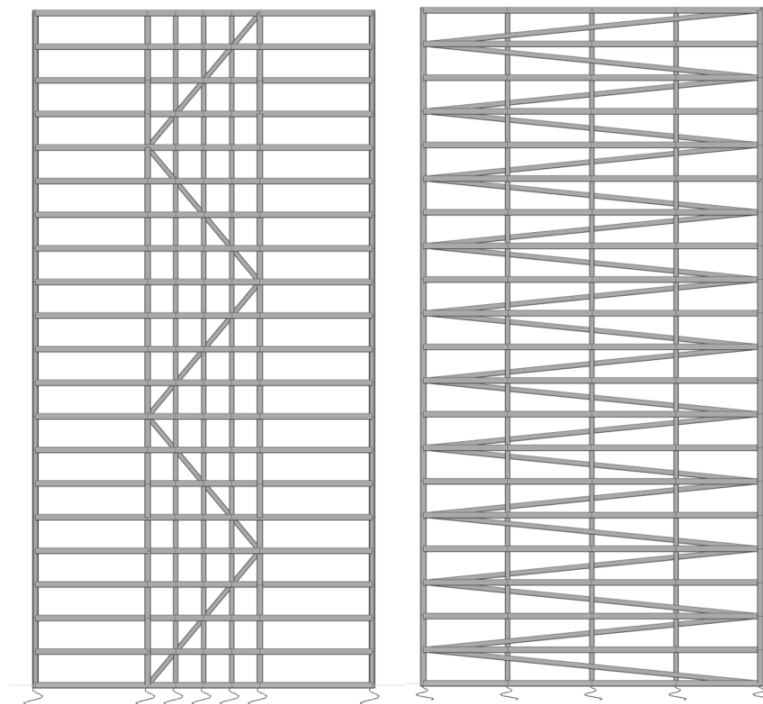


Figure 29: Configuration set-up for a rectangular megaframe

3.1.2.2.2 CIRCULAR

The circular megaframe is built up with a variable determining the amount of braces encircling the perimeter of the façade. Figure 30 illustrates the bracings of the circular megaframe, showing a configuration with 4 braces on the left and 16 braces on the right. The horizontal parameter in this system is the segmentation of the braces along each quarter of the façade. To illustrate the Figure 31 has been added. The figure shows the influence of the horizontal parameter, increasing the column density over the façade and raising the megaframe angle.

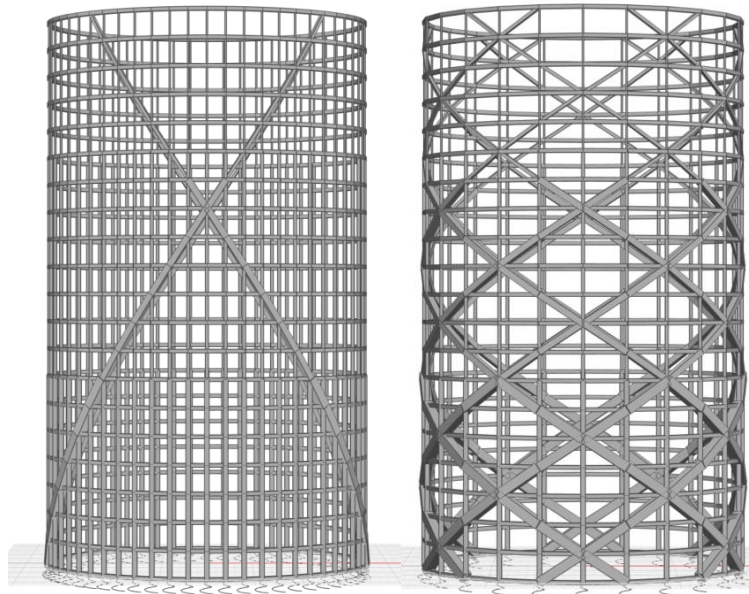


Figure 30: Configuration set-up for a circular megaframe

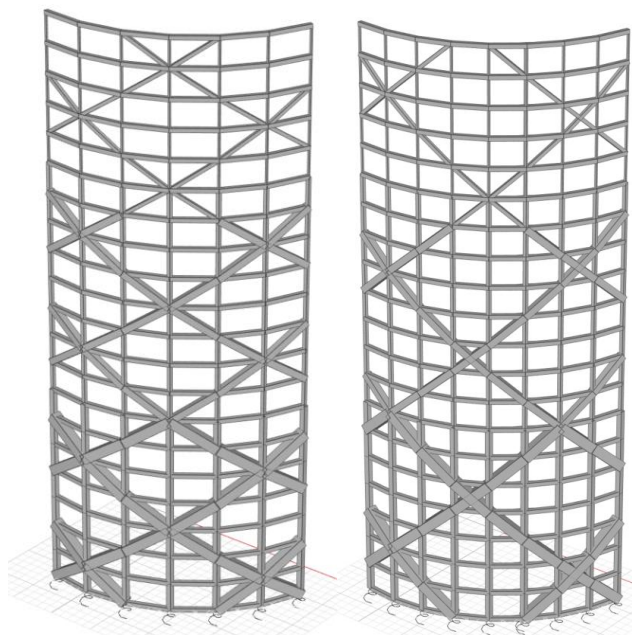


Figure 31: Circular megaframe horizontal parameter – 6 horizontal segments (left) and 7 horizontal segments (right)

3.1.3 INTERIOR SYSTEMS

Interior systems are the structural systems which primarily ensure stiffness on the inside of the structure, secondly these systems are known to provide passage through the floors to ensure vertical transport. The internal structures in this thesis are the CLT core, braced core and the combination of each with an outrigger structure.

3.1.3.1 BEAMS

Type	f_{mk} [N/m ²]	E [N/m ²]	ν	G [N/mm ²]	ρ [kg/m ³]	Width [mm]	Depth [mm]
GL32h	32	14 200	0.43	65	440	300	300

Table 6: Specific values GL32h beams

3.1.3.2 INTERNAL COLUMNS

Type	f_{mk} [N/mm ²]	E [N/mm ²]	ν	G [N/mm ²]	ρ [kg/m ³]	Width [mm]	Depth [mm]
GL32h	32	14 200	0.43	65	440	500	500

Table 7: Specific values GL32h internal columns

3.1.3.3 CLT CORE

Core stability systems are known for having high global stiffness as it is a composition of 4 continuous shear walls, placed perpendicularly with respect to one another. This shear-resistant element is most commonly built from reinforced concrete, as concrete allows the system to be poured into one element, allowing the system to also resist large moments. To this point, limited theory is available on CLT cores, which is why several assumptions need to be made:

1. U shaped cores

As stated in previous sections, the core system does not only serve as a stability system, a core also has the purpose of allowing vertical transport through the building. Typically, means of vertical transport such as elevators or staircases are located in the building's core. Specifically, when considering fire safety in high-rise structures, it is crucial to have unobstructed escape routes in the structure. However, most importantly, the area within the four shear walls that are specified as the core should be accessible from the outside. To be able to model a CLT core with these types of openings the CLT core is modelled as two U-shaped sections, connected by hinged links on each floor, as can be seen in Figure 32. By modelling the CLT core as such, in the primary direction the core would still have two shear walls orthogonal to its respective axis. In the secondary direction each shear wall will be split into two segments, connected with hinged links at every floor.

By adding hinged links, axial loads from one U-section to the other can be transferred, allowing both segments to cooperate in withstanding lateral loads, displayed in Figure 33. Although less global stiffness will be generated by the double u-shaped core segments when compared to a whole closed core, hinged links will allow some support between the segments and assure that the core is modelled more realistic.

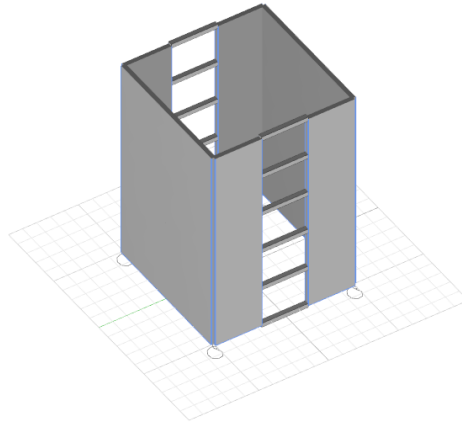


Figure 32: CLT core is modelled as two U-shaped sections, connected by hinged links on each floor

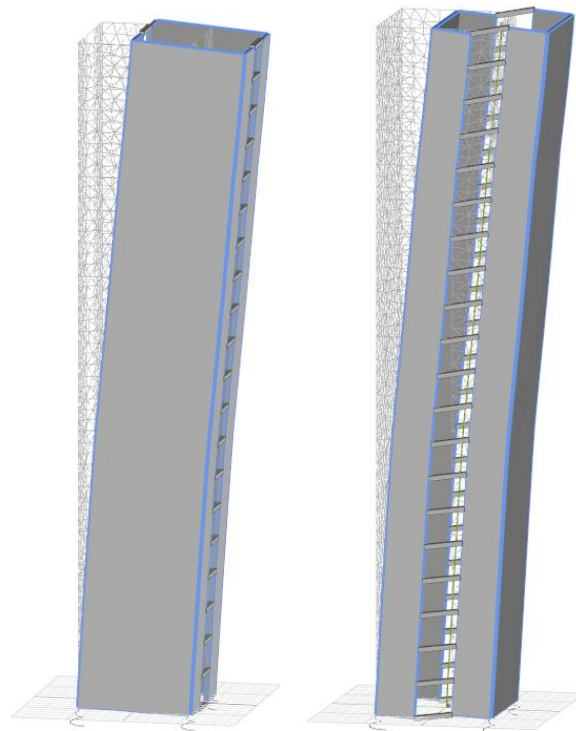


Figure 33: Allowance U-section segments to cooperate in withstanding lateral loads

2. Isotropic CLT properties

All CLT elements are modelled disregarding their orientation, therefore the anisotropic characteristic of cross-laminated timber can also be disregarded. By modelling CLT elements with isotropic properties, the shear strength in every direction will be equal, discounting orientations. Material properties of the CLT core are shown in Table 8 below.

3. CLT connections

For the CLT core it is found that the connections are governing for assessing its structural performance (Polastri et al., 2018). A reduction factor is inserted in the model to reduce the CLT core's bending properties to a level where it would replicate a CLT core with corresponding connections. Verhaegh et al. (2020) proposes that the global stiffness is reduced by 70% when considering the behaviour of its panel-to-panel connections. The reduction factor is therefore set to a factor 0.3 on the bending stiffness. Adjusted material properties can be seen in Table 8 below.

	$E_{0,mean}$ [N/m ²]	ν	G [N/mm ²]	ρ [kg/ m ³]	Thickness [mm]
CLT310	7340	0.3	500	500	310
CLT310*	2200*	0.3	500	500	310

Table 8: Material properties corrected by the reduction factor (own reduction)

3.1.3.4 BRACED CORE

The braced core system is built up from edge columns, beams and braces as shown in Figure 34 with dimensions found in Table 9.

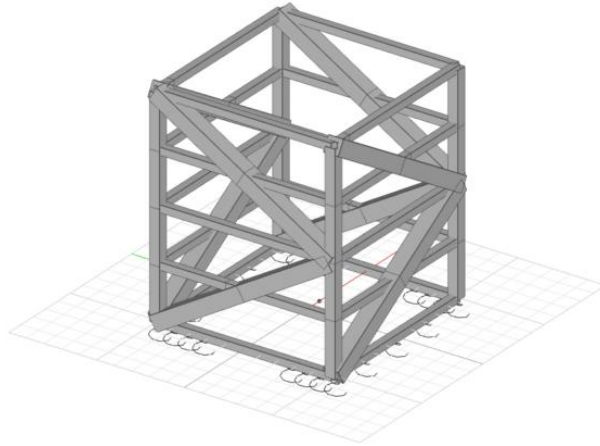


Figure 34: Braced core

Type	Dimensions	Material
Columns	550x550	GI32h
Beams	400x400	GI32h
Braces	800x800	GI32h

Table 9: Braced core system build up with dimensions and material

In addition, Figure 35 shows the orientation of brace spans over 2, 4 and 8 storeys respectively. A preliminary study shows best performance for 2 and 4 storey spans of the braced core (figure below), which is why the 8-storey span is disregarded onwards.

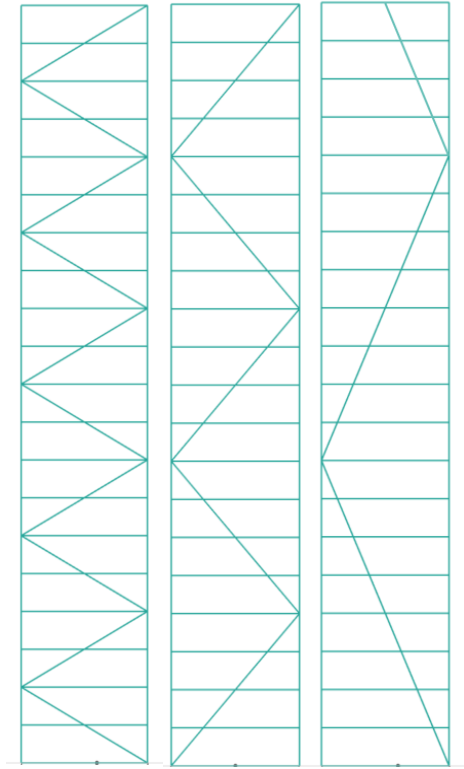


Figure 35: Orientation of the brace spans

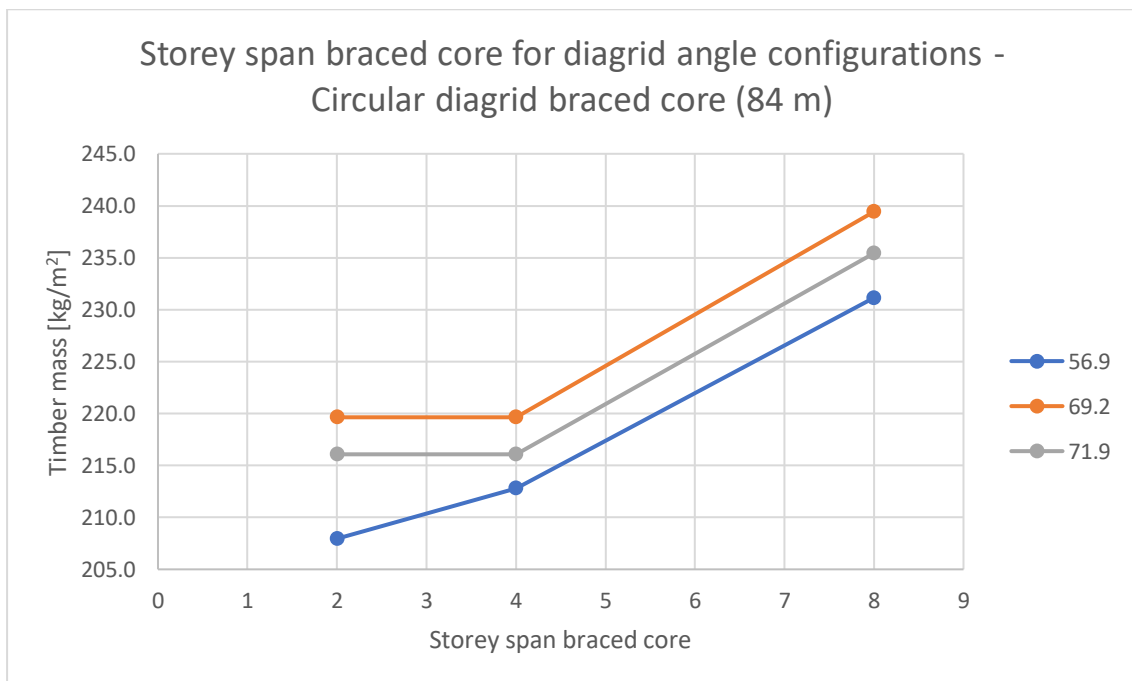


Figure 36: Storey span braced core for diagrid angle configurations.

3.1.4 OUTRIGGER

Two types of outrigger structures are assessed in this thesis: the outrigger in combination with a braced core and the outrigger in combination with a CLT core. In addition, the dimensions of the outrigger also differ for a circular floorplan and for a rectangular floorplan. As can be seen in Figure 37, the lever arm of the outrigger for the rectangular floorplan extends towards the façade of the structure, whereas the lever arm of the circular floorplan extends towards the inner column row. The latter is modelled as such to ensure that vertical loads of the outrigger located at the end of the lever arm are directly conveyed to the columns in axial compression or tension. Outrigger dimensions can be found in Table 10 below.

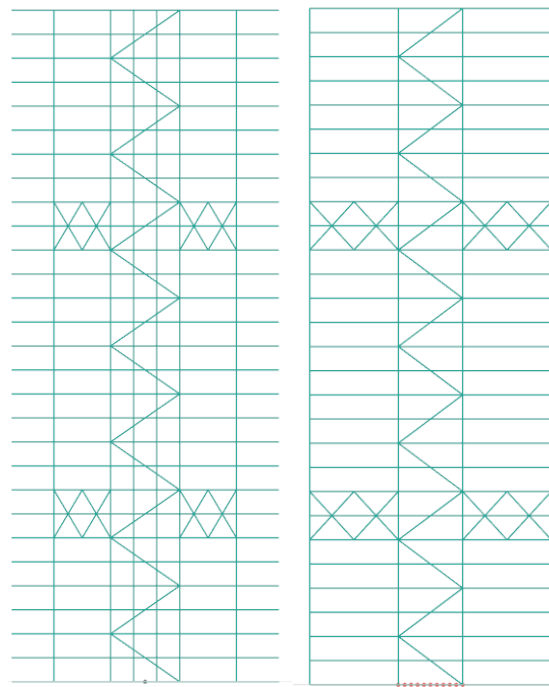


Figure 37: Lever arm of the outrigger

Type	Material	Dimensions
Outrigger brace	GI32h	350x350
Outrigger beam	GI32h	350x350
Internal column	GI32h	700x700 – 500x500 – 400x400

Table 10: Outrigger dimensions

Outrigger performance has been found to have varying performance at alternative outrigger heights (Nouri & Ashtari, 2015). In order to determine which outrigger heights are optimal for timber high-rise structures a preliminary study has been performed with an 84 m tall circular diagrid with a braced core outrigger, as can be seen in Figure 38. In the figure the height of the top outrigger is displayed on the x-axis whereas the height of the second (bottom) outrigger can be seen on the data labels shown in the figure. Both heights are displayed as percentages of the total height. This preliminary study shows that least accelerations achieved if the top outrigger would be at around 70% of the total height and the bottom outrigger at 30%. In order to verify the results Mcnabb and Muvdi (1975) has been consulted. The concerning paper suggests that ideal outrigger heights would be at around 31.2% and 68.5% which practically matches the results found in the preliminary study. Deviation from the values found in the paper might have occurred due to the fact that the relative outrigger height (with respect to the total height) is limited by the fact that outrigger heights should match floor heights. Furthermore, it is considered that outrigger heights at 30% and 70% are optimal which is why these two outrigger heights are fixed variables in the coming studies.

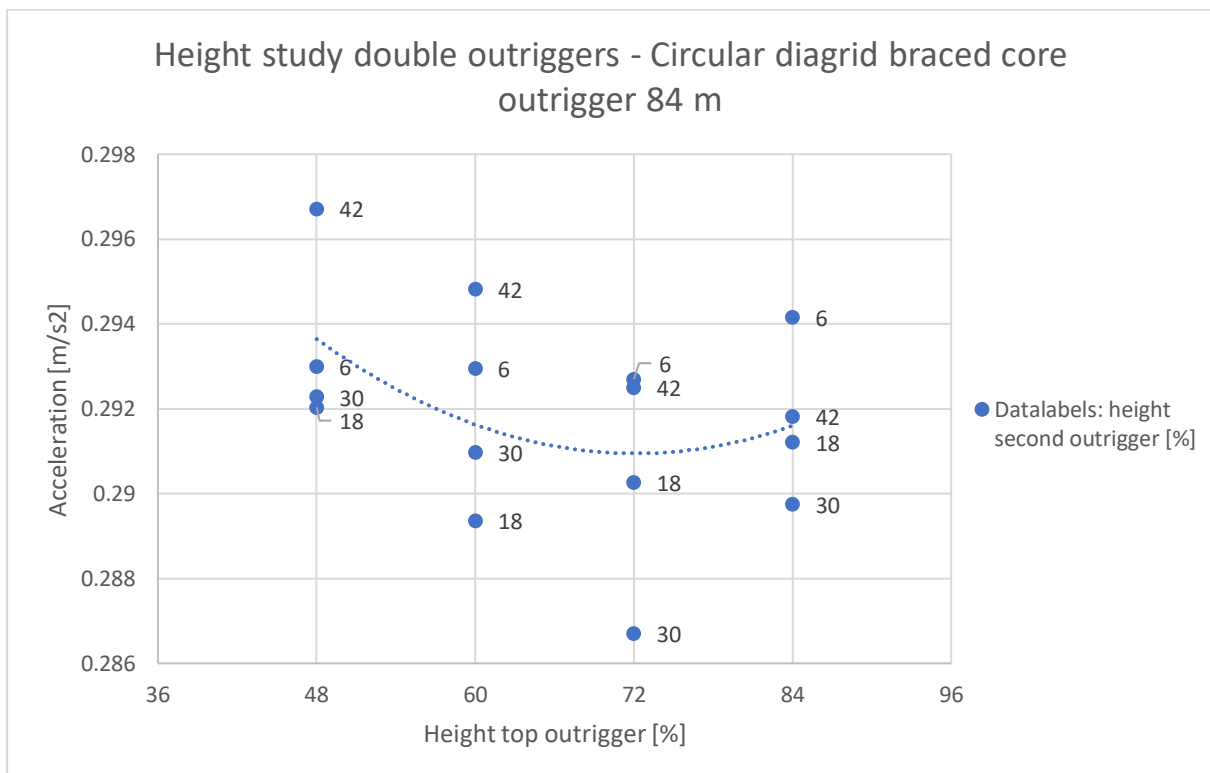


Figure 38: Outriggers height performance

3.2 ANALYSIS

3.2.1 GSA INPUTS

3.2.1.1 DAMPING

The damping in this thesis has been set at a value of 1%. According to Feldmann (2006), for timber structures, structural damping varies from 0.64 to 2.7%, depending on the type of structure, connections and finishing of the building. As researched by Feldmann (2006), lower damping values correspond to simpler structures, such as a timber tower used for a windmill, making the damping ratio used in this thesis rather conservative. Due to the large gap in literature on the damping coefficient for timber structures, it was assumed that it would be safer to assume lower damping, in order to get realistic results. Further on, as this thesis is a preliminary study, no detailed design is known to be able to determine which connections or cladding are used in the structure, making the approximation for damping a very rough estimate. Lastly, if all configurations are calculated with the same damping value, comparison between systems and influences of design considerations can still be made. A varying damping value would offset all trends equally, without changing the global behaviour of a structure.

3.2.1.2 CONNECTIONS

For modelling the connections in the model a few assumptions are made too. These assumptions are based on constructability and potential slip in the connections.

1. Constructability

Timber is an organic material where, unlike concrete or steel, it is extremely challenging to make moment resisting connections. In the scope of this research it has already been mentioned, in order to avoid achieving excessive moment capacities in timber connections, structural systems are chosen where the connections could be modelled as hinges. Only systems with shape-retaining configurations are studied in this research, meaning that the use of triangular shaped grid is highly preferred. In the model it is assumed that all joints are modelled as hinges, and that no rotational stiffness is added to the connection.

2. Slip

Although the connections are modelled as hinges, slip needs to be taken into account when modelling the structures. According to Hashemi et al, 2016, timber connections with slip friction improve the capacity to absorb dynamic energy in the structure. Meaning that by taking slip into account in the structural model, natural frequencies will decrease. Modelling of the slip is done by implementing an area modifier.

By decreasing the area of the elements the strain and deformation of the elements can be considered as slip in the connections. Table 11 below show the results for a study on the area modifier, for modelling slip in the connections. It can be seen that the natural frequency decreases when the slip effect increases. However, the acceleration increases with the decrease in frequency, meaning the too much slip is not desirable. For the structural model an area modifier of 0.75 is asserted to emulate realistic connection properties.

Area modifier	Natural frequency [Hz]	Acceleration
0.1	0.322	0.214
0.2	0.396	0.168
0.3	0.438	0.149
0.4	0.466	0.138
0.5	0.486	0.131
0.6	0.500	0.126
0.7	0.512	0.123
0.8	0.521	0.120
0.9	0.529	0.118
1.0	0.535	0.117

Table 11: Results study area modifier

3.2.1.3 SUPPORTS

The structure deflects due to two phenomena: the first one being the deformation of the structure, the second one is the deflection due to the rotation of the foundation, as seen in figure below. The total deflection is the sum of both alternatives, for which unity check calculations are done in further sections.

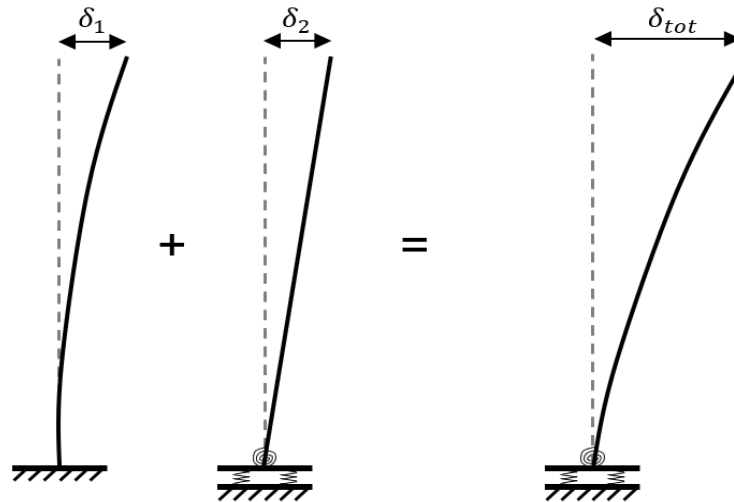


Figure 39: Deflections assumed due to building deformation and due to rotation of the foundation

For the translational stiffness at the supports it is assumed to apply foundation poles with the following properties.

E	20 000 N/mm ²
D	650 mm
L	25 m

Table 12: Concrete foundation pile properties

With compaction a compaction factor of 2.0 and a factor of dynamic stiffness of 1.5, the following equations can be applied.

$$k_{stat} = \frac{E * A}{L}$$

Equation 9: Static stiffness

$$k_{dyn} = 1.5 * k_{stat}$$

Equation 10: Dynamic stiffness

Resulting in a dynamic stiffness of 200 000 kNm. For this model, the stiffness in z-direction is most interesting, whereas the stiffnesses in x- and y-direction might be of less significance. It is assumed that the stiffness in x- and y-direction are about half of the stiffness of the z-direction.

Direction	Stiffness [kNm]
x	100 000
Y	100 000
z	200 000

Table 13: Directions and corresponding stiffness in kNm

3.2.1.4 LOAD COMBINATIONS AND LOADS

The load combinations applied in this thesis for sizing the structural elements based on strength can be seen in Equation 11, obtained from NEN-EN 1990+A1+A1/C2/NB:2019 eq. 6.10a & 6.10b.

$$6.10a: 1.1 \left(1.35G + \sum_{i \geq 1} 1.5\varphi_{0.1}Q_{k,i} \right)$$

$$6.10b: 1.1 \left(1.2G + 1.5Q_{k,i} + \sum_{i \geq 1} 1.5\varphi_{0.1}Q_{k,i} \right)$$

Equation 11: Load combinations applied for dimensioning on strength (a)(b) (NEN-EN 1990+A1+A1/C2/NB: 2019)

With G being the Dead Load and Superimposed Dead Load (values are in section 3.2.1.5) and Q being the Live Load on the structure, set at 1.75 kN/m².

For the modal analysis in GSA a different load combination is applied, as shown in Equation 12.

$$\text{Modal analysis: } DL + SDL + 0.1 * LL$$

Equation 12: Load combinations applied for modal analysis (NEN-EN 1990+A1+A1/C2/NB: 2019)

3.2.1.5 FLOOR LOADING

For the floor loading the dead load as well as the superimposed dead load are considered. The dead load is the result of the CLT260 element mentioned above.

Element	Load pressure [kN/m ²]
Dead Load	
CLT260	1.30
Superimposed Dead Load	
Floor finishing	0.73
Interior walls	0.50
Ceiling	0.30
Total SDL:	1.53

Table 14: Floor loading elements and corresponding load pressure

3.2.2 GSA OUTPUTS

First of all, the GSA model has been used to verify hand calculations made for determining axial loads in columns and diagonal elements. Axial loads found with this check are used to determine required element sizing based on ULS strength criteria.

In the workflow showed in section 3.1, it is shown that GSA has been used to calculate the weight, deflections and natural frequencies of the structure. The purpose of this section is to show the outputs of the finite element model made with GSA. The model assessed in this section is a 60 m tall circular diagrid with a diagrid angle of 71.9° and a CLT core, which can be seen in Figure 40.

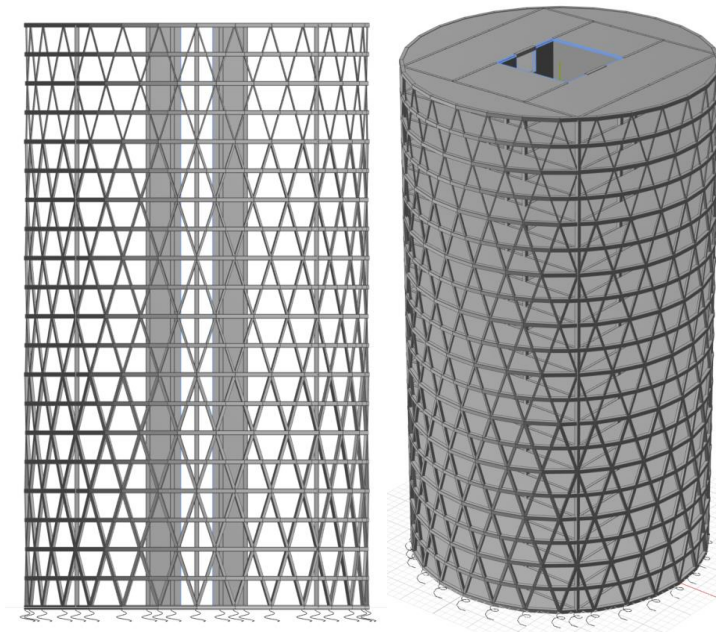


Figure 40: Display of plain model in GSA

Of the model shown in Figure 40 above, the deflections are determined due to the wind induced loads, which can be seen in Figure 41 below. The figure shows the deformed state on the left and structure with displacement contours on the right. As can be seen in the displacement legend on the top right, maximum displacement is 0.1750 m which is over $\frac{h}{500} = \frac{60}{500} = 0.12\text{ m}$, meaning that this configuration would not suffice.

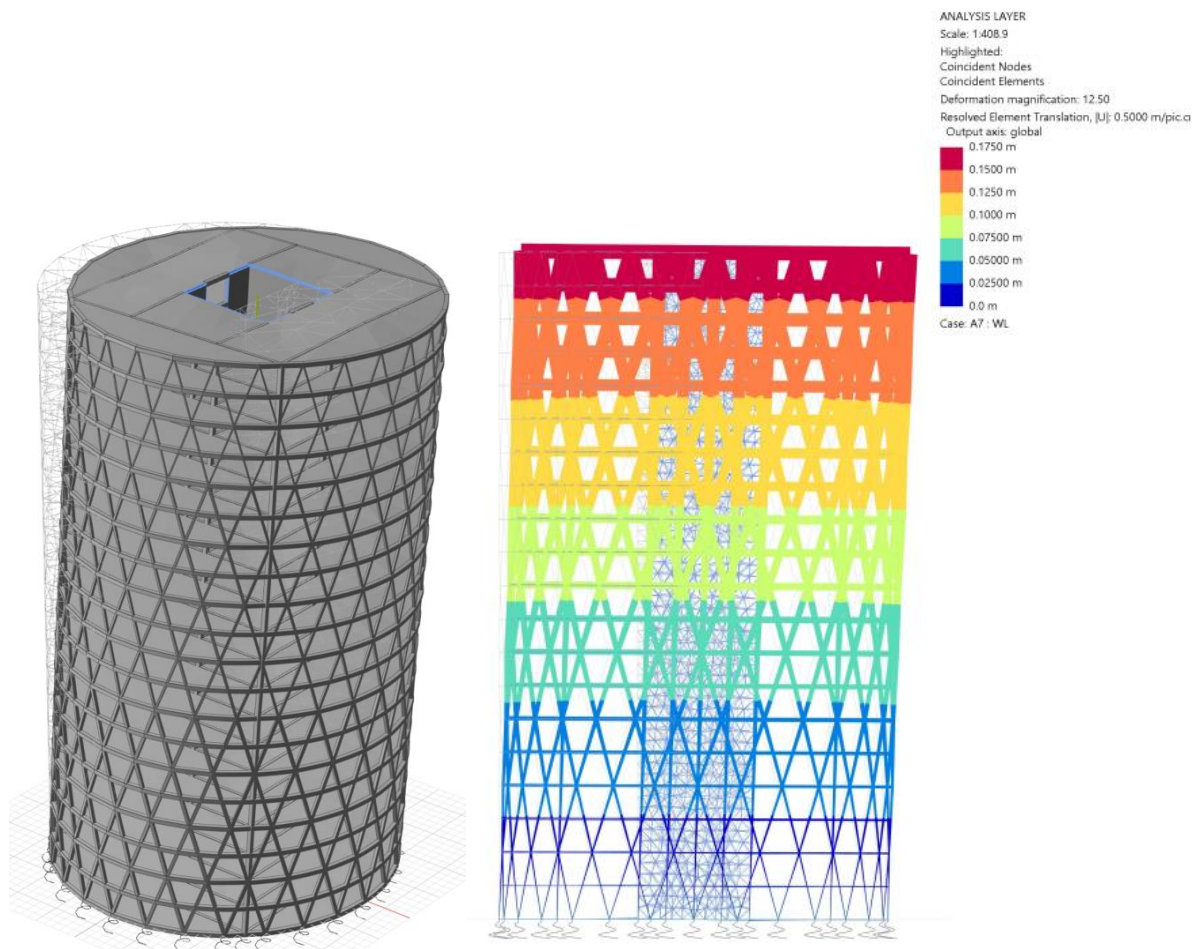


Figure 41: Deformation of a circular diagrid CLT cored structure

Additionally, GSA also does an accurate calculation of the natural frequency, as stated in the previous section. For finding the natural frequencies, eigenmodes of the structure are found by doing the modal analysis, as described with the load combination from section 3.2.1.4. Figure 42 shows the top view of the structure, where the first, second and third eigenmode are shown, corresponding to along- and cross-wind and torsional accelerations.

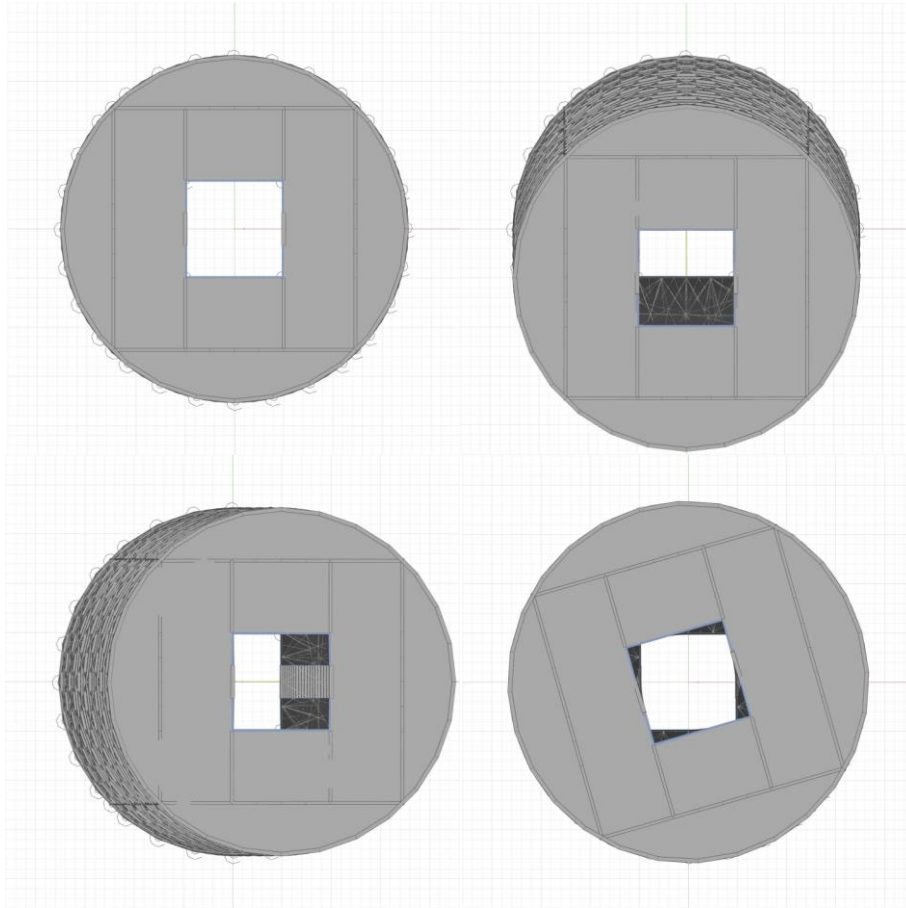


Figure 42: Top views of first three eigenmodes of the structure

3.3 ACCEPTANCE CHECK

In the parametric model there are several key performance indicators that need to be within a pre-set threshold in order to be able to compare systems to each other. The three main key performance indicators are called the acceptance levels in this thesis, consisting of acceptance levels for strength, deformation and acceleration. Whereas the acceptance level for strength and deformation are also known as the unity check, the acceptance level for acceleration is a benchmark for a combined acceleration and natural frequency in relation to the evaluation curves.

3.3.1.1 STRENGTH

The first acceptance level discussed is the acceptance level of strength of the elements. To avoid failure of an element, structural elements need to be checked whether the elements suffice based on the minimal strength requirements. In this thesis, all elements are checked on strength requirements from EN 1995-1-1: Eurocode 5: Design of timber structures and the Dutch National Annex, as explained in section 2.1.5, for which the calculations can be seen in Appendix A.

3.3.1.2 STABILITY

Acceptance levels of stability are more commonly known as the unity checks for lateral deformations in the serviceability limit state. For stability, there are two thresholds, both for the ultimate limit state (ULS) and serviceability limit state (SLS). In terms of ULS the threshold can be described as such that the moment due to vertical load needs to be higher than the moment due to horizontal loads. By ensuring higher vertical loads than horizontally, potential tipping of the building is avoided.

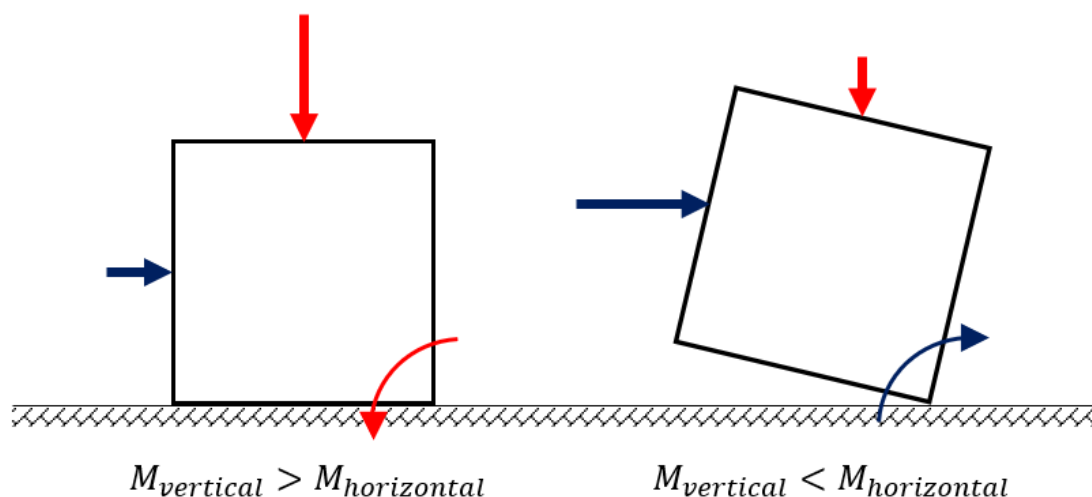


Figure 43: Stability thresholds and corresponding moments (van den Berg, 2012)

For the SLS stability threshold, Eurocode NEN-EN 1991-1-1 and the Dutch National Annex need to be consulted. The standard recommends maximum deflections based on the building height:

$$\delta_{max,SLS} = \frac{h}{500}$$

Equation 13: Max deflection, according to Eurocode 1

Assumptions are made to model the system as realistic as possible. With these assumptions the maximum deflections of the top nodes of the model are calculated with the help of GSA. The acceptance level is quantified as follows:

$$Acceptance\ level_{stability} = \frac{\delta_{max,top}}{\delta_{max,SLS}}$$

Equation 14: Stability acceptance level (Eurocode NEN-EN 1991-1-1)

3.3.1.3 ACCELERATION

As discussed in the introduction of the section, the acceleration acceptance level is composed of the acceleration and natural frequency of the structure. There are two types of acceleration curves considered in this thesis: evaluation curves according to ISO10137:2007(E) and according to NTA 4614-3/NEN6702. The Figure below shows evaluation curves according to both standards. Note that the evaluation curves depict the perception probability, ISO10137 curve 2 (orange) is estimated at 90% likelihood of perception. For both curves wind speeds are determined with a 1-year return period. For timber high-rise it is expected that wind-induced vibrations are more critical than for conventional high-rise structures, therefore the thesis will henceforth consider NTA 4614-3/NEN6702 standards. The criteria in these standards are less demanding causing the feasibility for timber structures to increase. Furthermore, the thesis is written in and focused on the Netherlands, which makes it argumentative to consider Dutch national standards. Lastly, since the problem definition states an increasing population growth and the housing shortage in the Netherlands, evaluation curve 2 from NTA 4614-3/NEN6702 is the guiding threshold for this thesis.

The acceptance level for wind-induced vibrations is calculated by performing a unity check of datapoint of the acceleration over the acceleration on the evaluation curve with corresponding frequency. The equation for the segment between 0.063 Hz and 1 Hz is:

$$a_{evaluation\ curve\ 2,\ NTA/NEN6702} = 0.04 * f_0^{0.453}$$

Equation 15: Equation for evaluation curve 2, according to NTA/NEN 6702

Acceptance level for the acceleration threshold is:

$$Acceptance\ level_{acceleration} = \frac{a_1}{0.04 * f_1^{0.453}}$$

Equation 16: Acceleration acceptance level

f_1 is the natural frequency calculated through GSA in the model

a_1 is the acceleration calculated in the Grasshopper script

By applying this approach for the acceptance level, the relative distance to the evaluation curve can be quantified with a single statistic, indicating a value below 1 when the threshold is satisfied.

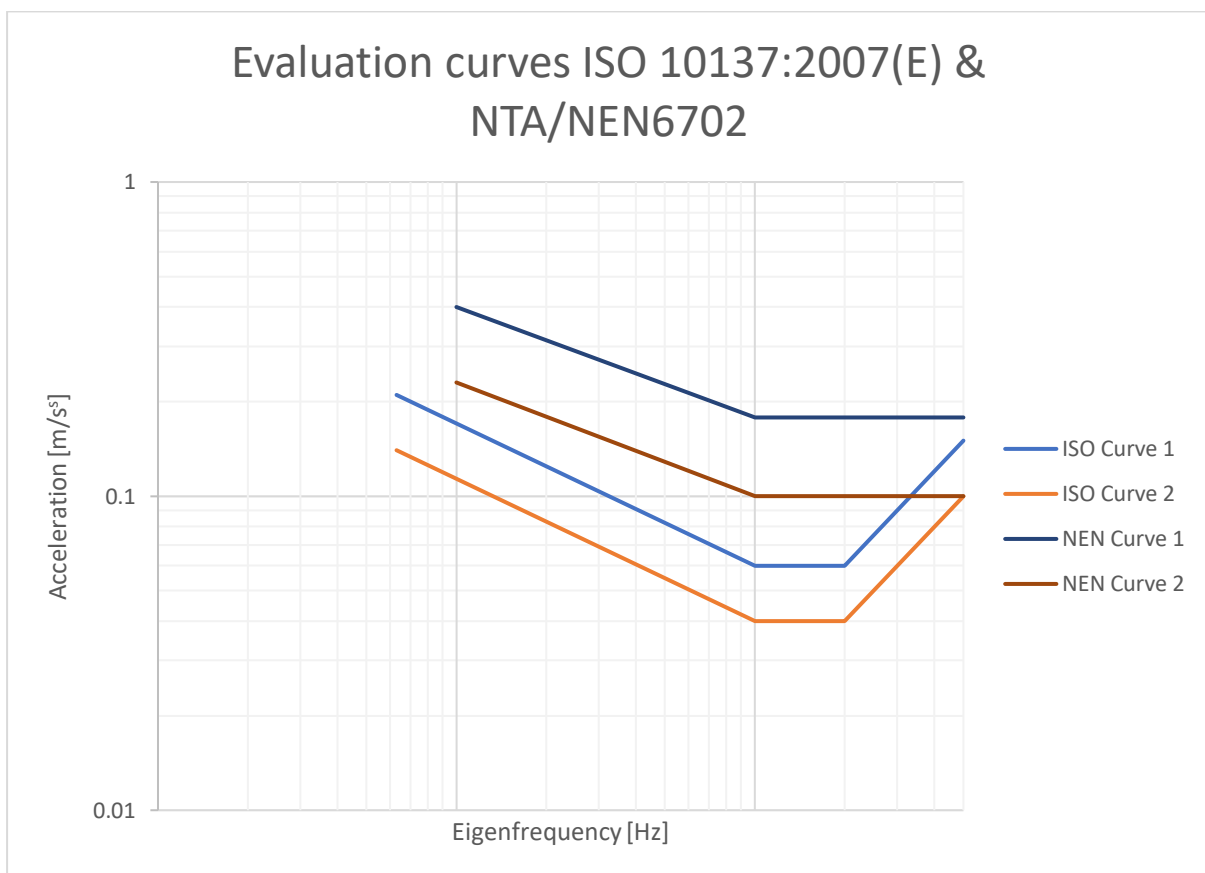


Figure 44: Evaluation curves ISO 10137:2007€ & NTA/NEN6702.

3.3.2 ELEMENT DIMENSIONS

Sizing of elements has been performed using the workflow in Figure 45 below. First the building geometry is set-up, as described in section 3.1. Then, based on the outcomes of the model in GSA (section 3.2), the axial loads through critical façade elements are calculated. Calculations for the critical façade elements are displayed in Appendix D.

With the critical loads found in Appendix D, structural elements are sized to fulfil the acceptance level of strength (as described in 3.3.1.1). Following the workflow from the figure below, the structural geometry is generated when elements are sized to fulfil the strength criterium. The structural model retrieves the mass, natural frequencies and deformation. Next, it is checked whether the structure's behaviour fulfils the acceptance level's thresholds (as described in section 3.3). If the acceptance levels are not met, the estimator function is consulted.

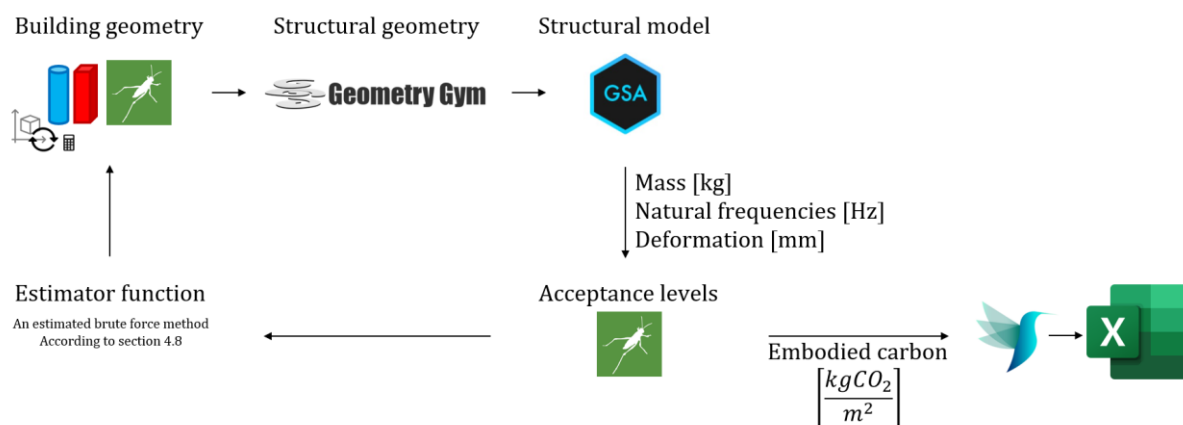


Figure 45: Workflow of the parametric structural model

The estimator function is a method developed to appropriately size elements in order to fulfil the acceptance levels of strength, stability and accelerations. The function is generated per structural system. The result of the estimator function is the factor by which the sizing of the elements should be multiplied if the elements are sized only for strength, in order to find a size that complies to all three criteria. A step-by-step approach, including problem statements, bottlenecks and the creation of such a function can be read in Appendix E.

4 RESULTS

In this section the results from the parametric structural model are displayed and assessed. For each set of results, key observations are noted, which are reviewed in the DISCUSSION. With the help of the estimator function (Appendix E), all results shown fulfil the acceptance level's threshold (section 3.3), with the governing failure mechanism being the along-wind acceleration. Therefore, it is assumed that comparison between results can be made.

The comparison is made based on the efficiency of the structure, measured in timber mass per square meter [kg/m^2]. By measuring the efficiency as such, material use of systems with varying shapes and heights can be compared.

4.1 GEOMETRY GENERATION

4.1.1 FLOORPLAN SHAPE

First, similar configurations are evaluated based on their behaviour for varying floorplan shapes. In Figure 46 below, a rectangular and a circular diagrid and CLT core system are compared. The effect of the circular floorplan shape is obvious, and increases for even taller structures, reaching a material saving of more than 50%.

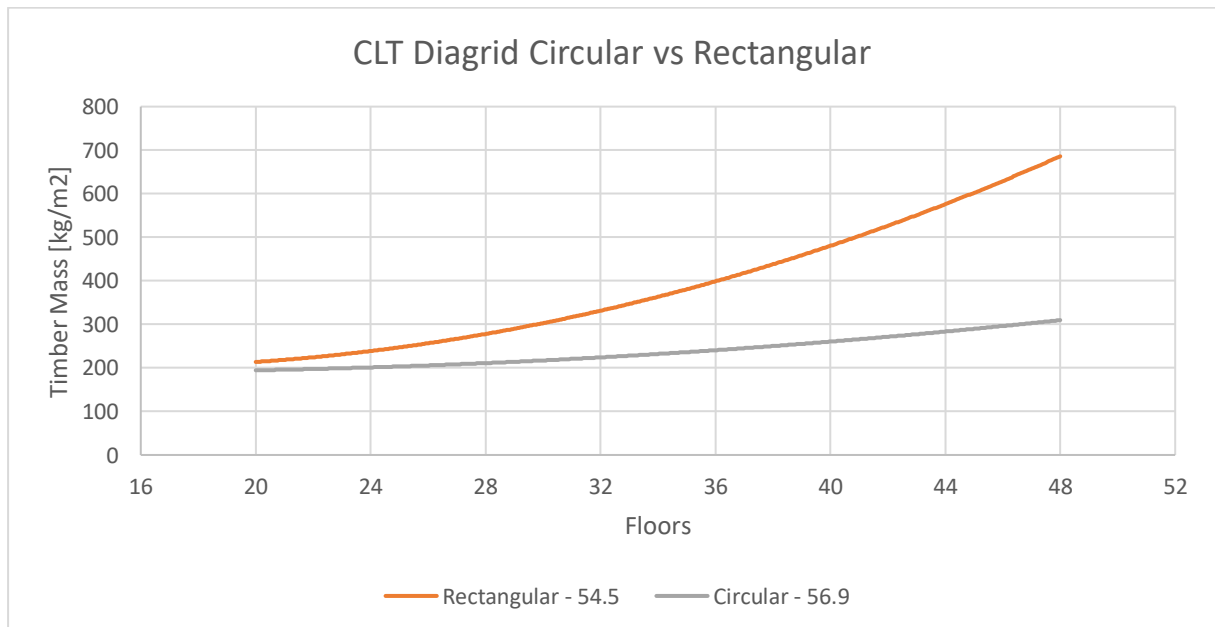


Figure 46: Diagrid structure with a CLT core, Circular vs. Rectangular

4.1.2 EXTERIOR SYSTEM

4.1.2.1 DIAGRID

		Horizontal segments				
		6			7	
	Storey span					
Rectangular	1	50.2°	---		54.5°	---
	2	67.4°	---	---	70.4°	---
Circular	1	52.7°	---		56.9°	---
	2	69.1°	---	---	71.9°	---

Table 15: Overview of configurations and corresponding diagrid angles.

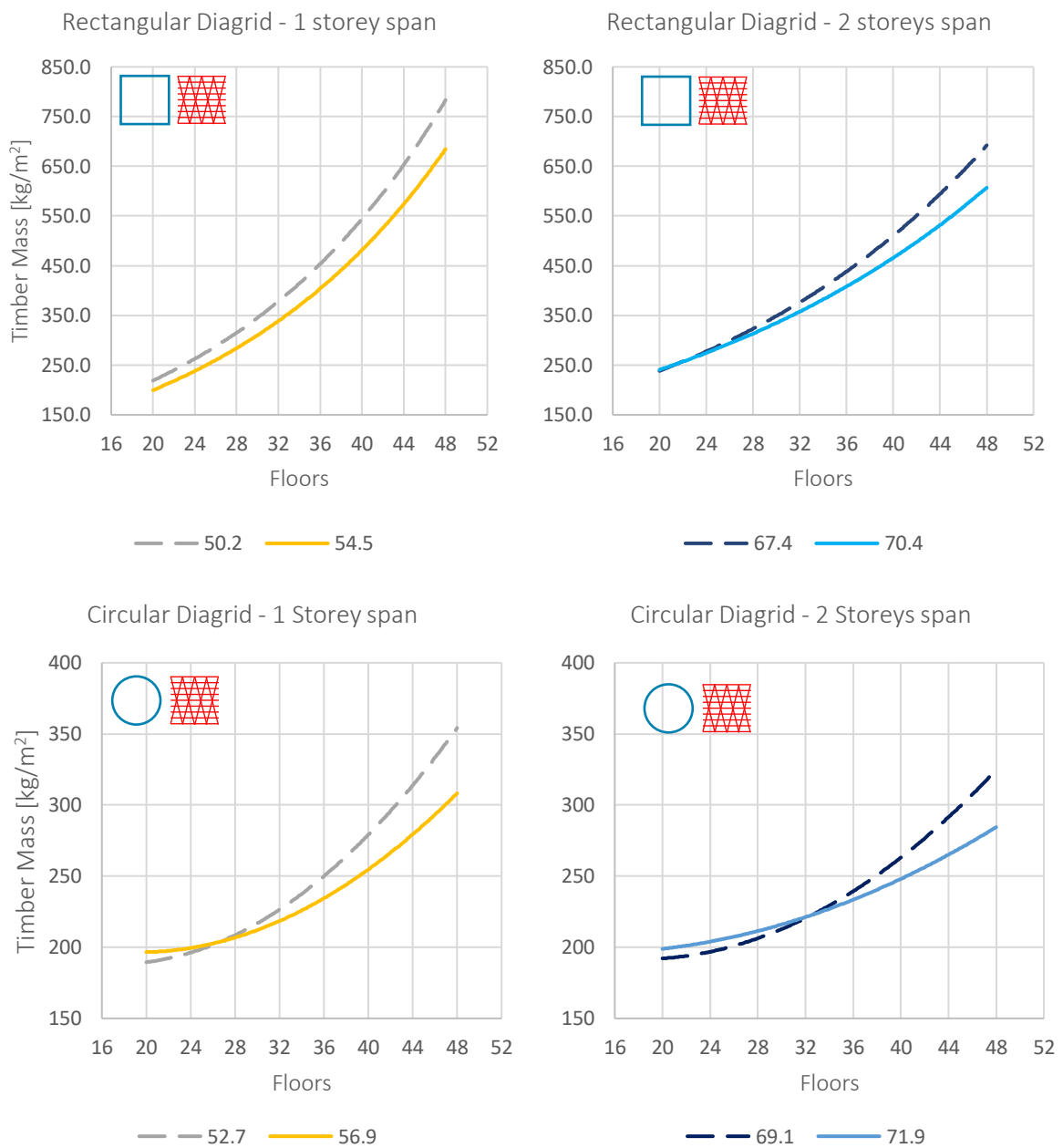


Figure 47: Comparison of Diagrid systems based on Timber Mass [kg/m²]

First, diagrid system configurations are analysed based on their material efficiencies. As can be seen in the Table 15, the diagrid angle is the result of two variables: the number of horizontal segments and the storey span of the diagrid. Out of 16 configurations the 8 best performing configurations are displayed in Figure 47, 4 rectangular and 4 circular configurations.

Figure 47 on the previous page shows the material use per configuration, in which the dotted lines indicate configurations with 6 horizontal segments, and continuous lines represent the results for 7 horizontal segments, as can be seen in Table 15.

Key observations from the diagrid configurations are:

1. Offset due to bay density

Configurations with 7 horizontal segments most often show less timber mass compared to its 6 segmented counterpart. This is especially the case for taller structures.

2. Varying slope due to diagrid angle

The slopes of the trendlines vary for alternative diagrid angles. Steeper trendlines occur for lower diagrid angles, trendline becomes more gentle for higher diagrid angles.

4.1.2.2 MEGAFRAME

Following the diagrid, the megaframe system is assessed on its performance.

When applied to a rectangular floorplan shape, the megaframe shows to be an inefficient exterior system. Preliminary results have shown that acceptance levels can only be met without outrageous element dimensions being applied. Figure 48 below shows a screen capture from GSA, showing the minimal element dimensions required in order to fulfil the acceleration acceptance levels, as seen in section 3.3.1.3.

For a 20-floor structure, the lowest altitude within the researched realm, this configuration requires 2500x2500 mm columns and 3500x3500 mm braces. Converging such large elements into one joint is considered to be extremely complicated and such element dimensions might obstruct too large façade segments, making it unappealing to live on these floors. Therefore, the rectangular megaframe is considered an unfeasible configuration.

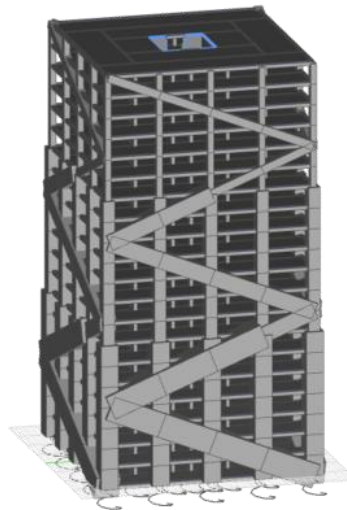


Figure 48: GSA capture for a 60 m Rectangular Megaframe that complies to acceptance levels

The megaframe does show satisfactory results when applied to a circular structure, for which the configuration can be seen in Table 16 and results are shown in Figure 49.

Megaframe angle		6 megaframe braces
Columns	10	47.5°
	12	52.7°
	14	56.5°

Table 16: Circular Megaframe configuration

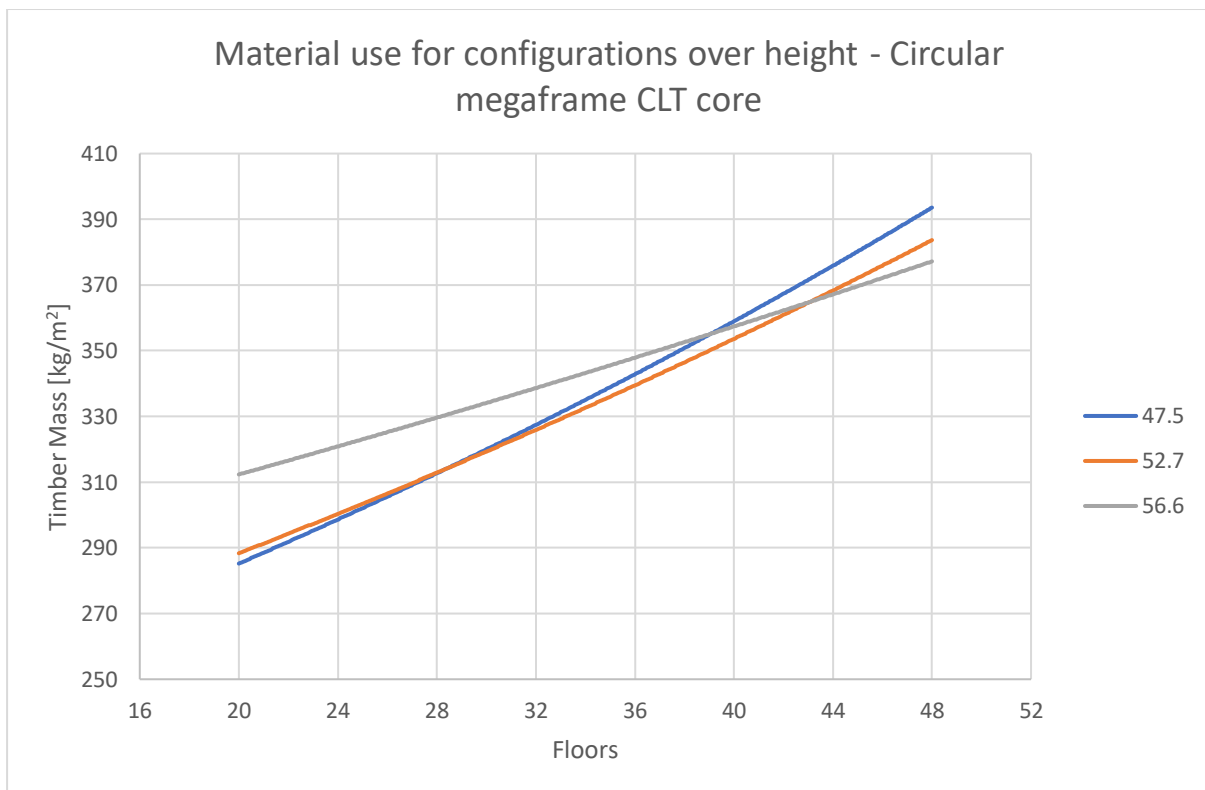


Figure 49: Timber mass for configurations over height - Circular megaframe CLT core

Key observations from Figure 49 show:

1. Varying slope due to megaframe angle.

For taller structure, larger megaframe angles show to be more efficient. Also, considering Table 16, the varying slope is related to the amount of columns per quarter of the façade (as explained in section 3.1.2.2, Figure 31). Therefore, more efficient taller structures could result from the increase in columns.

4.1.3 INTERIOR SYSTEM

The performances of the interior systems are compared based on fixed exterior systems, to be able to properly compare trends and performances. First, a comparison of interior systems with a diagrid is made. Evaluating the performances of a braced core (BC) to a cross laminated timber (CLT) core, as seen in Figure 50.

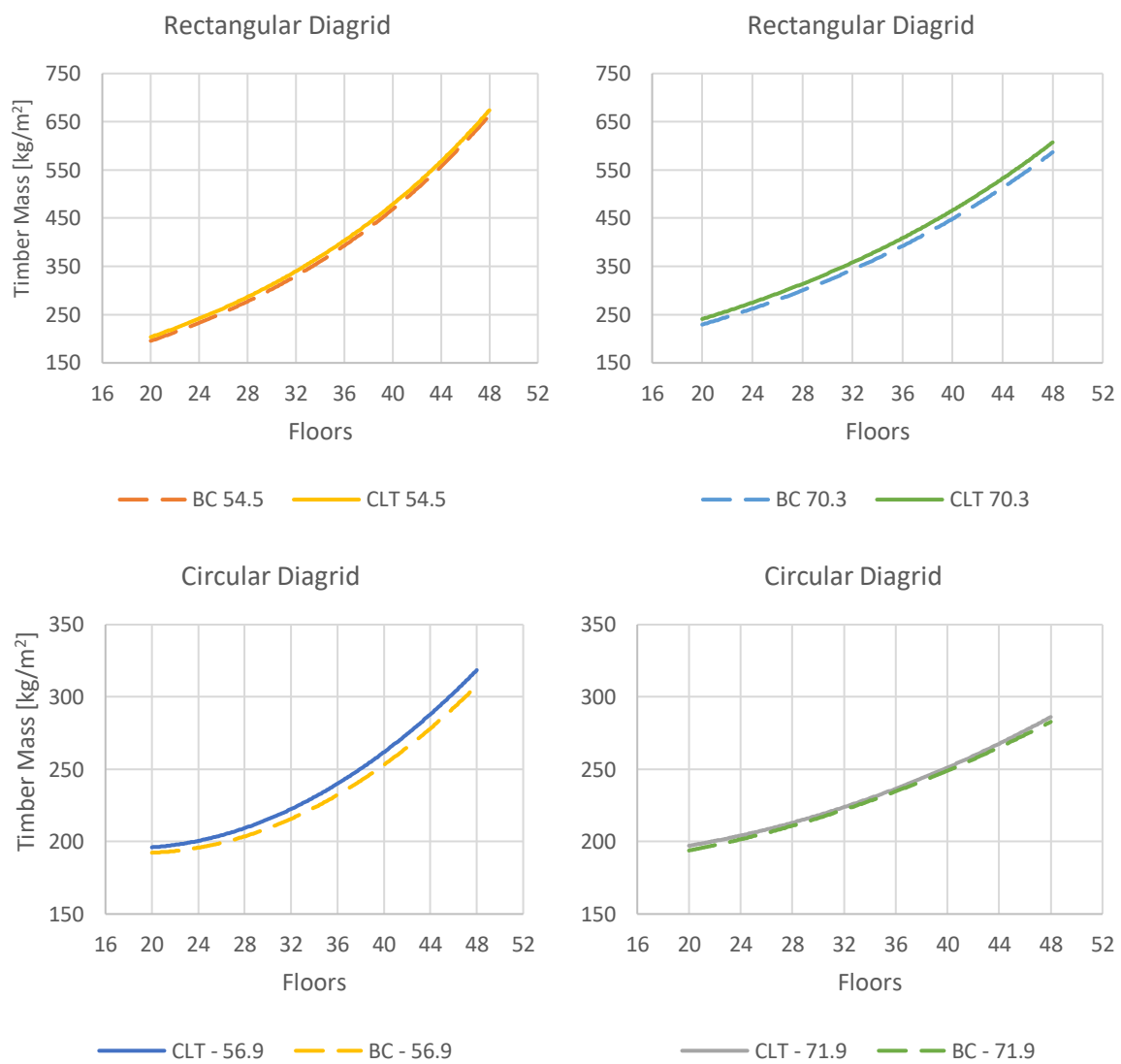


Figure 50: Comparison of interior systems of a Diagrid based on Timber Mass [kg /m²]

When assessing Figure 50 on the previous page the following remark is noted:

1. Constant offset rectangular structure

For the rectangular diagrid, a constant offset observed between the BC and CLT core configurations, suggesting an overall more material efficient performance for the braced core.

Next, behaviours of interior systems with the circular megaframe are analysed.

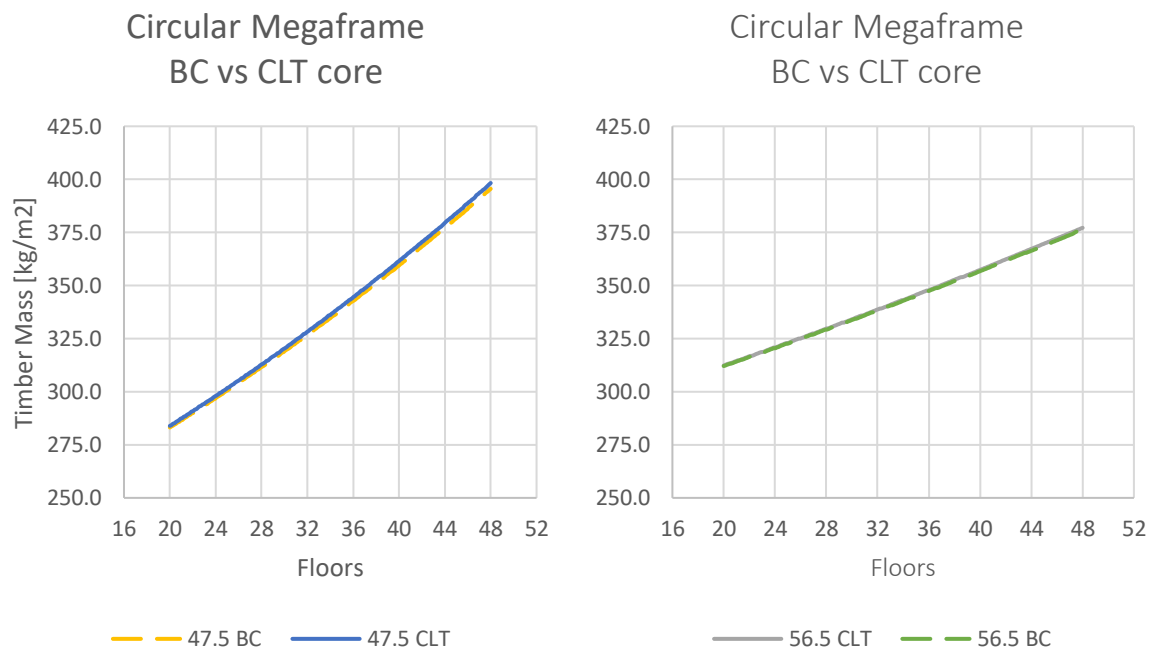


Figure 51 Comparison of interior systems of a Circular Megaframe based on Timber Mass [kg /m²]

Observations for the circular megaframe on interior systems are similar to the observations for the diagrid, which are described above.

4.1.4 OUTRIGGER

Moreover, configurations with added outriggers are studied, for which results with a diagrid system can be seen in Figure 52.

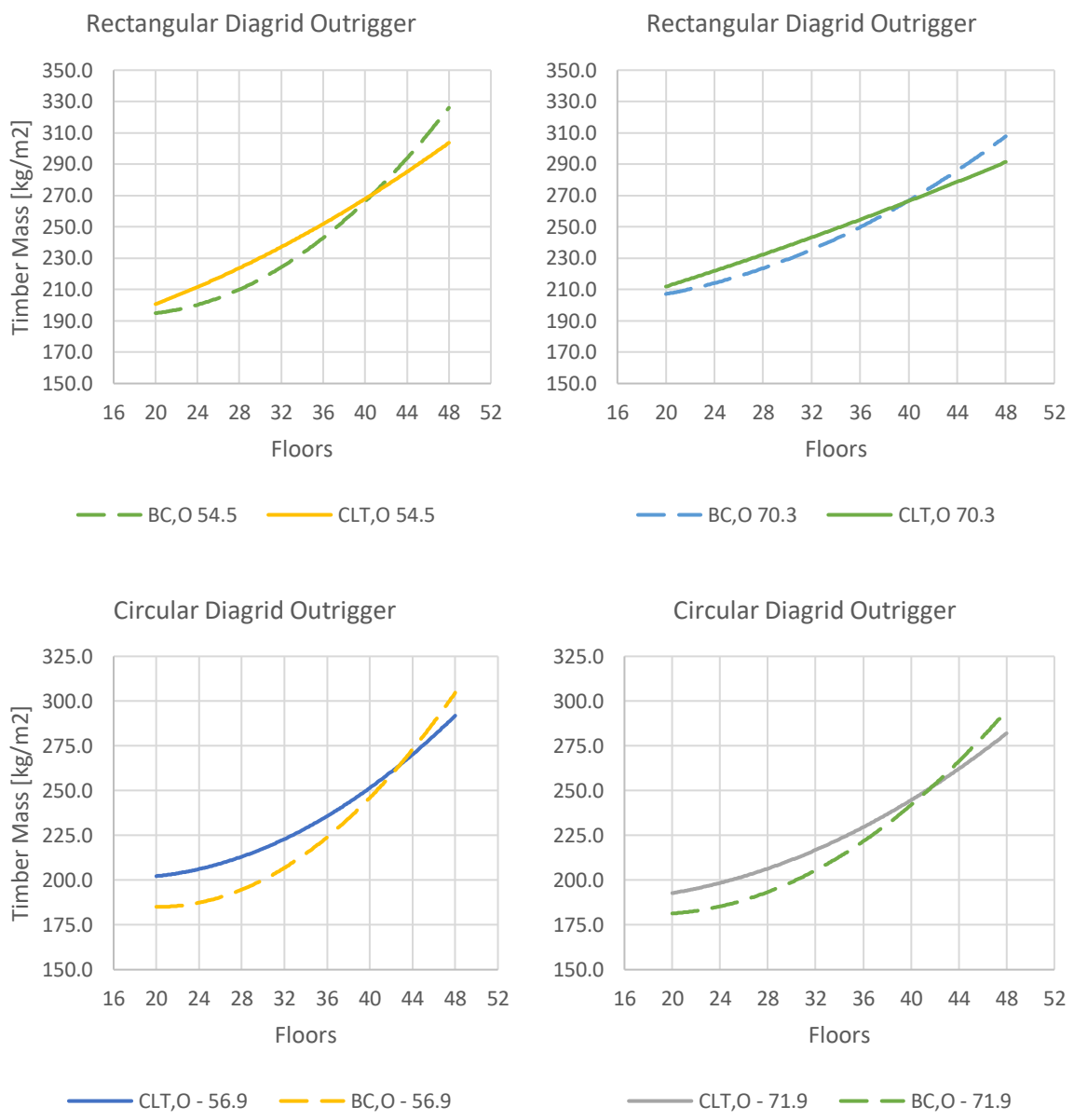


Figure 52: Comparison of outrigger systems of a Diagrid based on Timber Mass [kg/m²]

For the behaviour of the outrigger system, the following observations can be seen:

1. The outrigger system shows better performance when compared to the plain core systems (as seen in Figure 50, previous page). Effect on rectangular structure considerably higher than a circular structure.
2. The outrigger is more efficient combined with a braced core up to ± 40 floors, structures taller than ± 40 floors are more efficient with a CLT core.
3. The material efficiencies of an outrigger, especially combined with a braced core, seem to decrease exponentially over height.

Following the outrigger and diagrid studies, the effect of the outrigger with a megaframe is assessed in Figure 53.

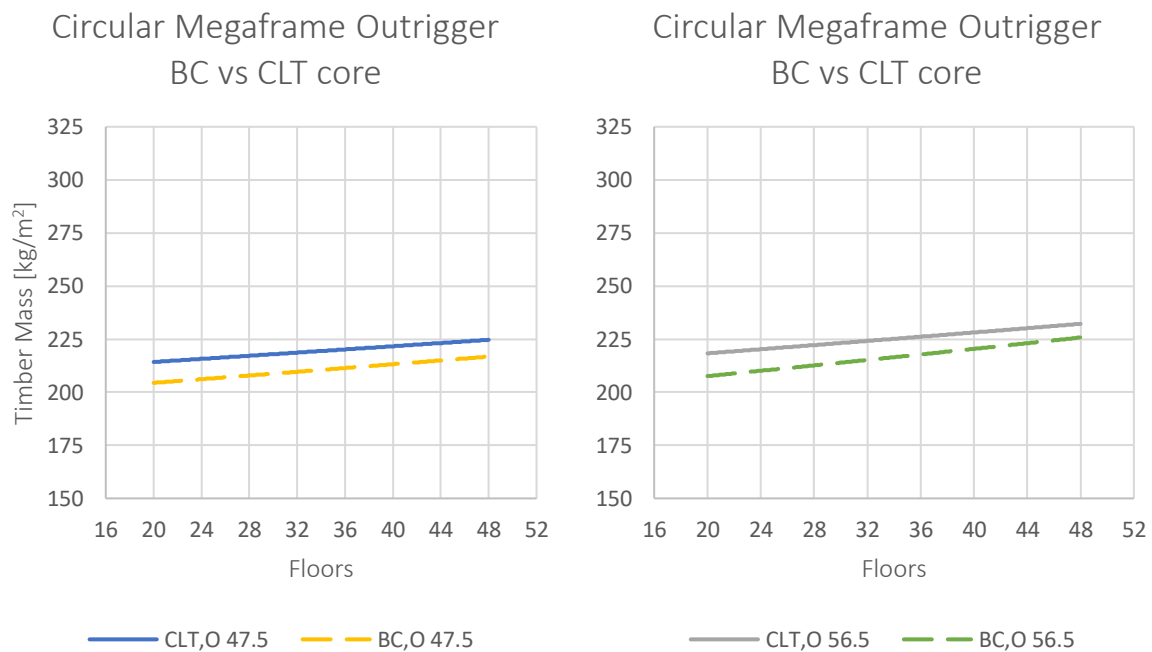


Figure 53: Comparison of outrigger systems of a Circular Megaframe based on Timber Mass [kg/m²]

From Figure 53 can be concluded that for a circular megaframe:

1. An outrigger with a braced core is more material efficient than an outrigger with a CLT core.

4.2 ANALYSIS

4.2.1 COMPARISON OF SYSTEMS

After comparing configurations within exterior systems, a comparison should also be made between varying systems. By making these comparisons, this thesis aims to produce design guidelines for realising efficient timber high-rise structures. When looking at Figure 54, showing most material efficient results from key configurations, it can be seen that:

1. Circular configurations are more efficient than rectangular configurations
2. Most material efficient configurations all belong to a system with an outrigger
3. The diagrid configuration is most efficient up to 33 floors, ± 100 m
4. The megaframe configuration is most efficient from 33 floors and higher

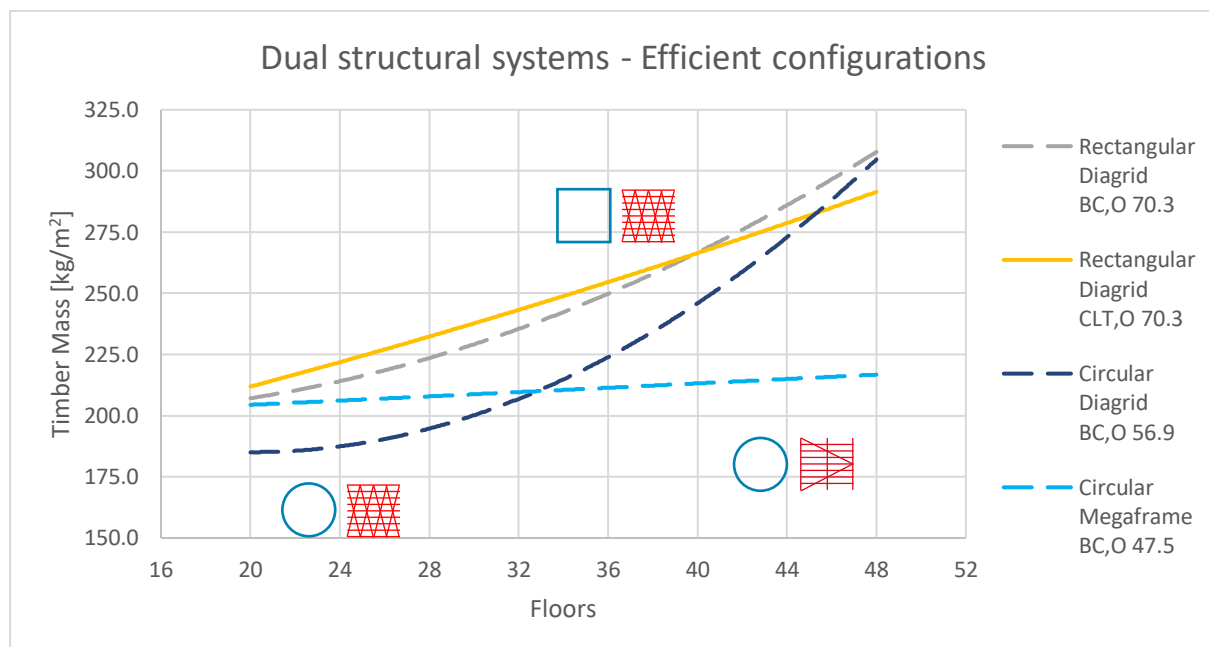


Figure 54: Comparison of dual structural systems – material use

4.2.2 MASS INFLUENCE

An analysis had been performed to study the influence of mass on the high-rise's accelerations. Adding mass might be a strategy for lowering material use by decreasing accelerations, requiring less stiff structures, as it has been found that the weight of the structure has a considerable influence on the structure's dynamic behaviour. Figure 55 shows the influence of increasing the superimposed dead load (SDL) on the building's accelerations for varying heights, showing a clear decrease in acceleration when more weight is added to the structure. As a design strategy, a method could be applied where mass is added to the structure, for example by adding material with a very low embodied carbon. By doing this the material use of structural elements is decreased while no structural timber is added.

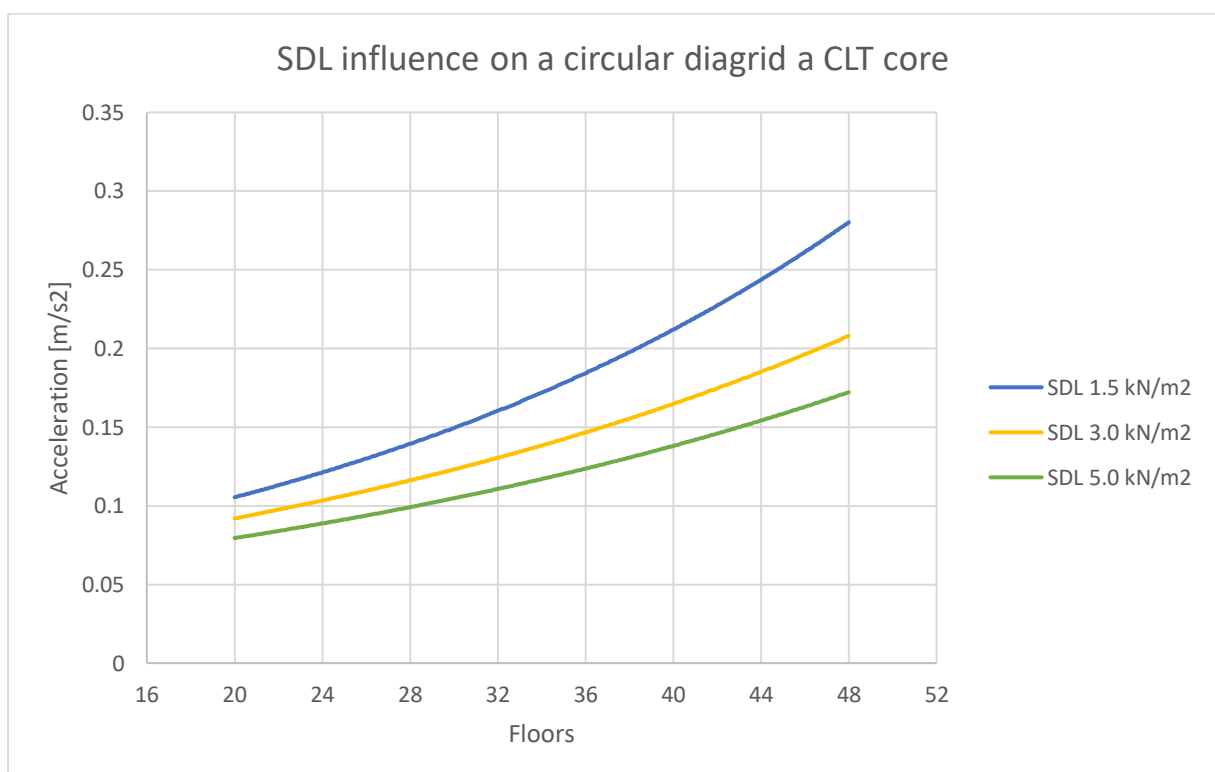


Figure 55: SDL influence on a circular diagrid with a CLT core

4.3 ACCEPTANCE CHECK

When considering interior systems for a timber dual-system high-rise structure, the accessibility of parts of the floorplan needs to be evaluated. Due to the fact that construction in timber is limited by joint rigidity, structural systems are studied that rely on hinged connections, hence the wide application of bracings. However, when applying a braced core or an outrigger system, it should be thought that braces obstruct the passage from one side of the system to the other.

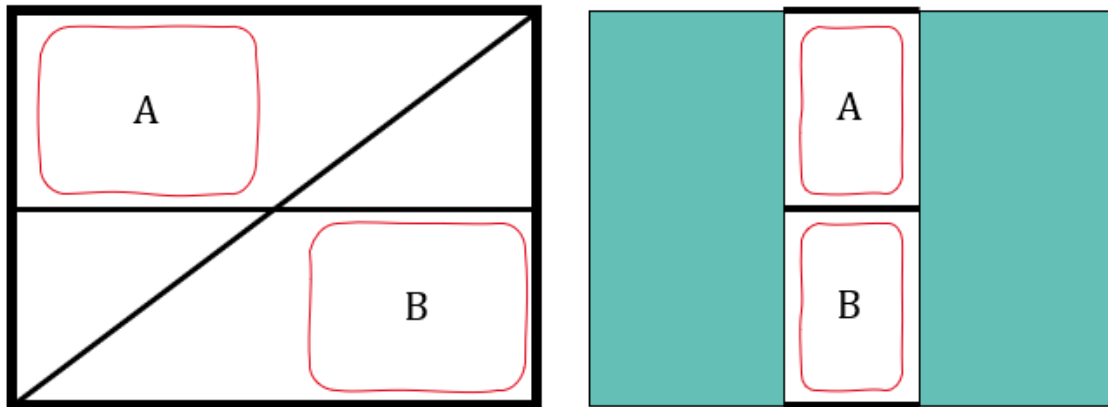


Figure 56: Accessibility of a braced core (left) and a CLT core (right)

As can be seen in Figure 56 above, the braced core (left) allows passage at an alternating location for each floor. While it allows passage, it still might not be ideal for implementation for a core system, when smooth vertical transportation through the system is desired. On the right of the figure, the CLT core system is displayed, where passages A and B are located at the same place within the core. Although a smaller area of passage is created for the CLT core (right), it might be more desirable as the layout of the vertical transportation system can remain unchanged for every floor.

Lastly, the outrigger system composes many difficulties when regarding the accessibility from one part of the system to the other. The outrigger bracings have a near 45° angle which highly obstruct any passage.

The accessibility of an outrigger system when applied to a circular floorplan is less problematic than a rectangular floorplan. Although the structure benefit most if the lever arms reach the façade, the floorplan is obstructed by it. Figure 57 shows the accessibility for a circular floorplan. The outrigger blocks parts of the effective floorplan but occupants are allowed to walk around the structural elements.

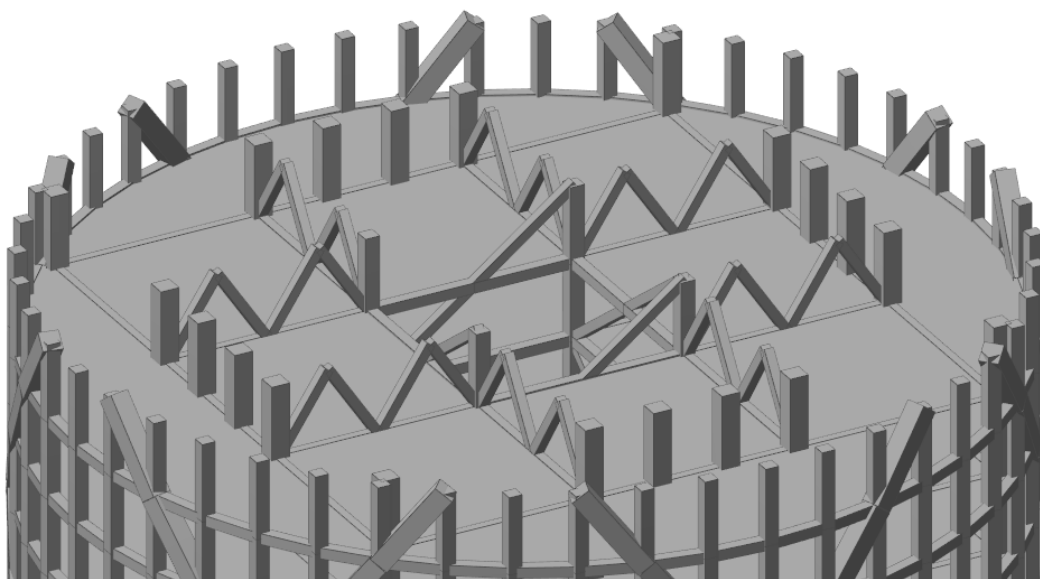


Figure 57: Cross-section of a circular megaframe with an outrigger showing the accessibility of the floorplan

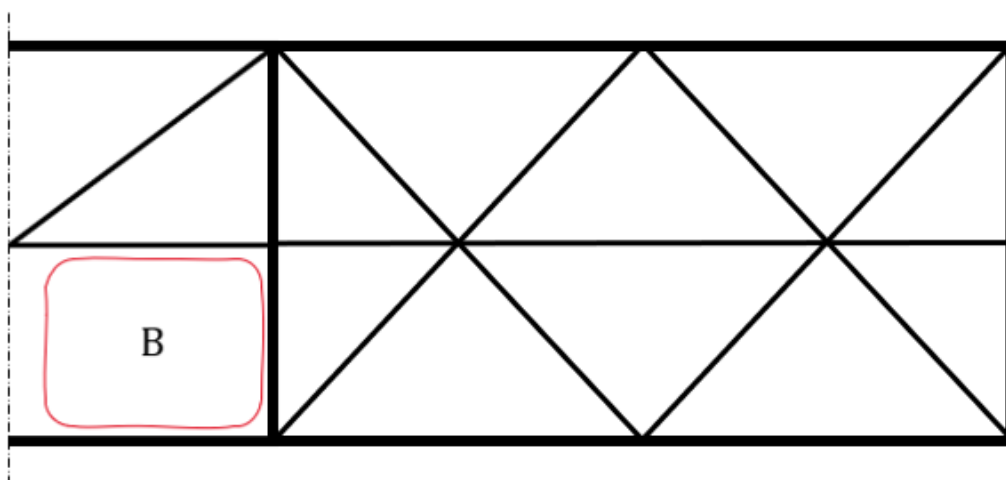


Figure 58: Accessibility of outrigger active floors

5 DISCUSSION

In this section of the thesis the results of the thesis are discussed, in order to analyse how dual structural systems can be applied for achieving desirable comfort levels in efficient timber high-rise. The outcomes of results are discussed in which assumptions made in the model are considered. The aim of this thesis is to study configurations of dual structural systems, assessed on their material efficiency.

5.1 GEOMETRY GENERATION

First the steps taken to generate the structure's geometry are discussed, following the workflow shown in Figure 59.

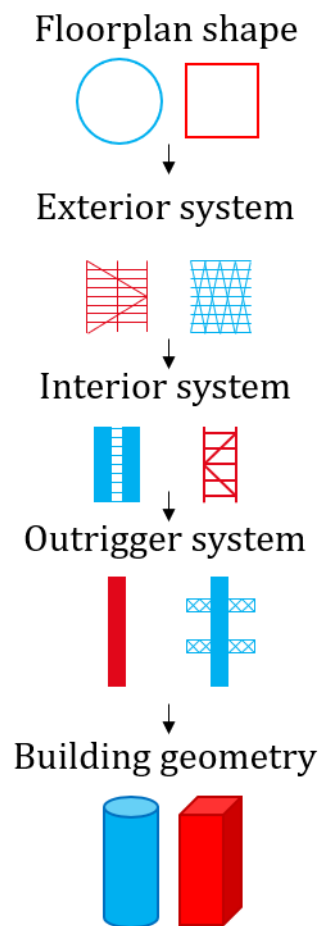


Figure 59: Workflow building geometry

5.1.1 FLOORPLAN SHAPE

Results have shown superior performances for circular floorplan shapes compared to rectangular shaped building. This can be related to the force coefficient factor (c_f), discussed in section 2.2.4. Due to the shape of the building, up to 75% higher accelerations are expected for a rectangular shaped building compared to a circular shape. However, due to the reduced width (30 m rectangular vs 35 m circular) and the design of the outriggers (section 3.1.4), the results show to be closer to each other than the force coefficient would suggest.

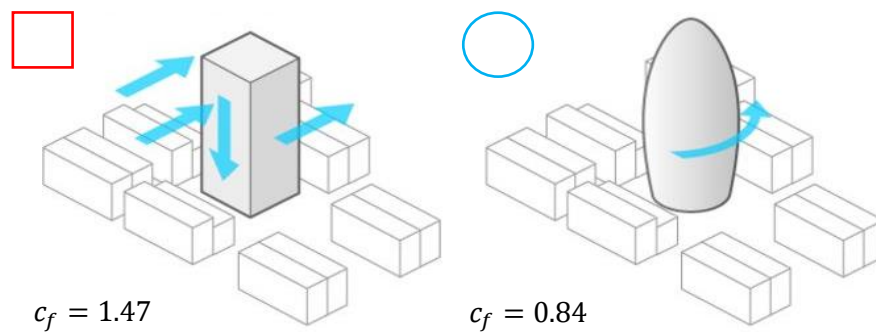


Figure 60: Floorplan shapes and their corresponding force coefficients

5.1.2 EXTERIOR SYSTEM

Exterior systems have a larger share in withstanding wind induced loads compared to interior systems, as their distance to the neutral axis is larger than that of a core system (Steiner's theorem). Improving the efficiency of the exterior systems therefore is more influential to the global efficiency than enhancing the interior system's effectiveness. For the exterior systems results have shown two influential parameters on the material use of the configuration:

1. Bay density
2. Brace angle

5.1.2.1 BAY DENSITY

Most material efficient results correspond to configurations with a higher bay density, shown in Figure 61 and visualized in Figure 62. This can be explained by the formula for bending stress distribution in combination with the moment of inertia using the parallel axis theorem (Steiner's rule).

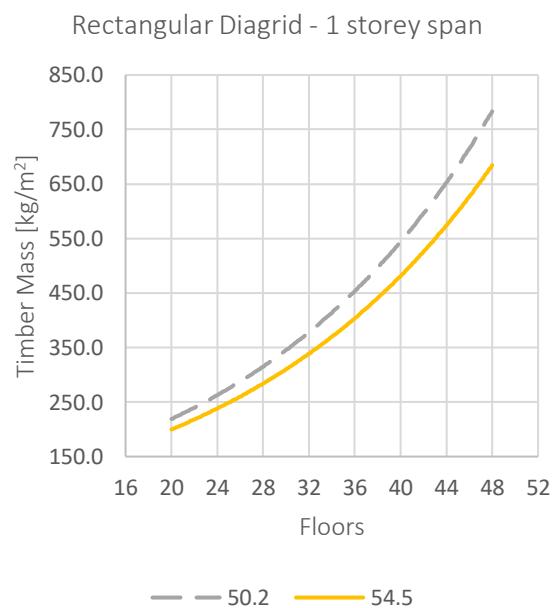


Figure 61: Rectangular Diagrid - Bay density

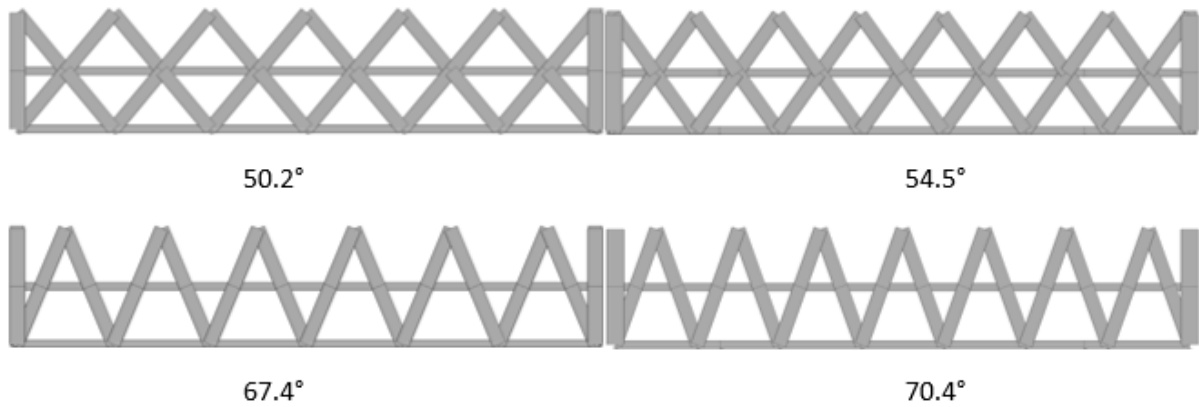


Figure 62: Visualisation of bay density for varying bay angles

The load at any given point along the stress distribution is influenced by the moment of inertia, whereas a higher moment of inertia results in smaller loads. The moment of inertia is largely affected by the amount of material along the façade, and the location of this material (Steiner's rule). Therefore, when the diagrid densifies, the share of Steiner's rule increases in the moment of inertia. Because of this relation it can be justified that by increasing the diagrid density, the required load resistance at any given point will decrease.

Moreover, a lower shear lag effect (section 2.2.5) is found when a larger bay density is present, resulting in a more linear stress distribution along the bays. When fewer horizontal segments are present critical bays must withstand higher loads compared to non-critical bays. Yet if all bays are sized equally, this results in over dimensioning of non-critical bays. Compared to a denser bay configuration, the non-critical bays are relatively higher oversized, resulting in less material use for the configuration.

5.1.2.2 BRACE ANGLE

Consecutively, results have shown that the most efficient bay angle varies over the height of the structure. As the structure grows taller, the optimal brace angle increases too, making it a valuable design consideration. This relation can be compared to the stress trajectories in a cantilever beam (Figure 63), which are similar for a tube system.

Stress trajectories show the course of the stresses over the profile of the beam. The nature of the stress trajectories is that stress paths cross the neutral axis at 45° and intersect orthogonally. Keeping these two properties into account, it is evident that for taller structures the stress trajectories occur over a longer length of the bottom stories, increasing optimum brace angles.

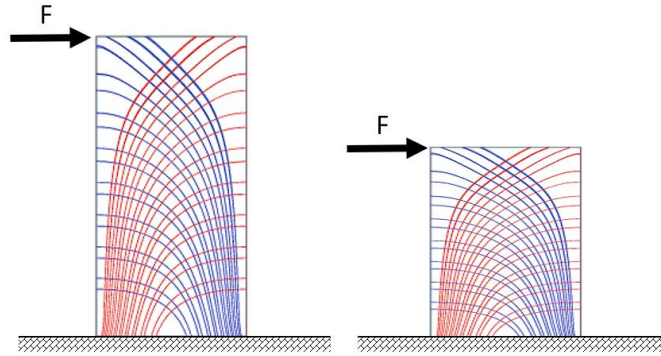


Figure 63: Relation bay angles and height for configurations

Additionally, Scaramozzino et al., 2022 confirm that the bay angle is depending on the behaviour of the structure. Stating that a 35° angle result in optimal shear resistance, whereas a 90° angle is optimal for bending resistance, as it is best to resist overturning moments.

As discussed in section 0, the relation between the bending and shear resistance determining the structure's natural frequency is set in dimensionless parameter α (Rossmann et al., 2015).

$$\alpha^2 = \frac{(GA)_{tot}}{(EI)_{tot}}$$

Equation 17: Dimensionless parameter α (Rossmann et al., 2015)

With shear and bending stiffnesses:

$$GA = \frac{F * h}{\delta}, \quad EI = \frac{1}{3} * \frac{F * h^3}{\delta}$$

Equation 18: Shear and bending stiffness

And Van Oosterhout's approximation for the natural frequency:

$$n_{1,x} = f(\alpha h) * \sqrt{\frac{q_w * h}{\mu * \delta_{max}}}$$

Equation 19: Natural frequency (Van Oosterhout, 1991)

Combining Equation 17, Equation 18 and Equation 19 prove that for taller structures, the bending stiffness' share increases in the determination of the natural frequency. As the bending stiffness becomes increasingly dominant, a larger brace angle is more efficient for taller structures.

5.1.2.3 RECTANGULAR MEGAFRAME

The rectangular megaframe has been discarded in advance because results have shown that unrealistic dimensions were required for a 60 floors configuration, making the rectangular megaframe not feasible for efficient timber high-rise. However, a critical view on the creation of the rectangular megaframe pinpoints model assumptions which lead to a design with decreased stiffness.

In the structural model, elements are spanning between each node, modelled as free rotating hinges. Therefore, no continuous elements are present in the structure. As a result, negligible bending moments are present in the megaframe's façade elements. In the structure, maximum bending moments of 2500 Nm are perceived.

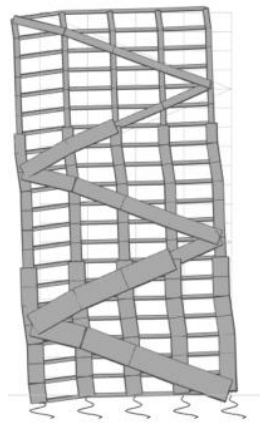


Figure 64: Deformed view of the rectangular megaframe

Due to the absence of continuous elements, the system lacks stiffness. Therefore, larger deformations and worse dynamic behaviour occur (Figure 64). Continuous façade columns would result in a stiffer structure with higher bending moments in the façade elements. Ideally, the façade columns would span between the end points of the braces, assuring an efficient and shape retaining exterior system.

5.1.3 INTERIOR SYSTEM

To explore the effects of dual structural systems for efficient timber high-rise, the performance on interior systems needs to be analysed. This analysis is shown in Figure 65, showing the comparison between a braced core system and a CLT core system in combination with a rectangular diagrid. The figures show a consistent better performance for the braced core alternative compared to the CLT core, as the graph shows a continuous equal offset for each configuration.

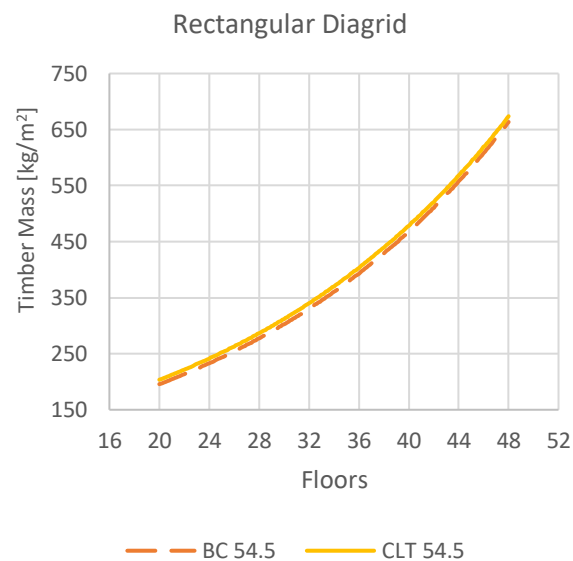


Figure 65: Timber mass for configurations over height - Rectangular diagrid braced core vs CLT core

To study the source of the constant offset, the core participation of the 70.3° configurations is studied (Figure 66). As both the braced and CLT core contribute to less than 2% of the total stiffness, Figure 65 cannot be interpreted as such that the braced core is more efficient than a CLT core. In fact, the difference in material use solely depends on the weight difference per m² of the interior systems, as exterior systems are sized identical. Results from Figure 66 show that for dual systems in timber high-rise, plain cores assessed in this thesis barely contribute to the global stiffness of the structure.

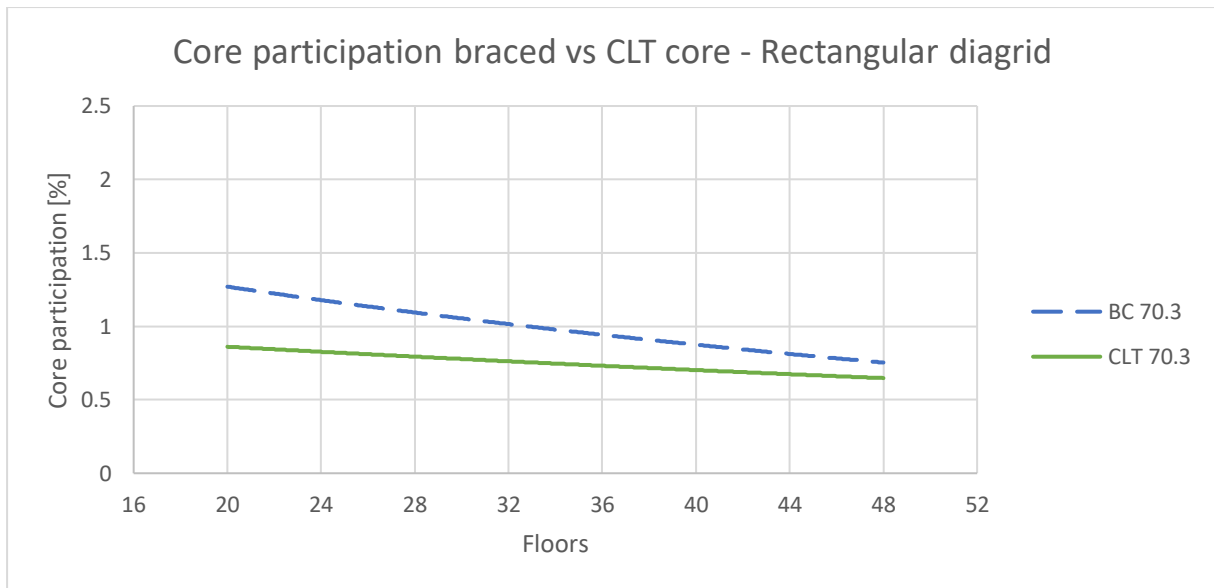


Figure 66: Core participation of a braced core and a CLT core – rectangular diagrid

Two design assumptions could cause the low participation for plain cores in this thesis: the diaphragm action of the CLT floors and the stiffness of the interior system.

Due to the modelling of the CLT floors, which have been modified with a lower bending stiffness to resemble hinged connections of the 2D elements in GSA, the diaphragm behaviour may be reduced. However, the influence of the degraded diaphragm action on the interior system's participation is insignificant, as the core participation varies within a 1% range for a 20% – 100% range of bending stiffness modifier.

Furthermore, the negligible core participation is a consequence of the bending stiffness proportions of the interior and exterior systems, being $6.89 \cdot 10^{11} \text{ N/mm}^2$ and $2.53 \cdot 10^{13} \text{ N/mm}^2$, respectively (calculations in appendix F). Therefore, the interior system has a stiffness of 2.72% of the exterior system's stiffness, clarifying its insignificant contribution.

In order to effectively apply dual structural systems for timber high-rise, interior systems should be stiffer, contributing for a larger share in the global stiffness. Without additional interior stiffness, the duality of these configurations is negligible and the interior systems only contribute in carrying vertical loads. Several variables could be explored to improve interior system's stiffness:

1. System dimensions
 - a. As described by Steiner's theorem, increasing the distance from an element to the neutral axis improves its capability to withstand overturning moments. Increasing the interior system's width and depth will increase its stiffness.
 - b. Increased sizing of structural elements improves the interior system's stiffness (Steiner's theorem).
2. Material properties
 - a. Material properties such as the strength, bending- and shear modulus affect the interior system's stiffness. Utilizing alternative materials such as concrete or steel would highly improve the interior system's stiffness, which is out of the scope of this thesis.
3. Connections
 - a. All joints (except for the CLT core's) in this thesis have been modelled to be perfect hinges, assuming no rotational stiffness is allowed in the connection. Section 2.1.4 states that adding rigidity to a timber connection might be either complex or incredibly expensive. The interior system's stiffness could be increased if semi-rigid connections are assumed.
 - b. For a timber interior system the connections are largely influential for the rigidity of the system. For CLT cores, the performance is governed by the connections between CLT panels. In this thesis, orthogonally connected CLT panels have been modelled with rigid connections. To resemble governing connections the stiffness of the CLT core has been reduced with 70%, as proposed by Verhaegh et al. (2020). To study the influence of the CLT core stiffness reduction on the global performance, Figure 67 and Figure 68 are created. Both figures clearly show that the influence on the structure's acceleration is nihil, which can be explained by the negligible participation of the interior system.

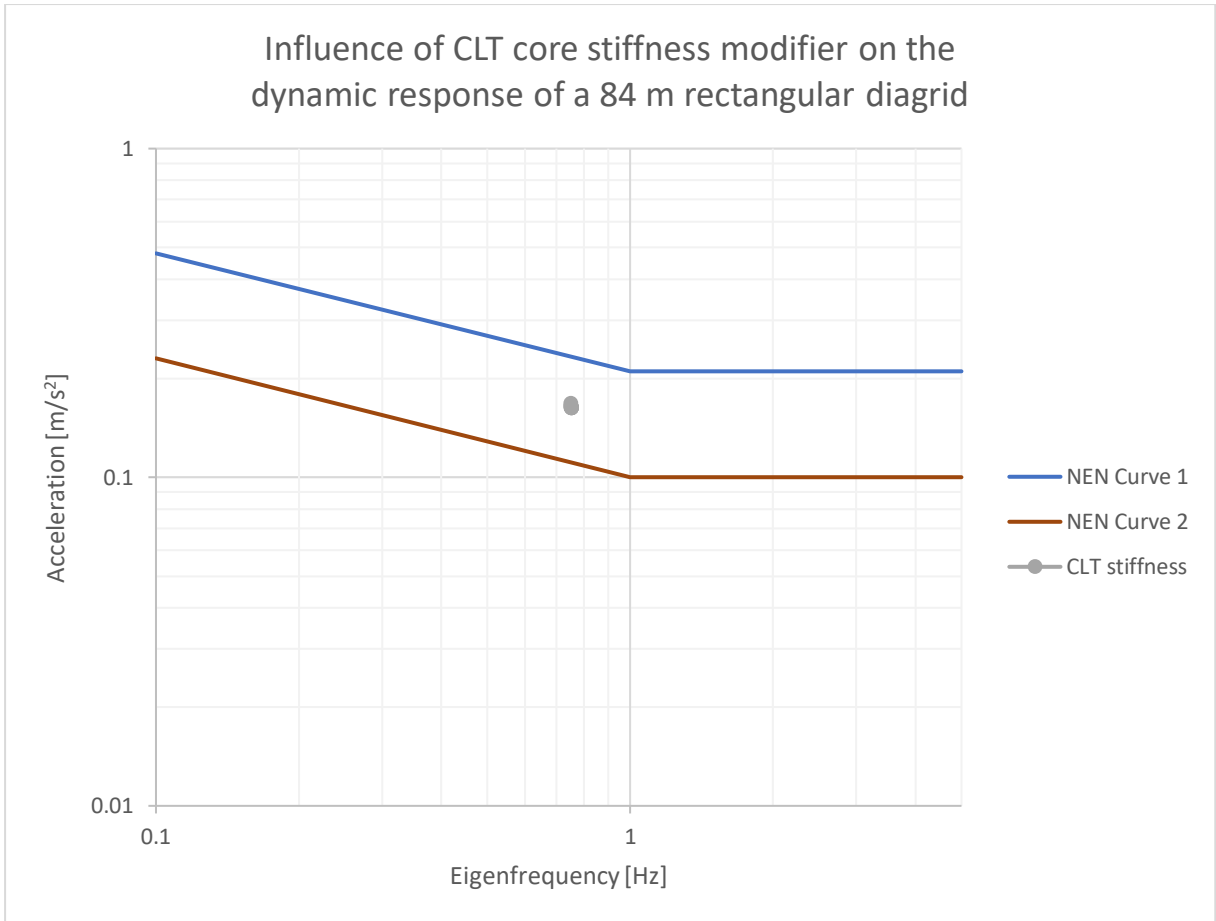


Figure 67: CLT core stiffness influence based on NEN6702 evaluation curves

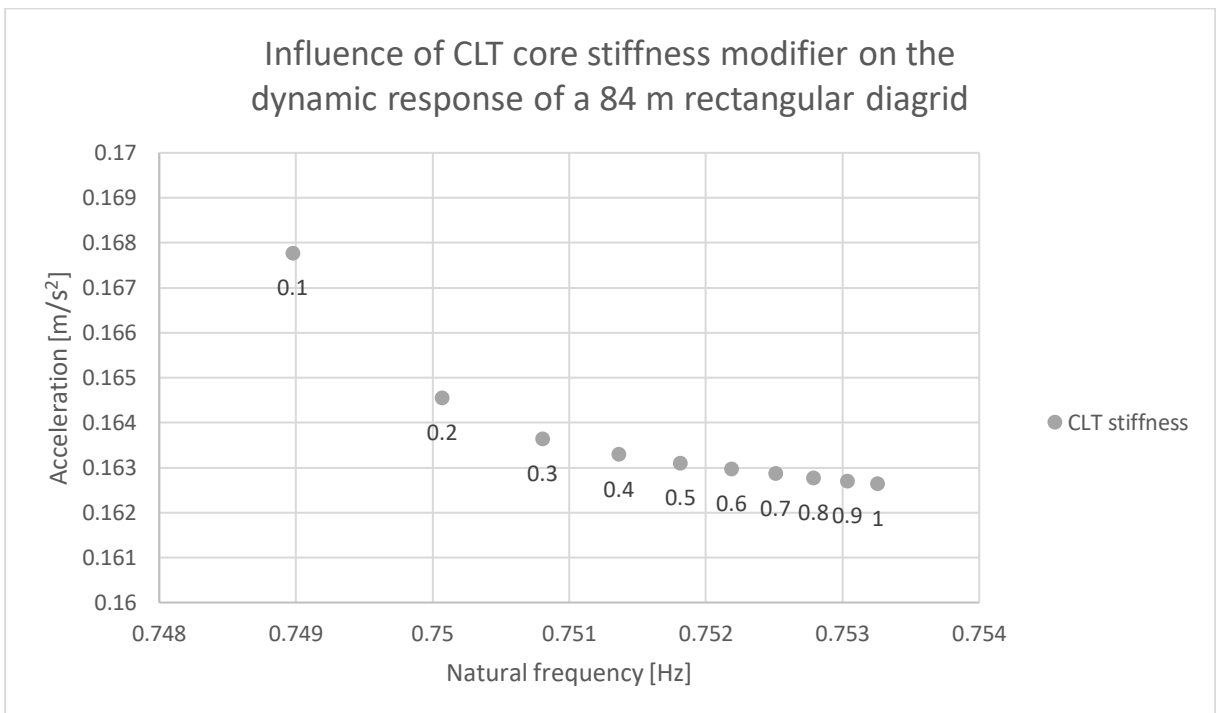


Figure 68: CLT core stiffness influence - detailed view

5.1.4 OUTRIGGER

To improve the dual performance of interior and exterior systems the outrigger system is studied. Results show the outrigger structure to be most effective when applied to a rectangular structure. This result can be traced back due to the design considerations made for a circular and a rectangular outrigger, as seen in Figure 69.

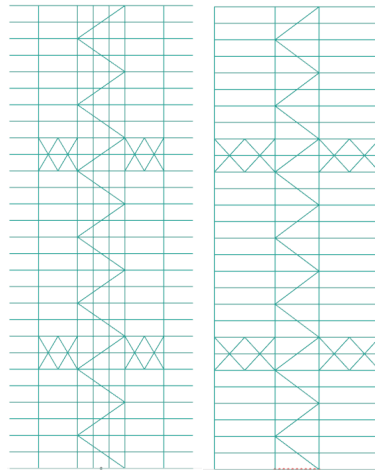


Figure 69: Lever arm of the outrigger

Varying lever arm lengths for circular and rectangular alternatives are caused by the configurations of structural elements. The outrigger systems are an extension of the core dimensions, spanning from the core perimeter towards the façade perimeter. Misalignments of the outrigger and diagrid joints are inevitable as multiple configurations of horizontal segments and storey spans are studied (Figure 70).

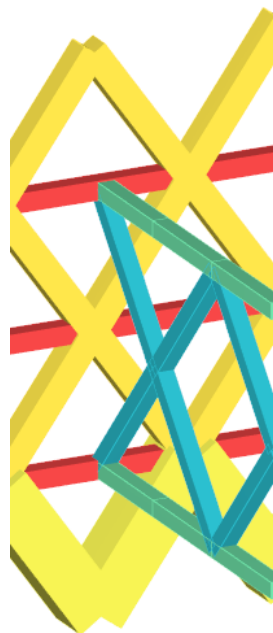


Figure 70: Misalignment of outrigger system and diagrid joint

This misalignment would be detrimental for the efficiency of the outrigger structure, as axial loading is transferred at the lever arm's ends. More efficient load transfer would occur when the lever arm ending is supported by an element that is proficient at axial loading. A column (Figure 71) would improve the efficiency of the system compared to a spanning beam (Figure 70).

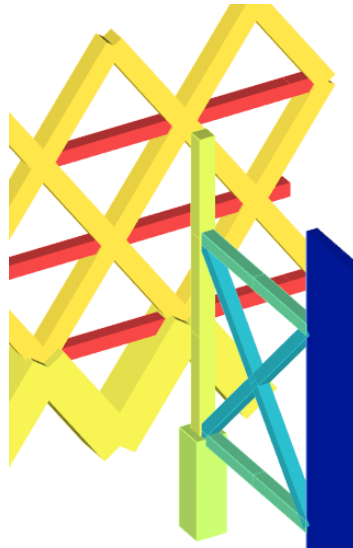


Figure 71: Outrigger lever arm supported by a column

Due to the preferred loading mechanism at the lever arm ends of the outrigger, the circular structures have been modelled with stiff arms extending towards the row of internal columns, allowing axial loading. Rectangular structures are modelled with façade reaching lever arms. If the outrigger is modelled as has been done in Figure 70, the large loads from the outrigger system must be withheld by the spanning façade beam, which is unfavourable as the bending resistance of the beam becomes highly critical. In this thesis, it has not been checked whether the loaded façade beams of the rectangular outrigger would satisfy unity check for strength (as described in section 3.3.1.1). Moreover, by increasing the stiff-arm length of the outrigger, the moment capacity of the outrigger will progressively be improved.

Moreover, an outrigger system functions as a connection between opposing facades. The occurring mechanism can be compared to the addition of extra webs over the cross-section of the structure, increasing the collaboration of opposing façades (flanges) and thus increasing the global stiffness.

Figure 72 depicts the participation of the exterior system on the structures moment resistance, showing a higher participation for structures with an outrigger. By adding outriggers, opposing facades are activated to resist overturning moments, efficiently utilising the opposite flanges of the structure.

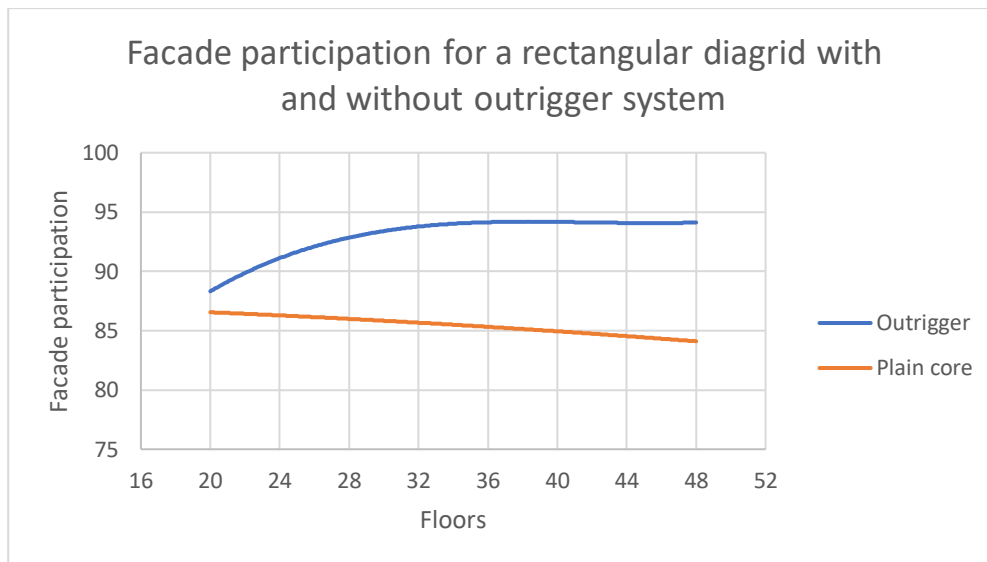


Figure 72: Core participation for a rectangular diagrid (54.5°) with and without outrigger system

Figure 72 shows a stagnated façade participation for an outrigger configuration from 28 floors onwards. As overturning moments increase, the flow of forces through the structure’s changes. Due to the misalignment of the outrigger arm and the diagrid joint, the flow of moment resisting forces prefers to follow the most efficient load path, utilising the internal columns of the structure and increasing their participation, as can be seen in Figure 73.

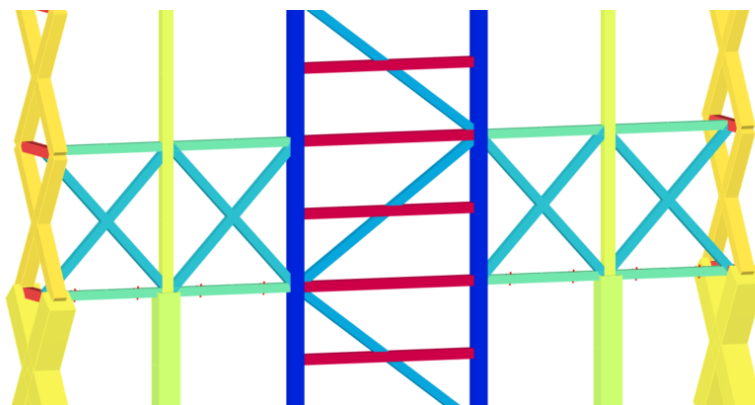


Figure 73: Cross-section of a diagrid system with a braced core and outrigger

Figure 74 shows the increased axial loading of internal columns due to the wind load only, showing a clear increase for structures taller than 28 floors, corresponding with the stagnating façade participation.

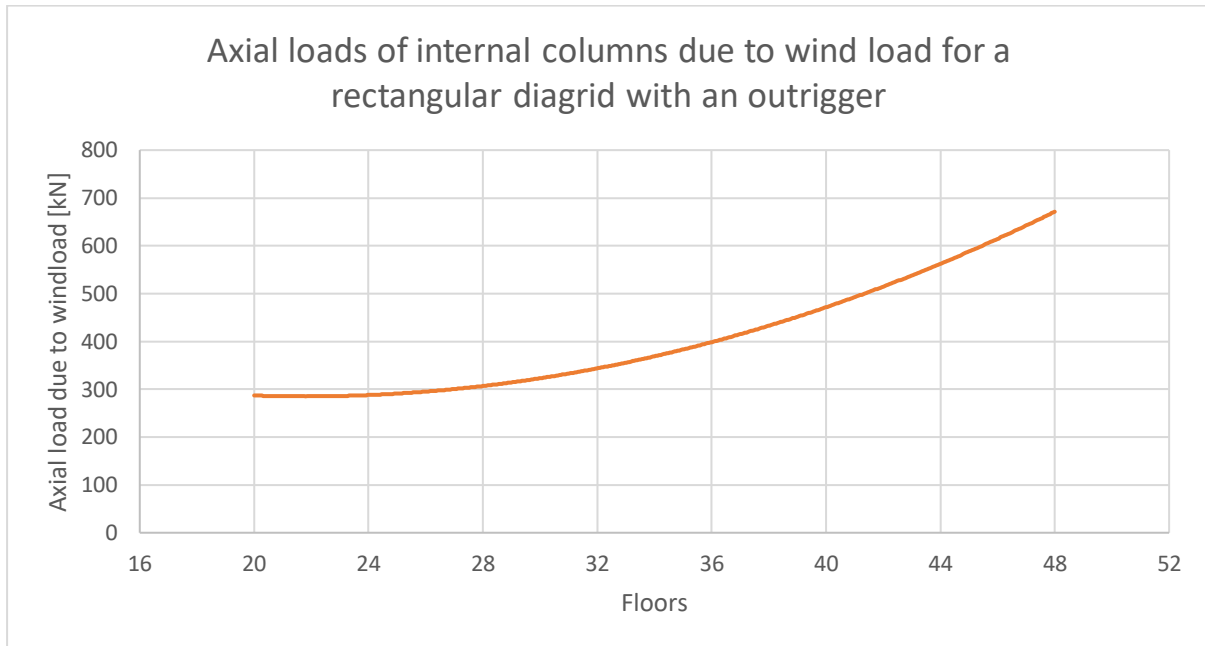


Figure 74: Axial loads of internal columns due to wind load for a rectangular diagrid with an outrigger

Moreover, Figure 75 shows that the outrigger performs different when attached to a braced core (BC) or a CLT core, a trend that has been seen for all configurations.

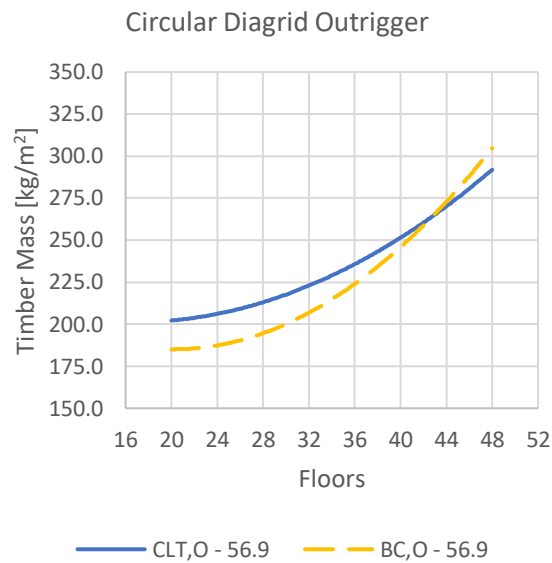


Figure 75: Circular diagrid outrigger - BC vs CLT core

The more efficient performance of a braced core for lower structures is due to the activation of internal columns for resisting overturning moments, the internal columns being located below the lever arm tips. Table 17 shows the axial loads in interior columns due to a constant wind load, displaying an increase in axial loads of 15% for the braced core and increase of 61% for the CLT core. Moreover, the ratio BC:CLT core of axial loading shifts from 2:1 to 1.4:1, a significant reduction of the dominance of the braced core.

Interior system \ Floors	20	48	Increase
Braced Core	600 kN	690 kN	15 %
CLT Core	300 kN	484 kN	61 %

Table 17: Axial loads internal columns for a Circular Diagrid Outrigger

This shift in effectiveness from the braced core to the CLT core is clarified by the deformation behaviour of a braced frame and a cantilevered beam, which resemble the braced core and the CLT core respectively. As the exterior diagrid deforms as a cantilevered beam (2.3.2), the deformation of the CLT core follows the same deformation path. Resulting in larger deflections for taller structures, activating larger axial loads in outrigger supporting columns. In contrast, the braced frame (BC) seemingly has larger deformations at lower heights and straightens at taller heights, decreasing its deformation and thus the activation of internal columns.

Lastly, application of an outrigger structure to a megaframe can reduce material use up to 46%, from 402 kg timber per m² to 216 kg/m². When an outrigger is applied to the megaframe, the system is less susceptible to brace angles for determining its structural efficiency, as combining diagonal braces and vertically oriented columns offer efficient load paths to enable shear and bending stiffness. Smaller megaframe angled configurations are more efficient as a lower megaframe angle implies less columns being added in the façade (as explained in section 3.1.2.2.1). Additional columns might become unnecessary and ineffectively increase the material use.

In conclusion, by adding an outrigger to a rectangular diagrid system, the material use can be reduced from 590 kg/m² to 290 kg-/m², a reduction of nearly 50%. This reduction corresponds to the increased contribution to the global stiffness of the façade active system and activation of internal columns to resist overturning moments. For the internal columns to be effectively activated, interior systems need to be chosen based on the structure's height, as the axial loading of the columns depend on the interior system's deformation. Due to an outrigger the façade participation can reach up to 94%, compared to the 84% of a plain core.

5.2 ANALYSIS

5.2.1 COMPARISON OF SYSTEMS

When comparing most efficient configurations of alternative systems, results in section 4.2 have shown an intersection between the trendlines of the circular diagrid and megaframe. At ±33 floors, the circular megaframe, combined with a braced core and an outrigger has shown to be the most efficient structure.

Properties of the megaframe are superior bending stiffness, as the columns are vertically oriented, being the most efficient for resisting overturning moments. As described in section 5.1.2.2, Equation 19 (the approximation for the natural frequency by Van Oosterhout, 1991), a higher bending stiffness – shear stiffness ratio results in a lower natural frequency.

Therefore, Figure 76 has been created, showing the ratio of the bending stiffness compared to the shear stiffness for the circular diagrid (most efficient up to 33 floors) and the circular megaframe (most efficient for 33 floors and higher). As can be seen in the figure below, both trendlines also intersect at 33 floors, confirming that a high bending stiffness – shear stiffness ratio is desired when designing efficient timber high-rise.

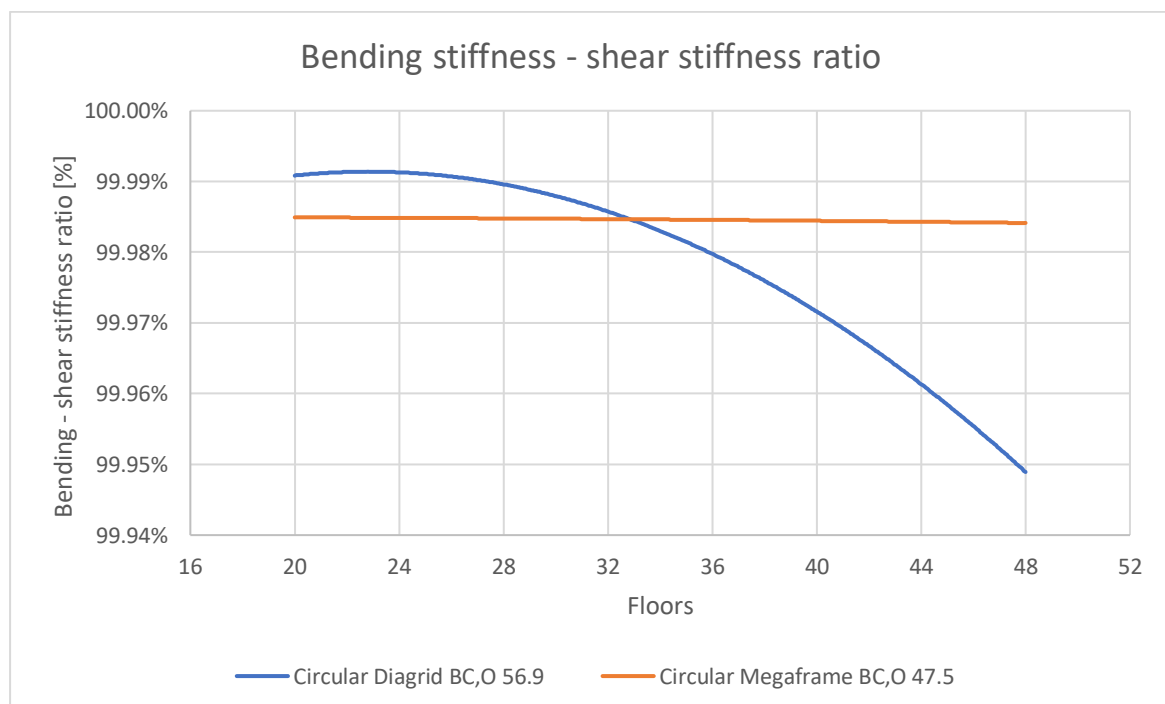


Figure 76: Shear and bending stiffness ratio Circular Diagrid and Megaframe

5.2.2 ESTIMATOR FUNCTION

Element sizing in this thesis is performed to fulfil acceptance levels thresholds (section 3.3). To be able to have proper sizing per configuration, the workflow from Figure 77 has been set-up, as discussed in section 3.3.2.

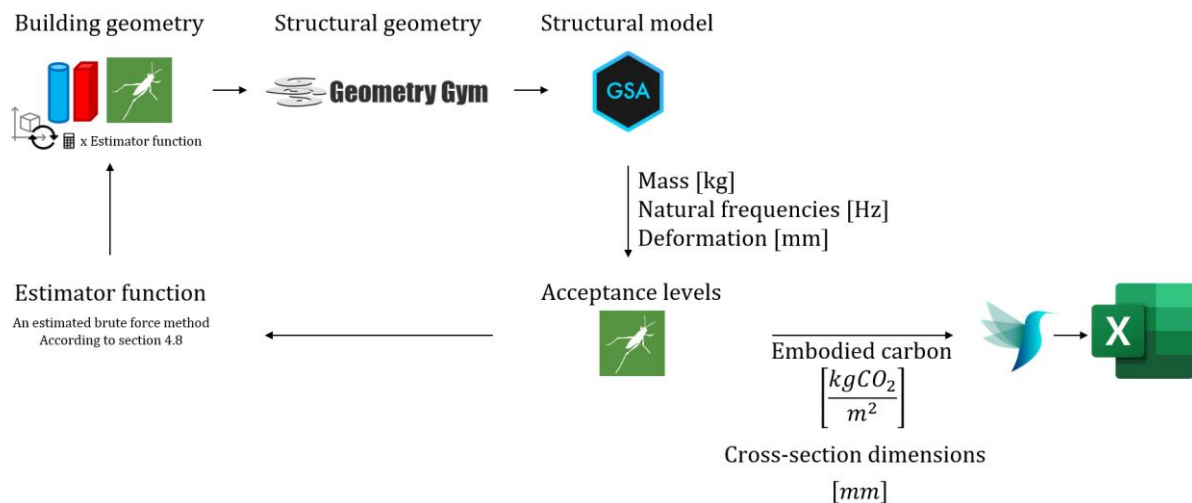


Figure 77: Workflow parametric model showing dimensioning method

Whereas the development of the estimation function offers an adequate adjustment to compromise between accuracy and speed of the brute force method, there still is a range of accuracy present in the results found in the thesis. The aim of the estimator function is to calculate numerous variants within manageable time and to make alternative configurations comparable, which is assumed to be possible if acceptance levels are within the 0.9 – 1.0 range. However, this range still implicates a 10% variance of the results, which is significant when looking at timber mass levels.

The objective of this thesis is focused on making substantiated comparisons between configurations varying in shape, height, interior- and exterior systems in a preliminary phase, for which less detailed designs are perfectly usable. If configurations are created using the same assumptions, justified comparisons can still be made, making the estimator function a sufficient approach, as the course of the results is roughly unaffected.

5.2.3 DAMPING

An increased damping coefficient would improve the efficiency of a timber high-rise. Although not influencing the duality of structural systems, higher damping would reduce the accelerations of the structure, reducing the material use. This thesis considered a damping coefficient of 1.0%, a conservative value for timber structures. Feldmann (2006) proposes that the damping coefficients for timber structures might range between 0.64 – 2.7 %, meaning that for timber structures larger damping coefficients are achievable. When designing with high damping coefficients, it should be considered that the governing mechanism might not remain the high-rise accelerations, instead lateral deformations in the serviceability limit state becomes governing.

Moreover, damping was found to be higher when considering slip in timber connections (Feldmann, 2006). In this thesis, the axial stiffness of the timber elements was reduced by reducing the EA of the element, to have the axial deformation resemble a slip allowance in the connection. Due to the lack of literature on the topic, the influence of the slipped connections on the damping coefficient have not been studied in this thesis. However, when designing timber high-rise, damping is a largely influential variable by which the material efficiency can be improved, making it an essential design parameter.

5.3 ACCEPTANCE CHECK

5.3.1 ELEMENT DIMENSIONS

The workflow is set-up to increase element dimensions until acceptance levels are met. Therefore, results of this thesis can show optimal design configurations involving 3500 x 3500 mm dimensions, which is extremely unrealistic.

Element dimensions need to be evaluated on their feasibility based on the constructability of the joints and the density of the façade. The constructability of connections becomes problematic when large element cross-sections need to be fitted into one joint. To put element dimensions into perspective the sizing of elements in Mjøstårnet are assessed, as discussed in section 2.3.1. For Mjøstårnet, element sizing of the edge columns is up to 1485 x 625 mm, and sizes of the glulam braces are up to 625 x 990 mm. Therefore, for dimensioning of braced elements, max dimensions of 1000 x 1000 mm are considered to be achievable.

As shown in Figure 78, cross-sections of key configurations vary from 500 x 500 mm to 1750 x 1750 mm, making the rectangular and circular diagrid configurations unfeasible for structures taller than 29 and 34 floors, respectively. The megaframe configuration shows smallest element dimensions, which can be clarified by the presence of columns in the façade. Therefore, braces are not required to transfer vertical loads, and sizes can thus be smaller. In Figure 78, the continuous lines represent results that are achievable within the feasible realm of timber high-rise, which in this thesis is determined by the design of Mjøstårnet. The dotted lines represent results that may not be feasible yet, showing which boundaries should be pushed.

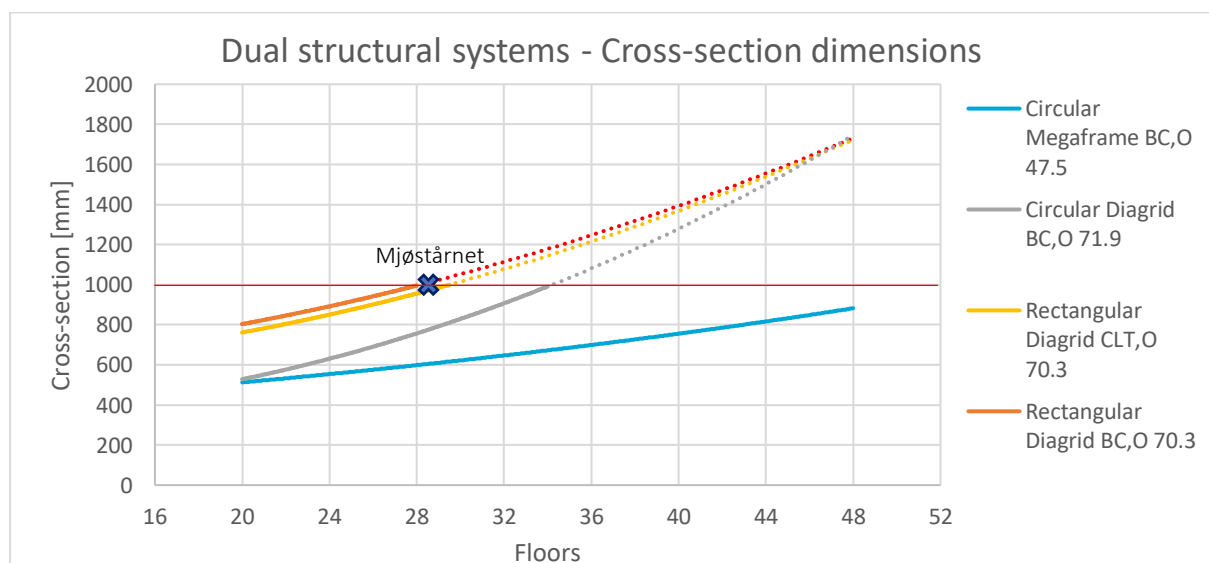


Figure 78: Comparison of dual structural systems – element cross-sections

5.3.2 ELEMENT LOADS

To be able to compare the results found in this thesis within the realm of existing timber high-rise structures, the maximum axial loads of the circular diagrid and megaframe are compared with the maximum loads in Mjøstårnet, occurring in its edge columns. Figure 79 below shows the maximum axial loads for the circular diagrid and megaframe from section 4.2.1.

The axial loads from the configurations analysed in this thesis do not occur in the edge columns. As the circular floorplan shape allow forces to flow smoothly through the façade, the edge columns are not critical in the design. Instead, internal columns below stiff arms of the outrigger are critically loaded.

If the design of Mjøstårnet would be considered as the boundaries for what would be achievable in timber high-rise, Figure 79 would suggest that the circular megaframe would only be achievable up to 37 floors, shown with the continuous line. Once again, the dotted lines resemble results that are beyond what is feasible for timber high-rise, as determined by the case of Mjøstårnet.

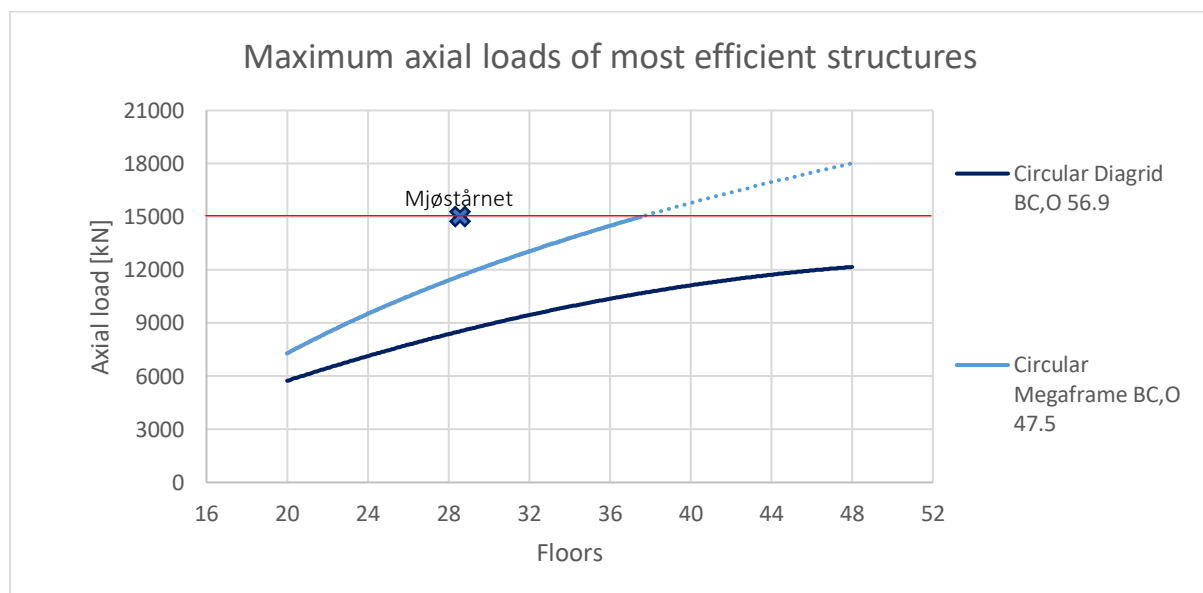


Figure 79: Maximum axial loads of circular diagrid and megaframe

5.3.3 DESIGN CODES

This thesis evaluates the dynamic behaviour based on the design codes set-up in the NTA 4614-3 and NEN6702 standards, both corresponding to the Dutch standards. Compared to the ISO10137:2007(E) standards, the Dutch standards allow more noticeable and frequent vibrations at top floors of the structure. It should be considered that the findings of this thesis comply to the Dutch standards, meaning that if these findings are to be compared to ISO principles, considerably less material efficient timber high-rise is realisable.

In addition to this, when assessing the National Building Code of Canada (NBCC, 2005), design checks should only be fulfilled when several conditions apply to the structure. Whereas in the case of timber high-rise the design checks should always be performed. These design checks are only depending on acceleration of the system, and are independent of the natural frequency, resulting in a broader spectrum of allowance. Furthermore, the Japanese building codes given by the Architectural Institute of Japan (AIJ, 2004) are put together in the AIJ-GBV-2004 standard. It is noteworthy that these standards do not operate as a criterium, instead the standards are set up as a guideline stating the probability of perception of the building's occupants, making it up to the building owner to determine which threshold is aspired. Even though ISO standards would show less efficient timber high-rise structures, following the Canadian and Japanese standards would allow for more design configurations requiring less material to be constructed compared to the configurations made in this thesis, as permitted by the Dutch standards.

6 CONCLUSION

In this section the outcomes of this thesis are summarized and concluded. This is done in an effort to give answer to the main research question of this thesis. The main research question reads:

“How can dual structural systems be applied for achieving desirable comfort levels in efficient timber high-rise”

Key observations on *how* to use dual structural systems for achieving efficient timber high-rise are:

1. Dual structural systems can achieve up to 50% material reduction if systems are connected with an outrigger, increasing the participation of the exterior system by 10%.
2. The effect of dual structural systems without an outrigger is negligible, as the stiffness of a timber core system is below 3% of the global stiffness.
3. The effectiveness of a configuration depends on the bending stiffness – shear stiffness ratio. A higher ratio results in lower natural frequencies, decreasing the required material.
4. Most efficient configurations are shown in Figure 80, with continuous lines showing feasible results, as discussed in sections 5.3.1 and 5.3.2. Dotted lines resemble results that are beyond the, to this point, viable realm for timber high-rise structures :
 - a. 20 – 33 floors, a circular 56.9° diagrid with a braced core and an outrigger system shows to be the most efficient alternative
 - b. 33 – 37 floors, a circular 47.5° megaframe with a braced core and an outrigger system shows to be the most efficient alternative

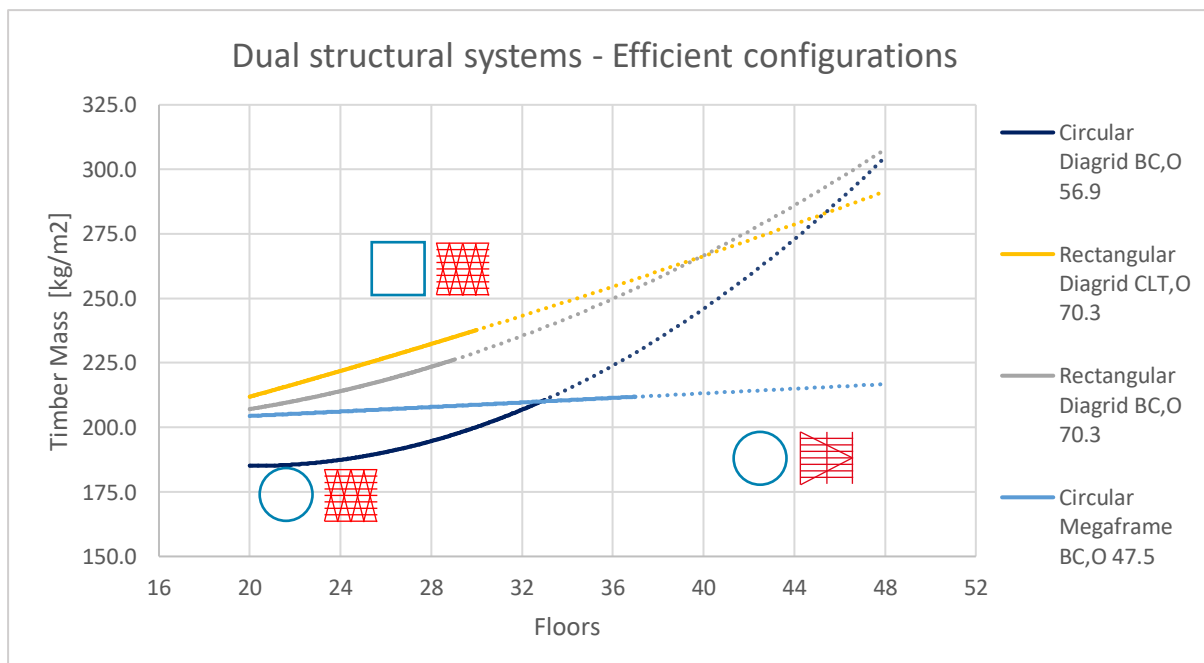


Figure 80: Dual structural systems - configuration effectiveness

Abovementioned observations are substantiated by the following conclusions:

1. Floorplan shape

Rectangular shaped structures ($c_f = 1.47$) can have up to 75% higher accelerations compared to circular shaped structures ($c_f = 0.84$), due to the influence of the force coefficient (c_f). More efficient timber high-rise can be achieved by designing circular shaped structures, as seen in Figure 80.

2. Bay density

An increased bay density lowers the stresses along the perimeter and the shear lag effect, resulting in smaller critical loads and over-sizing of non-critical elements. Element dimensions are reduced for increasing bay densities. The addition of columns (in a megaframe) further densifies the façade, increasing the bay density effect.

3. Brace angle

The brace angle of the diagrid affects the material efficiency at varying heights. For taller structures, bending resistances become more influential over shear resistances, altering the optimal diagrid angle from 30° (shear) to 90° (bending moments). Also following the course of the stress trajectories, visualized in Figure 81. The megaframe is not impacted by the brace angle, as braces and columns collaborate in resisting shear and bending in the structure.

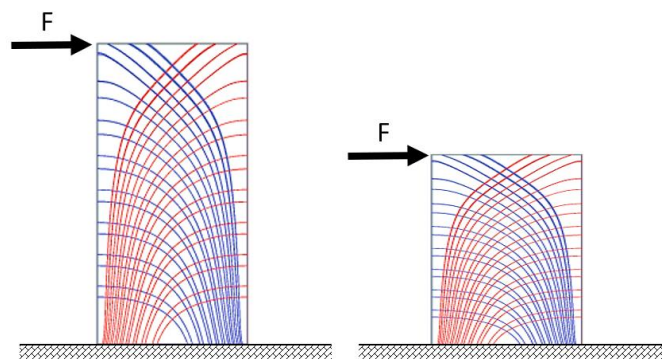


Figure 81: Relation bay angles and height for configurations

4. Interior system's stiffness

Timber-only plain cores (CLT core and braced core) show a negligible contribution to the global stiffness of a timber high-rise. Less than 2% collaboration is clarified by the proportions of stiffnesses of interior and exterior systems, interior stiffens being just 2.7% of the exterior stiffness. For dual structural systems to be applicable with a plain core, stiffer interior systems need to be applied. Recommendations for stiffer interior systems are found in section 0.

5. Outrigger

Outrigger systems can reduce the material use by 50% compared to a plain core structure. The outrigger effect is largest when:

- i) Outrigger arms reach to the façade. Façade reaching outriggers have longer lever arms and connect opposing facades. Therefore, outriggers act as additional webs, activating both flanges to resist bending moments, increasing façade participation from 84% to 94%.
- ii) Outriggers and façade nodes are aligned. Aligning lever arm tips with nodes of the exterior system avoids loading of spanning elements. Instead, when outriggers are connected to the façade node, axial loading is allowed in the exterior system.
- iii) The core system of the outrigger is selected as such that deformations of the system are largest. Larger deflections of the interior system result in higher axial loads at lever arm ends, increasing the moment resisting capacity.

6. Superimposed dead load

Increasing the super imposed dead load by 1.5 kN/m^2 can reduce accelerations by 20% for tallest configurations, resulting in less stiffness of the interior and exterior systems. If the added material holds low embodied carbon, increasing the super imposed dead load might be a strategy to reduce the structural material needed.

7 RECOMMENDATIONS FOR FURTHER RESEARCH

As a final step, this thesis encountered numerous gaps in literature and design strategies which require further studying in order to increase the feasibility for timber-only high-rise structures to be realised.

Force coefficient influence on timber high-rise design

This thesis explored the influence of the force coefficient on the design of a timber-only high-rise structure. Whereas this thesis only compared a circular or a rectangular shape, a large spectrum of influence parameters is available in order to reduce the total wind force on a body. Studies have shown positive influence of the force coefficient of twisted, inclined and interrupted facades or facades with rounded edges in order to reduce the total wind pressure. Further studies that aim to explore design strategies for realising timber high-rise structures should be performed on the influence of unconventional façade shapes for reducing lateral wind loads.

Rigidity timber connections

In this thesis the connections are assumed to be perfectly rotating hinges as a simplification because adding rigidity to timber connections is found to be a complex and expensive procedure. Further on, the influence of rotational stiffness in joints on the structure's global stiffness and dynamic behaviour might offer interesting studies. For timber-only high-rise to be realisable it is necessary to acquire a high global stiffness to which the rotational stiffness might be useful.

CLT core

To be able to properly model the behaviour of CLT cores, further studies and research is required to gain ample knowledge in order to properly design such a system. Many studies are convinced by the potential of the CLT core but further study and implementation needs to be performed to accurately design a CLT core and predict its performance.

Damping due to slip

For high-rise in general, but especially for timber high-rise where the dynamic behaviour is more critical, the influence of damping on the structure needs to be further explored to be able to satisfy the dynamic criteria with less material. This thesis implemented slip in the connections, in an attempt to simulate its energy absorption and consider it to be additional structural damping. To be able to properly exert slipped connections as a method to increase the damping coefficient, further studies are required to make proper assumptions on the influence of slip on the damping coefficient of the structure.

Dual structural systems

Whereas this thesis focused on dual structural systems in terms of interior and exterior systems, there are many combinations of systems that show potential for realising timber high-rise. Further studies should be performed on the efficiency of other combinations of dual structural systems, as combining systems have been proven to be an effective approach for timber high-rise, when connected to one another. Research should not only be limited to one structure or shape as bundling structures might be an adequate approach for an efficient design. For example, by linking two rectangular towers with a diagrid system by applying mass glulam braces, as is proposed for the River Beech Tower (see Figure 82).



Figure 82: River Beech Tower (Perkins Will, 2016)

Lastly, when considering dual structural systems in order to realise sustainable high-rise, it should be considered that constructing a timber-only high-rise might not be the most efficient approach. Although this thesis aims to research possibilities for timber-only structures, big improvements on carbon emissions can be made when a large share of element are constructed in timber, compared to a conventional non-timber design. In order to realise low carbon high-rise structures, findings from this thesis should be applied on how to apply and improve dual structural systems. Yet further studies might be relevant on which systems should be constructed in what material, in order to develop the most efficient, serviceable and realistic design.

8 BIBLIOGRAPHY

- A Smith B. Coull. *Tall Building Structures: Analysis and Design*. John Wiley Sons. Inc, 1991.
- Abrahamsen, R. (2017), *Mjøstårnet – Construction of an 81 m tall timber building*. Internationales Holzbau-Forum IHF 2017. https://www.forum-holzbau.com/pdf/31_IHF2017_Abrahamsen.pdf
- Abrahamsen, R. (2017). *Mjøstårnet-Construction of an 81 m tall timber building*. In Internationales Holzbau-Forum IHF (pp. 1-12).
- Arup. (2022). *Circular Buildings Toolkit*. Retrieved on 19 July 2022, van <https://ce-toolkit.dhub.arup.com/strategies>
- Ashtari, S. (2012), *In-plane Stiffness of Cross-laminated Timber Floors*. THE UNIVERSITY OF BRITISH COLUMBIA. https://central.bac-lac.gc.ca/.item?id=TC-BVAU-43504&op=pdf&app=Library&is_thesis=1&oclc_number=1032936627
- Blass, H. J., & Sandhaas, C. (2017). *Timber Engineering - Principles for Design*. Van Haren Publishing.
- Boafo F, Kim J-H, Kim J-T (2016) *Performance of modular prefabricated architecture: case study-based review and future pathways*. Sustainability 8:558. doi:10.3390/su8060558
- Climate Change Committee. (2019). *UK housing: Fit for the future?* <https://www.theccc.org.uk/publication/uk-housing-fit-for-the-future/>
- College Physics*. 2012. Retrieved 10 January 2014.
- Eckelman, C. A. (1998). *The shrinking and swelling of wood and its effect on furniture*. Purdue University Cooperative Extension Service.
- Ehrhart, T., Steiger, R., & Frangi, A. (2017). A non-contact method for the determination of fibre direction of European beech wood (*Fagus sylvatica* L.). *European Journal of Wood and Wood Products*, 76(3), 925–935. <https://doi.org/10.1007/s00107-017-1279-3>
- Ellen MacArthur Foundation. (2016). *The Circular Building in the Built Environment*. <https://www.arup.com/perspectives/publications/research/section/circular-economy-in-the-built-environment>
- Ellen Macarthur Foundation. (z.d.). *New to circular economy overview*. Visited on 8 februari 2022, van <https://ellenmacarthurfoundation.org/topics/circular-economy>
- EN 1991-1-4: *Eurocode 1: Actions on structures - Part 1-4: General actions - Wind actions*. (2010).
- Fang, D. & Liu, C. (2021, oktober). Mechanical characteristics and deformation calculation of steel diagrid structures in high-rise buildings. *Journal of Building Engineering*, 42, 103062. <https://doi.org/10.1016/j.jobe.2021.103062>
- Feldmann, H. & Huang, A. (2006). *Dynamic properties of tall timber structures under wind-induced vibrations*. Wood Conference of Timber Engineering

- Fleming, P., Smith, S., & Ramage, M. (2014). *Measuring-up in timber: A critical perspective on mid-and high-rise timber building design*. *Architectural Research Quarterly*, 18(1), 20–30. <https://doi.org/10.1017/S1359135514000268>
- Fu, F. (2018), *The shear lag effect*. Design and Analysis of Tall and Complex Structures, 2018 <https://www.sciencedirect.com/topics/engineering/shear-lag-effect>
- G van Oosterhout. Wind-induced dynamic behaviour of tall buildings. 1996
- Ghattas, R., Gregory, J., Noori, M., Miller, R., Olivetti, E., & Greene, S. (2016, October). *Life Cycle Assessment for Residential Buildings: A Literature Review and Gap Analysis*. MIT Concrete Sustainability Hub. https://dspace.mit.edu/bitstream/handle/1721.1/104794/LCA%20of%20Buildings_Updated%20Report_October%202016.pdf?sequence=4&isAllowed=y
- Green, M. (2012). *The case for tall wood buildings*.
- Gregoletto, D., & Da Luz Reis, A. T. (2019). High-rise buildings in the perception of the users of the urban space. *Cadernos Proarq*, 19, 90–110. https://cadernos.proarq.fau.ufrj.br/public/docs/Proarq19_HighriseBuildings_GregolettoReis.pdf
- Hafner, A., & Schäfer, S. (2017). Environmental aspects of material efficiency versus carbon storage in timber buildings. *European Journal of Wood and Wood Products*, 76(3), 1045–1059. <https://doi.org/10.1007/s00107-017-1273-9>
- Hashemi, A., Masoudnia, R., & Quenneville, P. (2016). A numerical study of coupled timber walls
Hasslacher Group, 2022, *From woods to wonders*, <https://www.hasslacher.com/data/dateimanager/broschuere/HNT-Brettschichtholz-EN.pdf>
- Horowitz, C. (2016). *Paris Agreement*. *International Legal Materials*, 55(4), 740-755. doi:10.1017/S0020782900004253 <https://doi.org/10.1016/j.conbuildmat.2016.05.160>
- IEA (2018a), *World Energy Statistics and Balances 2018*, www.iea.org/statistics and IEA Energy Technology Perspectives buildings model, www.iea.org/buildings
- Issa, C. A., & Kmeid, Z. (2005). Advanced wood engineering: glulam beams. *Construction and Building Materials*, 19(2), 99–106. <https://doi.org/10.1016/j.conbuildmat.2004.05.013>
- Kim, J., & Lee, Y. H. (2010). Seismic acceptance level evaluation of diagrid system buildings. *The Structural Design of Tall and Special Buildings*, 21(10), 736–749. <https://doi.org/10.1002/tal.643>
- Kwok, K. C. S. (1982). Cross-wind response of tall buildings. *Engineering Structures*, 4(4), 256–262. [https://doi.org/10.1016/0141-0296\(82\)90031-1](https://doi.org/10.1016/0141-0296(82)90031-1)
- Leichti, R. J. et al. (2000). THE CONTINUUM OF CONNECTION RIGIDITY IN TIMBER STRUCTURES. *Wood and Fiber Science*, 32(1), 11–19. <https://core.ac.uk/download/pdf/236633215.pdf>

Leonard, J. (2007), *Investigation of Shear Lag Effect in High-rise Buildings with Diagrid System*. Massachusetts Institute of Technology. <https://dspace.mit.edu/bitstream/handle/1721.1/39269/170876656-MIT.pdf?sequence=2&isAllowed=y>

Leško, A. (2016). Modern Moment Resisting Timber Connections – Theory and Numerical Modelling. *Procedia Engineering*, 153, 400–406. <https://doi.org/10.1016/j.proeng.2016.08.140>

Liu, C., Li, Q., Lu, Z., & Wu, H. (2017). A review of the diagrid structural system for tall buildings. *The Structural Design of Tall and Special Buildings*, 27(4), e1445. <https://doi.org/10.1002/tal.1445>

McNabb, J.W. and Muvdi, B.B. (1975), “Drift reduction factors for belt high-rise structures”, *Engineering Journal* 3rd Quarter, 88-91.

Merza, N. & Zangana, A. (2014). *Sizing Optimisation of Structural Systems of Tall Buildings*. CHALMERS UNIVERSITY OF TECHNOLOGY. <https://odr.chalmers.se/bitstream/20.500.12380/200925/1/200925.pdf>

Metabolic (2020). *Assessing all materials consumed for building in the Netherlands*. Visited on 18 July 2022, from <https://www.metabolic.nl/projects/assessing-materials-consumed-for-building-in-the-netherlands/>

Moon, K. S., Connor, J. J., & Fernandez, J. E. (2007). *Diagrid structural systems for tall buildings: Characteristics and methodology for preliminary design*. *Structural Design of Tall and Special Buildings*, 16(2), 205–230. <https://doi.org/10.1002/tal.311>

Nijssen, R. (2020). *High-rise structures* [Presentatieslides]. TU Delft. <https://brightspace.tudelft.nl>

Nouri, F., & Ashtari, P. (2015). Weight and topology optimization of outrigger-braced tall steel structures subjected to the wind loading using GA. *Wind and Structures*, 20(4), 489–508. <https://doi.org/10.12989/was.2015.20.4.489>

NTA 4614-3 (nl) *Convenant hoogbouw-Deel 3: Constructieve veiligheid Covenant high-rise buildings-Part 3: Structural safety*. (2012).

Pavel, S. (2018). Circular Economy: The Beauty of Circularity in Value Chain. *The Asian Institute of Research Journal of Economics and Business*, 1(4), 584–598. <https://doi.org/10.31014/aior.1992.01.04.52>

Polastri, A., Izzi, M., Pozza, L., Loss, C., & Smith, I. (2019). *Seismic analysis of multi-storey timber buildings braced with a CLT core and perimeter shear-walls*. *Bulletin of Earthquake Engineering*, 17(2), 1009–1028. <https://doi.org/10.1007/s10518-018-0467-9>

Rijksoverheid. (2016). *Nederland circulair in 2050*.

Rossmann, J. S., Dym, C. L., & Bassman, L. (2015). *Introduction to Engineering Mechanics: A Continuum Approach, Second Edition* (2de editie). CRC Press.

Sanner, J. et al. (2017). River Beech Tower: A Tall Timber Experiment. *CTBUH Journal*, 2017(II), 40–46. <https://global.ctbuh.org/resources/papers/download/3348-river-beech-tower-a-tall-timber-experiment.pdf>

Scaramozzino, D., Albitos, B., Lacidogna, G., & Carpinteri, A. (2022). Selection of the optimal diagrid patterns in tall buildings within a multi-response framework: Application of the desirability function. *Journal of Building Engineering*, 54, 104645. <https://doi.org/10.1016/j.jobbe.2022.104645>

Schmidt Iii, R., Deamer, J., & Austin, S. (2011). *Understanding adaptability through layer dependencies*. In International Conference on Engineering Design.

SIS. Bases for design of structures 1–Serviceability of buildings and walkways against vibration. Tech. rep. SS-ISO 10137:2008. Swedish Standards Institute, 2008.

SOM. (2017). *Poly International Plaza*. Visited on 28 november 2021, from <https://www.som.com/projects/poly-international-plaza/>

Staub-French, S., Pilon, A., Poirier, E., Fallahi, A., Kasbar, M., Calderon, F., Teshnizi, Z., & Froese, T. (2021). *Construction process innovation on Brock Commons Tallwood House*. Construction Innovation. <https://doi.org/10.1108/CI-11-2019-0117>

Studiengemeinschaft Holzleimbau e.V. (2010, november). *Environmental Product Declaration (EPD-SHL-2010111-E)*. Institut Bauen und Umwelt e.V. <https://www.studiengemeinschaft-holzleimbau.de/publish/binarydata/downloads/2011/epd-shl-2010111-e.pdf>

Sukrawa, M., Pringgana, G., & Diva Tryatra Sanjaya, P. (2019). *Comparative analysis and design of tower using diagrid, conventional moment frame and braced frame system of steel structures*. <https://doi.org/10.1051/mateconf/201927601026>

Thanh Dat, B., Traykov, A. & Traykov, M. (2017). *Shear-lag effect and its effect on the design of high-rise buildings*. E3S Web of Conferences 33, 02001 (2018). <https://www.e3s-conferences.org/>

The World Bank. (2020). *Urban Development*. Visited on 18 July 2022, from <https://www.worldbank.org/en/topic/urbandevelopment/overview#:~:text=Globally%2C%20over%2050%25%20of%20the,1.5%20times%20to%206%20billion.>

TNO. (2021). *Circular construction with timber, and what's needed for serious scaling up*. Visited on 18 July 2022, from <https://www.tno.nl/en/tno-insights/articles/circular-construction-with-timber-and-what-s-needed-for-serious-scaling-up/>

United Nations. (z.d.). *Population*. Visited on 28 november 2021, from <https://www.un.org/en/global-issues/population>

Urban Taskforce. (2022, January). *High rise buildings to help Sydney become a green metropolis*. <https://www.urbantaskforce.com.au/wordpress/wp-content/uploads/2022/01/Standing-Tall-Urban-Ideas-January-2022.pdf>

Van der Lugt, P. (2012). *Carbon Storage Utilising Timber Products*. ENVIRONMENT INDUSTRY MAGAZINE. <https://www.accoya.com/app/uploads/2020/04/Carbon-Storage-Using-Timber-Products.pdf>

Vasseghi, A. & Khoshkalam, V. (2020, 23 april). Effect of Outrigger Panels on Seismic Performance of Steel Plate Shear Wall Structural System. *International Journal of Steel Structures*, 20(4), 1180–1192. <https://doi.org/10.1007/s13296-020-00350-4>

Verhaegh, R., Vola M., & de Jong, J. (2020). Haut – A 21 storey Tall Timber Residential Building. *International Journal of High-Rise Buildings*, 9(3), 213-220.
with slip friction damping devices. *Construction and Building Materials*, 121, 373–385.

WPMA. (2020). *NZ Wood Design Guides*. <https://www.wpma.org.nz/uploads/1/3/2/8/132870817/ch-2.1-trees-carbon-and-the-environment.pdf>

Znabei, T. (2020, september). *A Post-tensioned Cross-Laminated Timber core for buildings*. <http://resolver.tudelft.nl/uuid:a903744a-f70b-4370-9bf2-dd452f5a9833>

APPENDICES

A TIMBER CALCULATIONS

Assumptions:

- Service Class 3
- Permanent load duration class
- Fundamental combination of actions
- System strength factor, $k_{sys} = 1.0$
- Depth factor, $k_h = 1.0$
- Modification factor, $k_{mod} = 0.5$

Design resistances

Compressive strength along the grain

$$f_{c,0,d} = \frac{k_{mod} * k_{sys} * f_{c,0,k}}{\gamma_M}$$

Equation 20: Compressive strength along the grain

Bending strength

$$f_{m,d} = \frac{k_h * k_{mod} * k_{sys} * f_{m,k}}{\gamma_M}$$

Equation 21: Bending strength

Tensile strength along the grain

$$f_{t,0,d} = \frac{k_{mod} * k_{sys} * f_{t,0,k}}{\gamma_M}$$

Equation 22: Tensile strength along the grain

Shear strength

$$f_{v,d} = \frac{k_{mod} * k_{sys} * f_{v,k}}{\gamma_M}$$

Equation 23: Shear strength

Design stresses

Design tensile stress along the grain

$$\sigma_{t,0,d} = \left| \frac{N_{Ed}}{A} \right|$$

Equation 24: Design tensile stress along the grain

Design bending stress about the principal y-axis

$$\sigma_{m,y,d} = \left| \frac{M_{y,Ed}}{W_y} \right|$$

Equation 25: Design bending stress about the principal y-axis

Design bending stress about the principal z-axis

$$\sigma_{m,z,d} = \left| \frac{M_{z,Ed}}{W_z} \right|$$

Equation 26: Design bending stress about the principal z-axis

Crack factor for cracks cause by rapid drying

$$k_{cr} = 0.67$$

Net shear area

$$A_{net} = \frac{2 * k_{cr} * h * b}{3}$$

Equation 27: Net shear area

Design shear stress for shear in the y-y direction

$$\tau_{y,Ed} = \left| \frac{V_{y,Ed}}{A_{net}} \right|$$

Equation 28: Design shear stress for shear in the y-y direction

Design shear stress for shear in the z-z direction

$$\tau_{z,Ed} = \left| \frac{V_{z,Ed}}{A_{net}} \right|$$

Equation 29: Design shear stress for shear in the z-z direction

Unity checks strength

Compression

U.c. compressive stress, parallel to the grain

$$\eta_{c0} = \frac{\sigma_{c,0,d}}{f_{c,0,d}}$$

Equation 30: U.c. compressive stress, parallel to the grain

Tension

U.c. tensile stress, parallel to the grain

$$\eta_{t0} = \frac{\sigma_{t,0,d}}{f_{t,0,d}}$$

Equation 31: U.c. tensile stress, parallel to the grain

Shear

U.c. shear in the y direction

$$\eta_{V,y} = \frac{\tau_{y,Ed}}{f_{v,d}}$$

Equation 32: U.c. shear in the y direction

U.c. shear in the z direction

$$\eta_{V,z} = \frac{\tau_{z,Ed}}{f_{v,d}}$$

Equation 33: U.c. shear in the z direction

Combined bending and axial

U.c. bending and axial load

$$\eta_{M+N} = \frac{\sigma_{t,0,d}}{f_{t,0,d}} + \frac{\sigma_{m,y,d}}{f_{m,y,d}} + k_m * \frac{\sigma_{m,z,d}}{f_{m,z,d}}$$

Equation 34: U.c. bending and axial load

And

$$\eta_{M+N} = \frac{\sigma_{t,0,d}}{f_{t,0,d}} + k_m * \frac{\sigma_{m,y,d}}{f_{m,y,d}} + \frac{\sigma_{m,z,d}}{f_{m,z,d}}$$

Equation 35: Unity check bending and axial load

Unity checks stability

Slenderness – buckling

Slenderness ratio about y-axis (similar for z-axis)

$$\lambda_y = l * \sqrt{\frac{A}{I_y}}$$

Equation 36: Slenderness ratio about y-axis (similar for z-axis)

Relative slenderness ratio about y-axis (similar for z-axis)

$$\lambda_{rel,y} = \frac{\lambda_y}{\pi} * \sqrt{\frac{f_{c,0,k}}{E_{0,05}}}$$

Equation 37: Relative slenderness ratio about y-axis (similar for z-axis)

Straightness factor

$$\beta_c = 0.1$$

Instability factor y-axis (similar for z-axis)

$$k_y = 0.5 * (1 + \beta_c * (\lambda_{rel,y} - 0.3) + \lambda_{rel,y}^2)$$

Equation 38: Instability factor y-axis (similar for z-axis)

Instability factor y-axis (similar for z-axis)

$$k_{c,y} = \frac{1}{k_y + \sqrt{k_y^2 - \lambda_{rel,y}^2}}$$

Equation 39: Instability factor y-axis (similar for z-axis)

Slenderness – Lateral Torsional Buckling

Critical bending stress

$$\sigma_{m,crit} = E_{0,05} * \frac{0.78 * b^2}{h * l_{ef}}$$

Equation 40: Critical bending stress

Relative slenderness for LTB

$$\lambda_{rel,m} = \sqrt{\frac{f_{m,k}}{\sigma_{m,crit}}} \leq 0.75$$

Equation 41: Relative slenderness for LTB

Lateral buckling factor

$$k_{crit} = 1.0$$

Unity checks stability

Unity check flexural buckling

$$\eta_{\lambda} = \frac{\sigma_{c,0,d}}{k_{c,y} * f_{c,0,d}} + \frac{\sigma_{m,y,d}}{f_{m,y,d}} + k_m * \frac{\sigma_{m,z,d}}{f_{m,z,d}}$$

Equation 42: Unity check flexural buckling around the y-axis

And

$$\eta_{\lambda} = \frac{\sigma_{c,0,d}}{k_{c,z} * f_{c,0,d}} + k_m * \frac{\sigma_{m,y,d}}{f_{m,y,d}} + \frac{\sigma_{m,z,d}}{f_{m,z,d}}$$

Equation 43: Unity check flexural buckling around the z-axis

Unity check LTB

$$\eta_{LTB} = \frac{\sigma_{m,y,d}}{k_{crit} * f_{m,d}}$$

Equation 44: Unity check LTB

B ALONG-WIND ACCELERATIONS

Along-wind accelerations are the accelerations of the excitations in the same direction as the wind loads. These excitations result from frontal wind loads on the building's façade.

$$a_{along}(y, z) = \sigma_{a,x}(y, z) * k_p$$

Equation 45: Along-wind accelerations

$\sigma_{a,x}(y, z)$ *standard deviation of the characteristic along-wind acceleration*
 k_p *is the peak factor*

The standard deviation is calculated according to the following formula:

$$\sigma_{a,x}(y, z) = c_f * \rho * I_v(z) * v_m^2 * R * \frac{K_y * K_z * \varphi(y, z)}{\mu_{ref} * \varphi_{max}}$$

Equation 46: Standard deviation

c_f *is the force coefficient*
 ρ *is the air density*
 $I_v(z)$ *is the turbulence intensity at height (z)*
 v_m *is the characteristic mean wind velocity*
 R *is the square root of resonant response*
 K_y, K_z *is the size reduction coefficients*
 $\varphi(y, z)$ *is the mode shape*
 μ_{ref} *is the reference mass per unit area*
 φ_{max} *is the mode shape value at maximum amplitude*

For along-wind accelerations mode shape variations along the horizontal axis has uniform distribution and along the vertical axis have linear distributions (Eurocode 1, 2020)

$$\varphi(y, z) = \frac{z}{h}$$

$$K_y = 1$$

$$K_z = \frac{3}{2}$$

And the peak factor:

$$k_p = \sqrt{2 * \ln(v * T)} + \frac{0.6}{\sqrt{2 * \ln(v * T)}} \geq 3$$

Equation 47: Peak factor (Eurocode 1, 2020)

T is the average period of reference wind velocity ($T = 600$)

v is the estimation gust frequency

Gust frequency can be estimated with:

$$v = n_{1,x} * \sqrt{\frac{R^2}{B^2 + R^2}}$$

Equation 48: Gust frequency (Eurocode 1, 2020)

$n_{1,x}$ is the natural frequency

$$B^2 = \frac{1}{1 + \frac{3}{2} * \sqrt{\left(\frac{b}{L(z)}\right)^2 + \left(\frac{h}{L(z)}\right)^2 + \left(\frac{b}{L(z)} * \frac{h}{L(z)}\right)^2}}$$

Equation 49: Width structure (Eurocode 1, 2020)

b is the width structure

h is the height structure

$L(z)$ is the turbulence length scale

$$L(z) = L_t * \left(\frac{z}{z_t}\right)^\alpha$$

Equation 50: Turbulence length scale (Eurocode 1, 2020)

L_t is 300 m

z is the reference height

z_t is 200 m

$$\alpha = 0.67 + 0.05 \ln z_0$$

$$R^2 = \frac{\pi^2}{2 * \delta} * S_L * K_s$$

- δ is the logarithmic decrement of damping
 S_L is the spectral density function (non-dimensional)
 K_s is the size reduction factor

$$S_L = \frac{6.8 * f_l}{(1 + 10.2 * f_l)^2}$$

$$f_l = \frac{n_{1,x} * L(z)}{v_m(z)}$$

$$K_s = \frac{1}{1 + \sqrt{(G_y * \varphi_y)^2 + (G_z * \varphi_z)^2 + \left(\frac{2}{\pi} * G_y * \varphi_y * G_z * \varphi_z\right)^2}}$$

Equation 51: Size reduction factor (Eurocode 1, 2020)

$$G_y = \frac{1}{2}$$

$$G_z = 5/18$$

$$\varphi_y = \frac{c_y * b * n}{v_m(z_s)}$$

$$\varphi_z = \frac{c_z * h * n}{v_m(z_s)}$$

$$c_y = c_z = 11.5$$

When analysing the parameters used for calculating along-wind accelerations it can be seen that there are environment-dependent parameters such as air density and wind velocities and building-dependent parameters. Building dependent parameters include building measurements, damping coefficients, mass distributions and most importantly natural frequencies.

C ACROSS WIND ACCELERATIONS

Smith and Coull (1991) state that across-wind accelerations might become critical for more slender buildings that comply to the following criterium:

$$\frac{\sqrt{W * D}}{H} < \frac{1}{3}$$

Equation 52: Across wind accelerations criterium for slender buildings (Smith & Coull, 1991)

W is the width of the building

D is the depth of the building

H is the height of the building

When assessing Equation 52, it is clear that for a building with a width and depth of 30 m, across-wind accelerations should be investigated when building over 90 meters. Also, when increasing the size of one of the facades the probability of having critical across-wind accelerations decreases.

It is generally mentioned that it is difficult to calculate across-wind accelerations, and that only with wind tunnel tests accurate results can be found Smith and Coull (1991). However, according to Smith and Coull (1991) peak accelerations on top floors can be estimated with the following equations:

$$a_w = n_0^2 k_p [W * D]^{1/2} \left(\frac{a_r}{\rho * g * \sqrt{\beta}} \right)$$

$$a_r = 78.5 * 10^{-3} \left[\frac{V_H}{n_0 \sqrt{W * D}} \right]^{3.3}$$

Equation 53: Peak accelerations (Smith & Coull, 1991)

a_w is the peak acceleration

n_0 is the fundamental frequency

ρ is the average building density

g is the gravitational acceleration

β is the estimated critical damping ratio

D ELEMENT DIMENSIONS

In this thesis, the elements of the structural model are first sized based on the required sizing to be able to fulfil the unity check for strength. It is known that the load distribution is susceptible to the shear lag effect, resulting in a nonlinear distribution of forces along the perimeter of the building. The hand calculation provided in this section resemble the loads in the exterior elements and have consistently been confirmed and reconfirmed with the corresponding loads of the GSA model, in order to certify the found calculation approach. Yet it should be considered that part of the full lateral loads are also dissipated to other structural elements which are not considered in this calculation. This calculation's purpose is to be an estimation of actual loading, to be able to select appropriate and corresponding element sizes.

The lateral loads on the structure are withheld by both structural systems, in this case both the core and the façade have a share in resisting wind-induced moments. For the following calculations, it is assumed that 85% of the bending moment is resisted by the façade system, whereas the interior system is accountable for 15% of the resistance, as can be seen in the moment capacity participation in Figure 83. In addition, of the 85% of façade resistance, it is expected that half of the wind load flows through each flank of the building, as is seen in Figure 83.

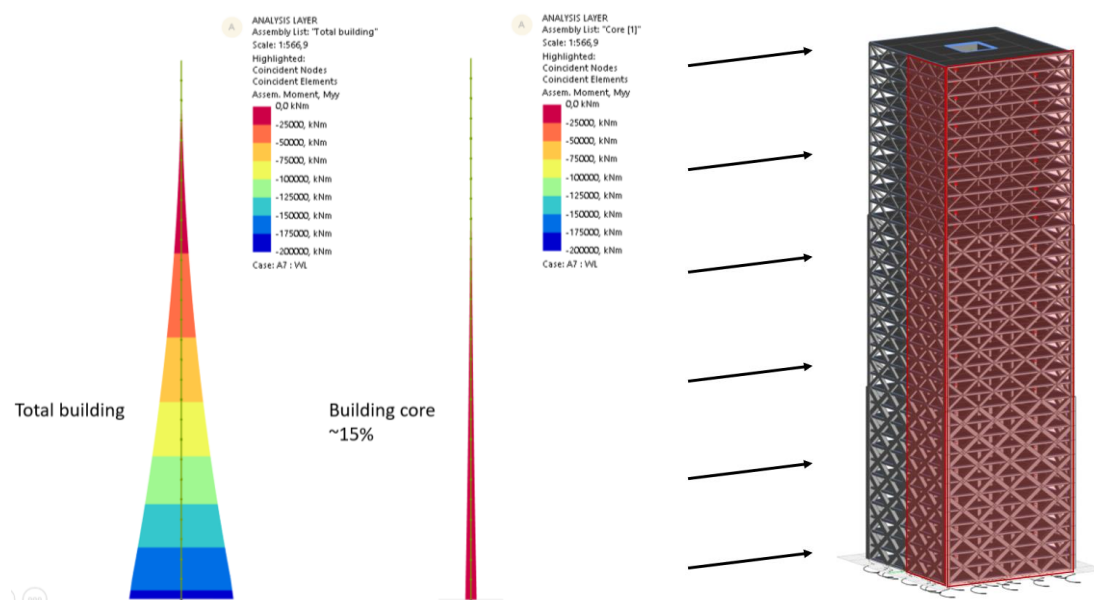


Figure 83: Core participation and wind distribution along the façade – due to wind induced loads

Figure 84 below shows the axial loads active for an 84m rectangular diagrid system. In the figure it can be seen that the exterior system is assessed, consisting of the diagrid bays and the edge column. Sizing of the elements will be done on diagonal elements and the edge column separately, as axial loads are

of different orders of magnitude. When assessing diagonal elements in the web of the flange of the structure, it can be seen that diagrid bays on the web part close to the edge column is susceptible to the highest loads. In addition, due to the diagrid behaviour, it can be seen that the orientation of the diagrid bay determines whether tension or compression occurs in the element. Not only is the direction of the loading mirrored along the web, the axial forces are also mirrored.

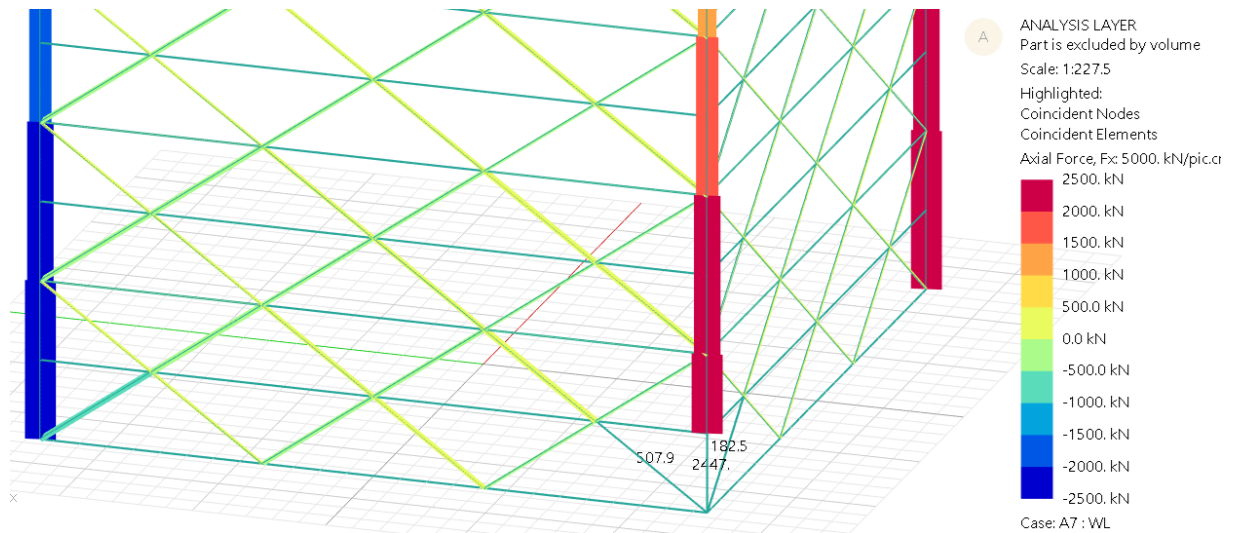


Figure 84: Axial loads for rectangular diagrid

For simplification of the calculation, compressive (blue) and tensile (red) elements are split in this calculation, as it has been found that they hold equal but mirrored loads (Figure 85). In the following assumption, the stress pattern along the perimeter could be resembled by Figure 85. Due to simplification, half the moment of each façade part is used.

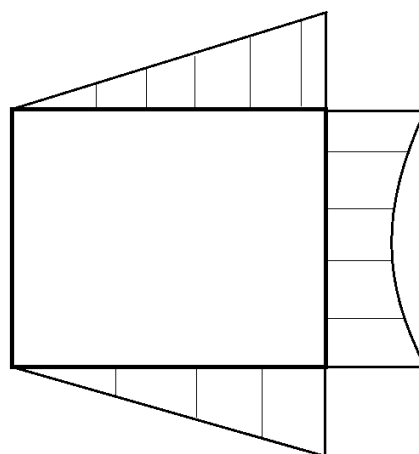


Figure 85: Assumed stressed distribution along the façade

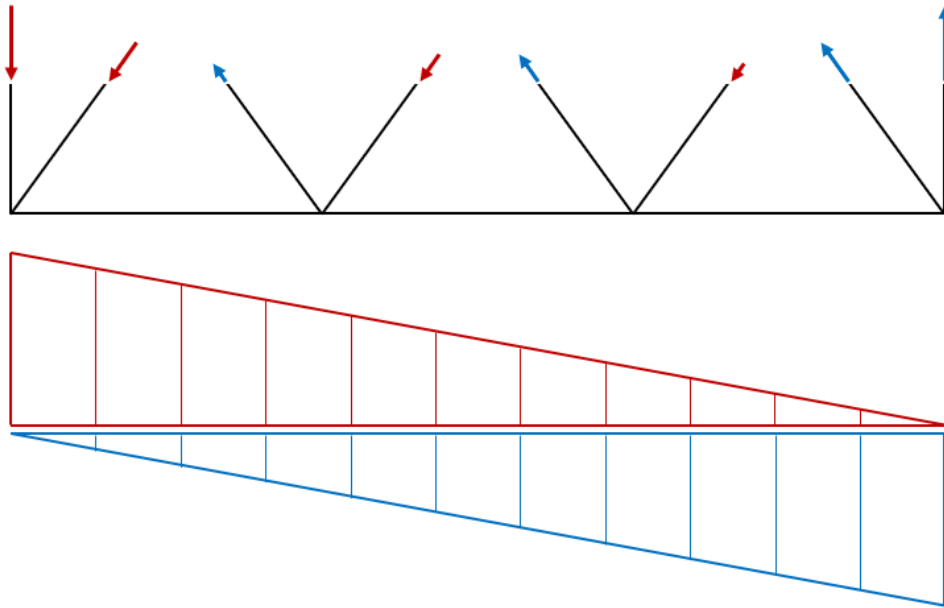


Figure 86: Stress distributions and axial loads for moment equilibrium

When considering Figure 86, reaction forces for the sections in tension and compression (which are split in this assumption) can be calculated using the following formulas:

$$\sigma_i = \frac{M * z_i}{I} = \frac{F}{A}$$

Equation 54: Stress equation used for hand calculation

And

$$\sum M_{(o,o)} = \sum F_i * r_i = 0$$

Equation 55: Moment equilibrium

With

$$M = \frac{1}{2} * \frac{1}{2} * 0.85 * M_{tot}$$

Equation 56: Assumption on moment for axially compressed elements

All together this results in:

$$F_{edge,column} = \frac{M - \sum(l_{bay,i} * F_{diagrid,v,i} + \dots + l_{bay,n} * F_{diagrid,v,n})}{\left(l_{tot} * \frac{A_d}{A_c} + l_{tot}\right)}$$

Equation 57: Hand calculation for finding axial load in edge column

l_{bay} is the length of the lever arm from the corresponding bay to the origin

l_{tot} is the total length, equal to the width of the building

$F_{diagrid,v,i}$ is the vertical reaction force of a diagrid element

A_d is the area of the diagrid

A_c is the area of the edge column

And

$$F_{diagrid,v,edge} = \frac{M * l_{tot}}{I} * A_d - F_{edge,column} * \frac{A_d}{A_c}$$

Equation 58: Hand calculation for finding axial load in diagrid

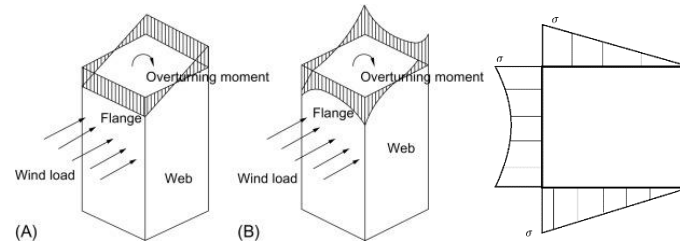


Figure 87: Axial stress distribution in the columns of the building in web as well as in flange panels (Fu, 2018)

Since the stiffnesses of dual structural systems are too complex to determine with hand calculations, GSA is needed to find the correct stiffnesses. With the structure's stiffness the building's deformation and natural frequencies can be determined. This is done in GSA.

The strength of the elements is determined with the hand calculation, based on the calculation for timber elements according to and complying to a unity check smaller than 0,8. For the dimensions complying to the strength unity check, also checks are done based on deformations and comfort levels at the top floor. Based on Figure 87 above, for an extreme slenderness it is assumed that strength will suffice ample, while deformation might suffice less and dynamic behaviour barely. Automatic dimensioning based on hand calculations can only be done on strength, however, through empirical research an estimator function might be found which can be applied to the parametric model. By finding and applying this estimator function, many adequate alternatives might be compared without over dimensioning the elements. In this way structural and typological alternatives can be compared on the same criteria, since all alternatives comply to three abovementioned unity check criteria.

E ESTIMATOR FUNCTION

In order to have a uniform approach for finding the estimator function factor for cross-section dimensions sized on strength a roadmap needs to be set-up. By consequently following the steps in the roadmap, estimator functions and results are gathered that are drawn up by the same principles.

Problem: Sizing of elements is done with a hand calculation for strength criteria. In addition, sizing could also be done for deflections with mechanical equations, which results to be complex with combined structural systems, which is why it is not done in this thesis. In conclusion, dimensioning of elements should be done based on deformation thresholds and dynamic criteria too, therefore sizing only for strength is insufficient.

Goal: The goal is to find an estimator function per structural system which is the factor by which the sizing of the elements should be multiplied if the elements are just sized only for strength, in order to find a size that complies to all three criteria.

1. Unity checks for strength, stiffness and accelerations should be within a range of $0.9 < 1.0$ to be able to make substantiated comparisons between outcomes.
2. A concrete step-by-step method should be drawn up, in order to ensure a universal approach is applied for each estimator function.

Bottlenecks:

1. Finding an estimator function is quite a rough estimation, and it is impossible to find one estimator function for all configurations. With the step-by-step method a plan is made to approach this problem and to generate various relevant estimator functions.
2. To find the coherence between empirical data, trendlines are applied for the estimator functions. By plotting trendlines the corresponding equations can be found in Excel, which can be seen as the estimator function equations. Problematic for a trendline is that it averages data points, meaning that it is inevitable that some data points are not satisfied with the estimator function, and some aren't.
3. Although the estimator function might give a proper estimation for which a certain share of configurations will suffice $u.c. < 1.0$, it is extremely hard (if not impossible) to estimate whether unity checks would be within the $0.9 < u.c. < 1.0$ criterium. Making it a manual iterative process, which is time consuming.
4. Finding, testing and verifying the estimator functions is very time consuming, especially when there are large differences in configuration acceptance levels.

The plan written in this section will be similar for all structural systems and floorplan shapes, however the results shown in this section are results of the circular diagrid CLT core only. The estimator function method has been systematically drawn up in the following steps:

1. Calibration model & first analysis
2. Determination of bandwidth
3. Dimensioning factor
4. Verification bandwidth
5. Adjusting estimator function
6. Verification estimator function

E.1 CALIBRATION MODEL & FIRST ANALYSIS

When taking bottleneck 4 into account, it is important to be aware of the time-consuming process, and to pre-evaluate configurations before running all the models and trying to find estimator functions for configurations that beforehand could be discarded. To be able to discard results premature, literature needs to be consulted and taken into account. Literature relevant for premature discarding can be found in chapter 3 in this thesis on acceleration levels and shear lag.

Now that the scope for the estimator function results is set, a first plain model has been analysed. The dimensioning of the elements is sized on strength only, meaning that no estimator function has been applied in this model.

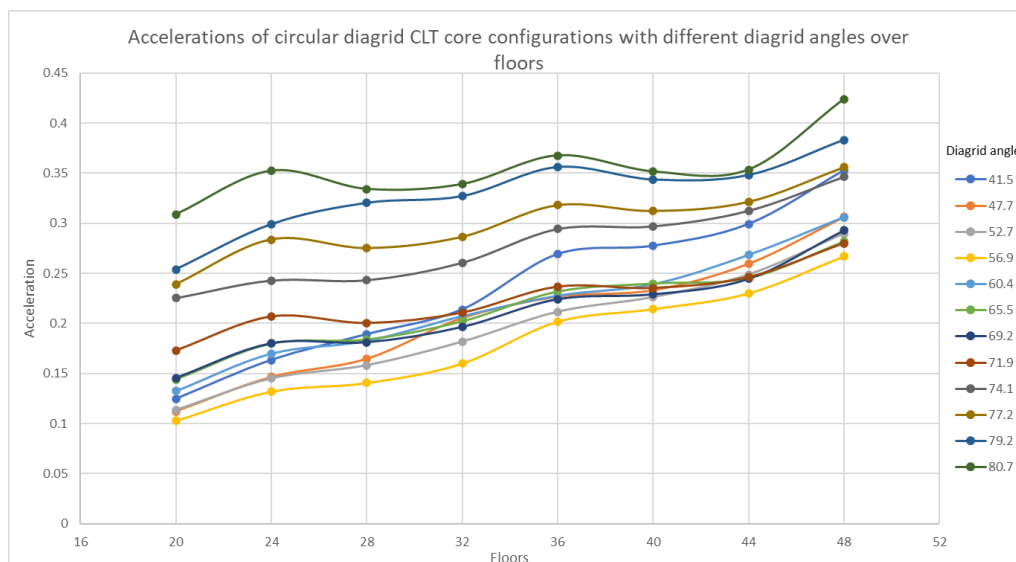


Figure 88: Accelerations of circular diagrid CLT core configurations with different diagrid angles over floors.

The figure above shows the accelerations of 12 different configurations of the diagrid system, each with a corresponding diagrid angle (as shown in the graph's legend). What is obvious from this graph is the

inferior acceptance level of the configurations with diagrid angles 74.1° and higher. The accelerations of the >74,1° configurations are in some cases up to 3 times as high as a lower angle configuration. The poorer acceptance level in combination with the findings from Kim and Lee (2010) make it straightforward that >74.1° configurations can be discarded before estimator functions are created.

E.2 DETERMINATION OF BANDWIDTH

When plotting a simplification of the graph above and discarding the $>74.1^\circ$ configurations, graph 46 below is created covering the results of the 8 residual configurations. Instead of looking at accelerations the graph plots overall acceptance level, giving an indication on how alternative configurations behave compared to each other based on serviceability. What is seen in the graph is that there are two lines following a similar course and two lines having separate slopes. The two lines with comparable slopes indicate the bandwidth for which the acceptance levels of 6 configurations are represented. Configurations with diagrid angles 41.5° and 71.9° perform differently, and trying to find an estimator function for a multitude of individually performing systems is not desirable. For the case of 71.9° diagrid angle, from 32 floors onwards the acceptance level enters the bandwidth of the bulk of configurations, from there on a general estimator function might apply for that specific system too.

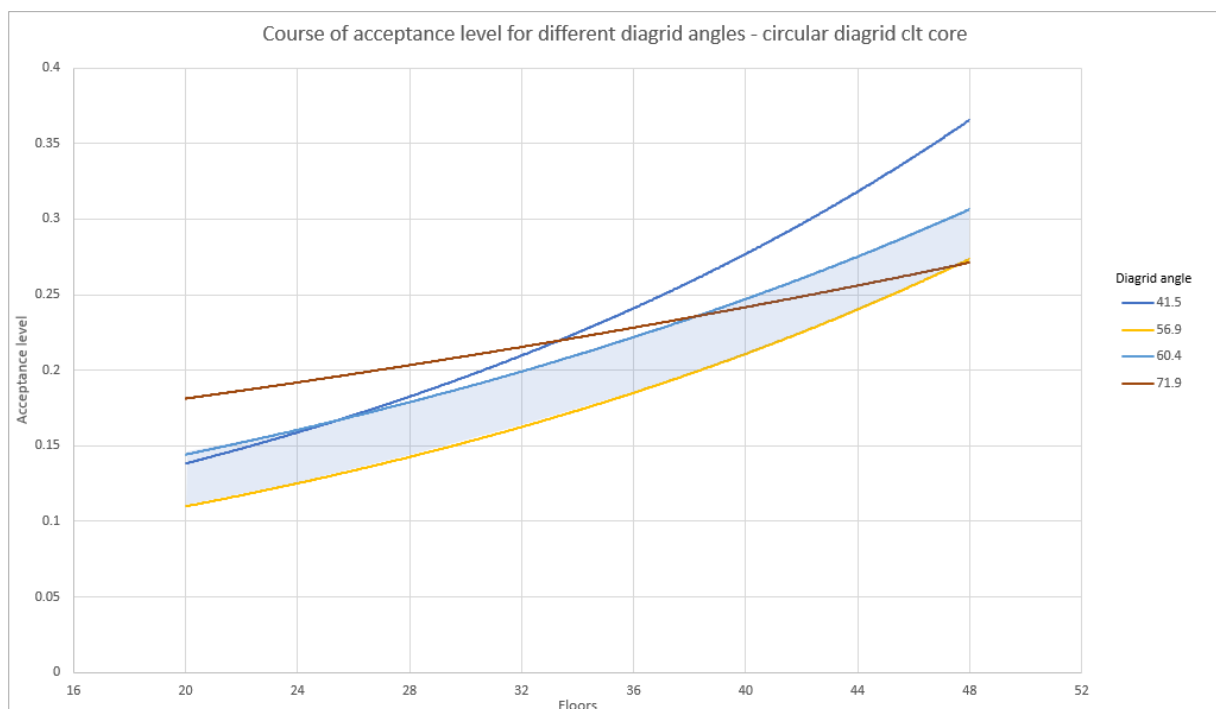


Figure 89: Course of acceptance level for different diagrid angles - circular diagrid CLT core.

Note that the bandwidth of the majority of configurations is defined by diagrid angles 60.4° and 56.9° . For finding an estimator function that applies to several configurations, first the estimator function for the maximum and minimum band width needs to be found. The next section elaborates on the process of finding an estimator function with the help of a dimensioning factor.

E.3 DIMENSIONING FACTOR

In this section the process for an estimator function with a dimensioning factor is explained. It is important to recall that diagrid angles 60.4° and 56.9° are respectively the upper and lower limit of the bandwidth of configurations for a circular diagrid CLT core. The steps described below will be done for both configurations, although to avoid repetitiveness in this thesis, only the approach for 60.4° (the upper limit) will be explained.

The goal of finding the dimensioning factor is to find for which element sizing, with respect to dimensioning of elements on strength, would make the configuration suffice serviceability acceptance level criteria. The dimensioning factor is a factor that is multiplied by the element cross-section measurements found by the strength dimensioning calculation. This factor is a parameter in the following study, varying from 1.0 to 6.0 with steps of 0.5. The model is ran with the following set-up:

Fixed parameters: Structural systems, floorplan shape, horizontal segments + storey span diagrid (diagrid angle)

Variable parameters: Height, dimensioning factor

Element sizing: Strength hand calculation + dimensioning factor (parametrized)

Results collected from this study are acceptance level values corresponding to the (over)dimensioning of elements. These results can be filtered on a certain acceptance level value (i.e. < 1.0) to see what sizing of elements is required to achieve desired serviceability levels. Figure 90 below shows the results for diagrid angle 60.4° .

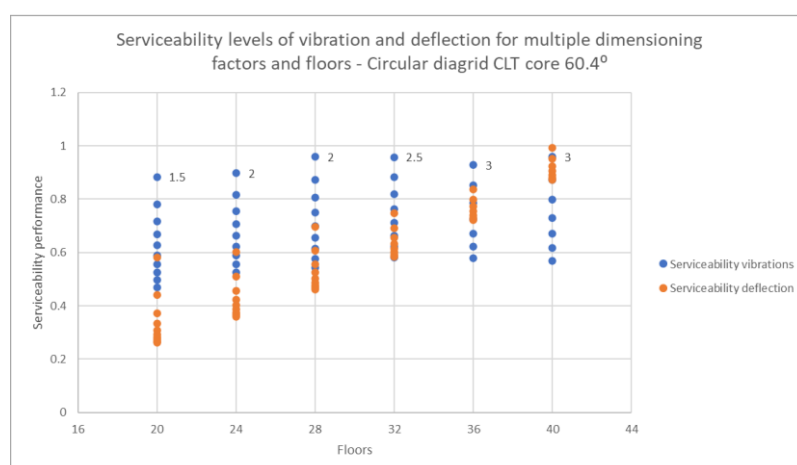


Figure 90: Serviceability levels of vibration and deflection for multiple dimensioning factors and floors.

As can be seen in the figure above, dimensioning factors are needed for the structure to suffice serviceability acceptance level. Also, in the case of 60.4° diagrid configuration, buildings higher than 40 floors are not feasible, as dimensioning factors higher than 6 are not sufficient. For heights over 40 floors deflection levels become governing, for which more material is required. In the table below required dimensioning factors are presented for configurations 60.4° and 56.9°.

Angle\floors (height [m])	20 (60)	24 (72)	28 (84)	32 (96)	36 (108)	40 (120)	44 (132)	48 (144)
60.4°	1.5	2	2	2.5	3	3	X	X
56.9°	1	1.5	1.5	1.5	2	2	2.5	3.5

Table 18: Dimensioning factors for different angles and floors

To find the coherence between dimensioning factors and sum of floors the results from the table above are plotted with a trendline in the graph below. The trendline equation is also plotted, giving a estimator function for the coherence of dimensioning factors for the upper and lower limits of the configuration bandwidth. Keep in mind that for a 60.4° angle diagrid, dimensioning factors are considered to be out of bounds, meaning that if the actual value would be plotted (a dimensioning factor ≥ 6), the trendline equation would be considerably higher.

Whereas Figure 91 presents the bandwidth of the acceptance level, Figure 91 below shows the bandwidth of estimator functions for approximating the dimensions to accommodate serviceability in the structure’s design. To mitigate bottleneck number 2) the nature of a trendline, it is considered to modify the trendline equation. By doing this, the goal is to cover more configurations with an estimator function. Note that the results are not modified, only the equation for approximating corresponding dimensions is adjusted.

For the following studies, bandwidths are modified as such that the trendline will go through the two upper points in order to cover all datapoints below the equation curve. Figure 91 depicts the increase of the trendline, where it can be seen how the modification ensures the trendline to incorporate more of the empirical datapoints.

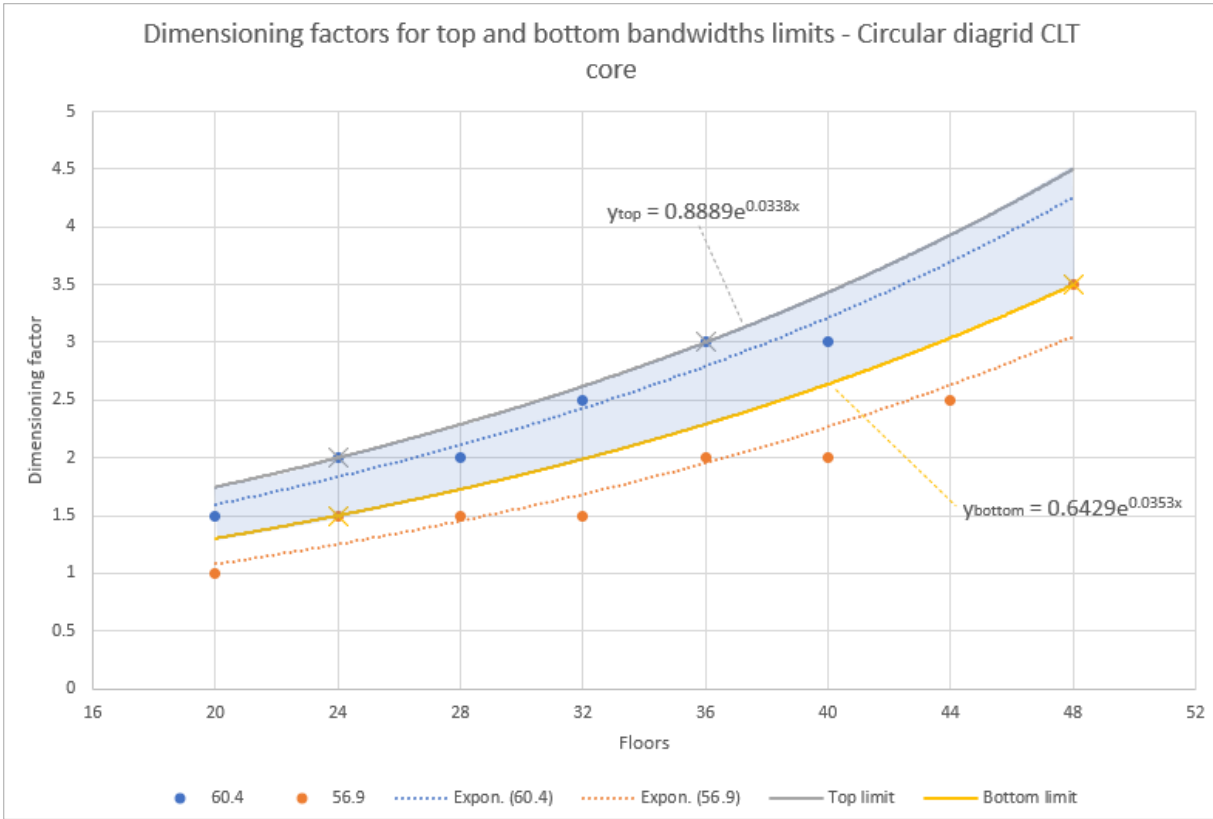


Figure 91: Dimensioning factors for top and bottom bandwidth limits

E.4 VERIFICATION BANDWIDTH

Next step is to verify the estimator functions found that are the top and bottom limit of the bandwidth. By running the model for the best and worst performing configuration and measuring the outcomes on serviceability, an estimation can be made of dimensioning factors for other configurations. For finding comparable outcomes, one should be mindful of the fact that acceptance level values should be within 0.9 and 1.0.

Furthermore it is also crucial to be keen on constructability, and to be realistic when evaluating results. To give an illustration, the top limit indicates that for 48 floors (a total building height of 144 m), dimensioning based on strength should be multiplied by almost 4.5. If not aware of the order of magnitude of these dimensions, highly unrealistic outcomes could be generated.

Figure 92 below shows the results for the upper and lower limit of the bandwidth for the seven configurations mentioned earlier. The top limit of the bandwidth ensures that 93% of configurations satisfy a acceptance level < 1.0. The 7% outliers are result of the dimensioning factor running out of bounds in the previous section. Remember that for 44 and 48 floors multiplying the strength sizing by 6 would not be sufficient. Meaning that the actual value should be higher, and a higher value would drastically increase the upper limit of the bandwidth. The 7% outliers that are well beyond the

serviceability acceptance level are discarded henceforth because the dimensioning of these elements are of an irrational magnitude (± 3000 mm).

Further on, the goal to have acceptance level between the values 0.9 and 1.0. The blue and orange double sided arrows show which range of the spectrum satisfies acceptance level criteria, and it also shows which parts are not covered by it. Since the top part of the spectrum is rejected, estimations for the middle and lower part are needed. Additional estimator functions are needed, which will be done in the next section.

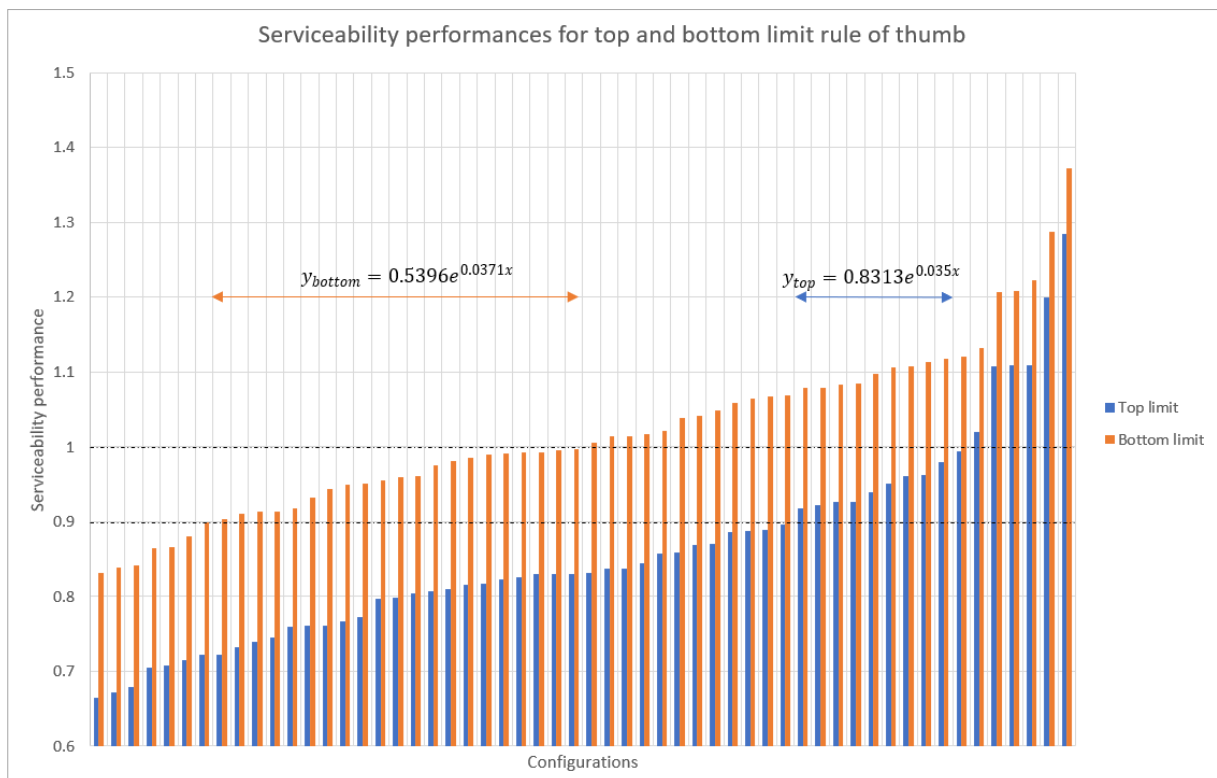


Figure 92: Serviceability performances for top and bottom limit estimator function

E.5 ADJUSTING ESTIMATOR FUNCTION

Estimator functions for top and bottom bandwidth do not cover all configurations with the required precision (within $0.9 < 1.0$ serviceability performance). Therefore two additional estimator functions are added to the spectrum, in the middle of the bandwidth and below the lower limit. By doing this, all configurations are analysed with additional estimator functions, meaning that different sizes are inputted in the model. The estimator function in the middle of the bandwidth is added because the top limit overperforms, serviceability performance is below 0.9. The function below the lower limit is added for the same reason, only now the bottom limit overperforms.

The middle estimator function is constructed as the middle value of the bandwidth, the under estimator function is set at 0.75 of the lower bandwidth. When analysing results from the second generation of estimator functions, it is seen that still there were configurations that were oversized, where acceptance levels were much below 0.9. Therefore, two additional estimator functions are added, to properly size all configurations. The last two estimator functions that have been added were the under_2 and under_3 functions, as can be seen in Figure 93 below. Table 19 below shows how each additional estimator function has been generated.

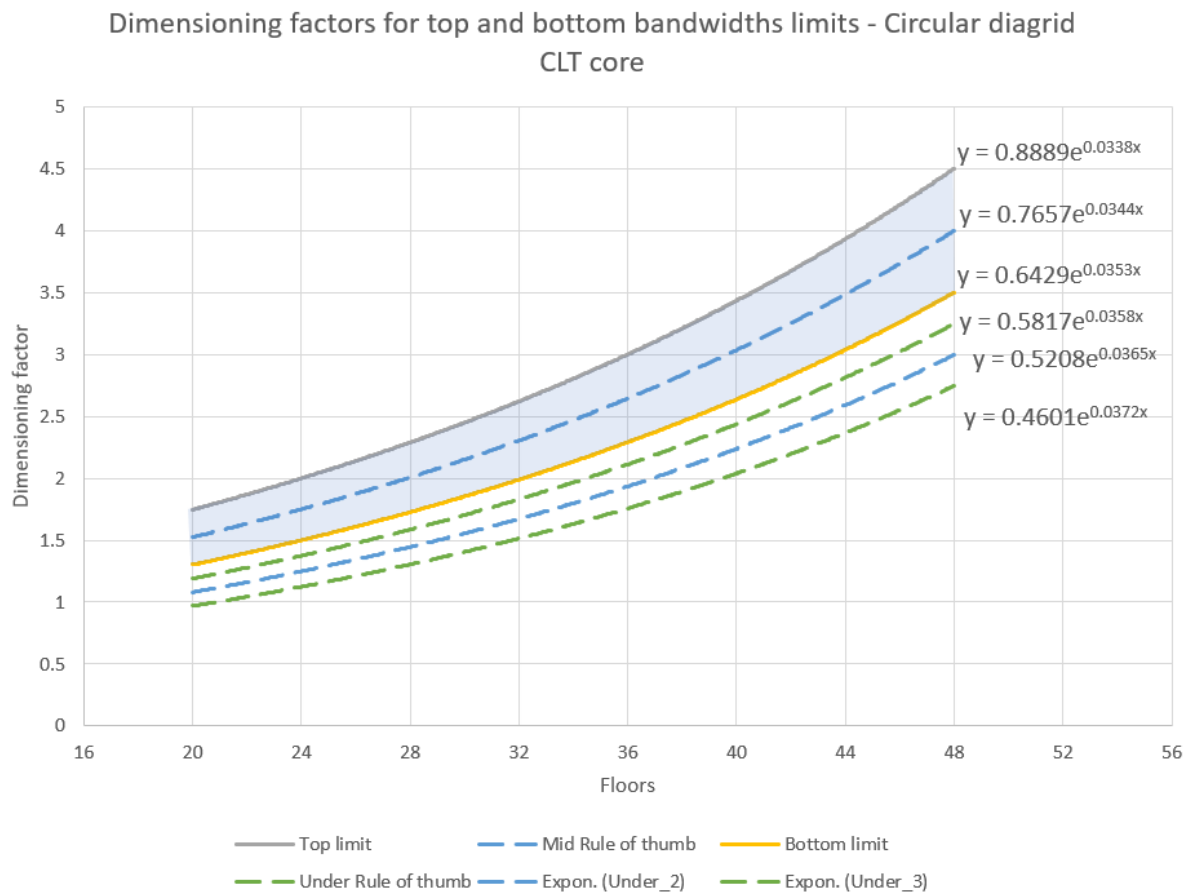


Figure 93: Dimensioning factors for top and bottom bandwidths limits.

Name	Set-up	Function
Top limit function	y_{top}	$y_{top} = 0.8889 * e^{0.0338x}$
Bottom limit function	y_{bottom}	$y_{bottom} = 0.7657 * e^{0.0344x}$
Mid function	$\frac{(y_{top} + y_{bottom})}{2}$	$y_{mid} = 0.6429 * e^{0.0353x}$
Under function	$y_{bottom} - \frac{(y_{top} + y_{bottom})}{4}$	$y_{under} = 0.5817 * e^{0.0358x}$
Under_2 function	$y_{bottom} - \frac{(y_{top} + y_{bottom})}{2}$	$y_{under,2} = 0.5208 * e^{0.0365x}$
Under_3 function	$y_{bottom} - \frac{3 * (y_{top} + y_{bottom})}{4}$	$y_{under,3} = 0.4601 * e^{0.0372x}$

Table 19: Set-up for creating estimator functions

E.6 VERIFICATION ESTIMATOR FUNCTION

Graph 51 below shows that all configurations comply to the pre-set criteria. Only the four configurations that are discarded earlier do not fulfil match this criterium.

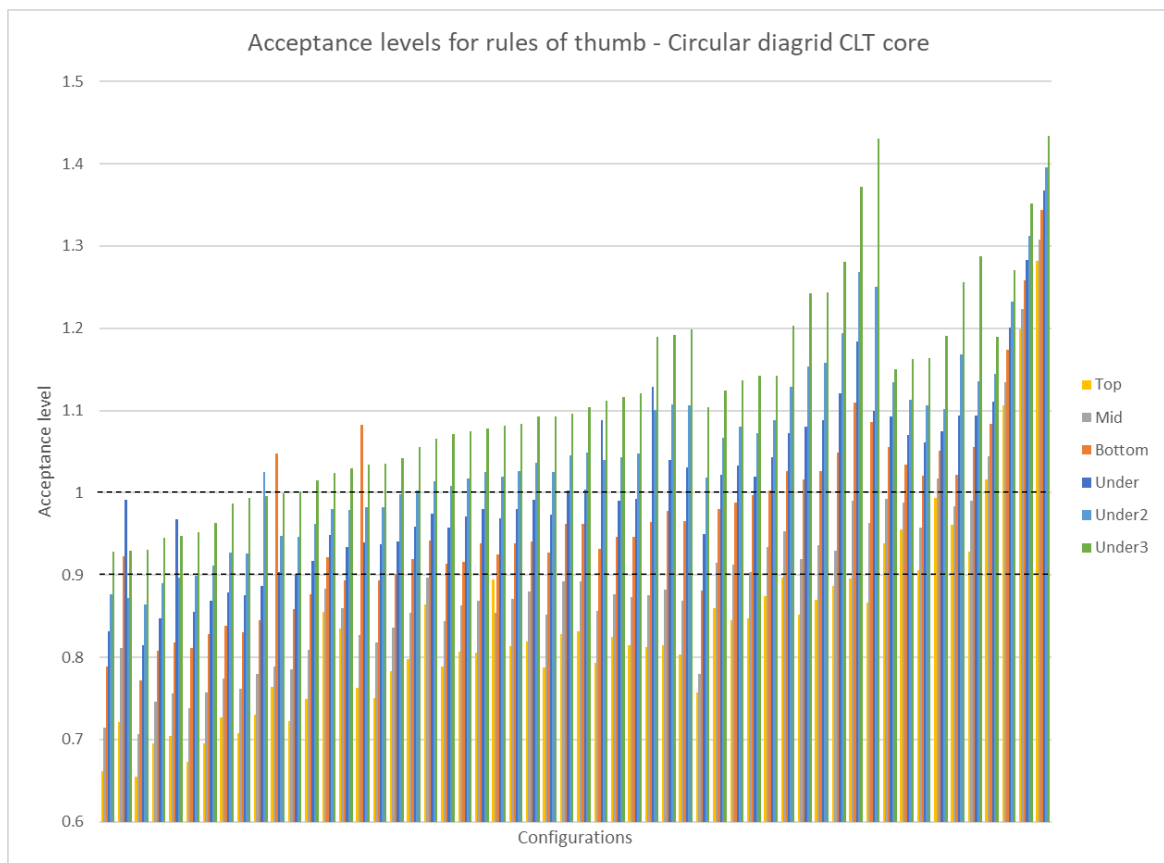


Figure 94: Acceptance levels for estimator functions.

F STIFFNESS CALCULATION CORE VS FAÇADE

Calculation of the stiffness of the interior system vs the exterior system has been performed with the help of the deflection of the system calculated by Oasys GSA (Figure 95: Simplified GSA models for finding deflection of systems) and Equation 59 below.

$$EI = \frac{P * h^3}{3 * \delta}$$

Equation 59: Bending stiffness

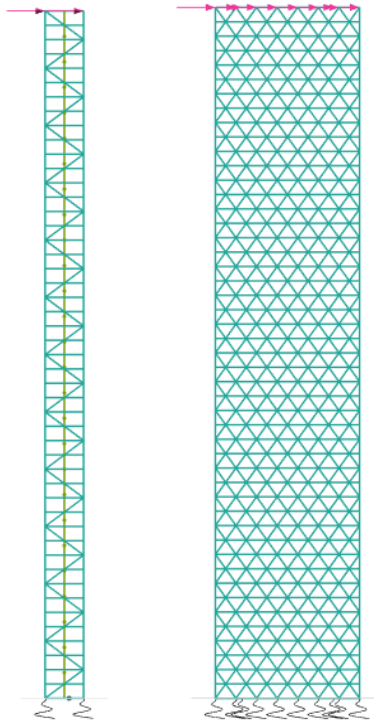


Figure 95: Simplified GSA models for finding deflection of systems